博士論文

Molecular nonadiabatic theory and its applications to field-induced dynamics

（分子の非断熱理論とその外場誘起動力学への応用）

花崎　浩太

Contents

General Introduction

Quantum-mechanical properties of molecules are closely dependent on their electronic states. In static problems, *ab initio* electronic state calculations [1] have been successfully applied to accurately reproduce a wide variety of molecular properties including structure, thermochemical and spectroscopic quantities. However, in dynamical problems where the Born-Oppenheimer approximation [2] breaks down, static *ab initio* calculations are no longer sufficient. Recent developments in laser techniques [3–8] have realized ultrafast intense laser pulse with fs to sub-fs time duration, intensity exceeding 10^{16} W/cm^2, which reaches electronic time scale and field strength exceeding that of a typical atomic Coulomb field. As a consequence, there has been growing interest in chemical reactions under controlled pulse field and real-time observation of electronic dynamics. These new types of experiments, which have been renewing our understanding on chemical bond formation and possible engineering applications. Resolving highly nonadiabatic electronic dynamics taking place in these experiments is hence one of the central tasks for theoretical study. This work is devoted for developing theoretical foundation of electron nucleus coupled nonadiabatic dynamics from modern standpoint as stated above.

Need for a new theory One may be skeptical of the need for 'new' theoretical approaches of quantum dynamics, which is perfectly described by the time-dependent Schrödinger equation. Nevertheless we have two motivations to seek for an 'improved' theory; (1) Needs for an appropriate representation for quantum-mechanical description of a given phenomena : We have to seek for such representation that best describes the underlying physics and most likely to contribute to our understanding. (2) Needs for an appropriate computational method that compromises between the requirement of accuracy and currently available resources: We have to find out such a numerical scheme that achieves requirements within available resources. These points will be further specified in later discussion.

Formal description of nonadiabatic dynamics We start our discussion from the formal theory of (non)adiabatic dynamics. The quantum-mechanical states of an electron-nucleus coupled system can be described as

$$|\Omega\rangle\!\rangle = \int d\mathbf{R}|\mathbf{R}\rangle|\Psi:\mathbf{R}\rangle = \int d\mathbf{R}|\mathbf{R}\rangle \sum_{\alpha} |\Phi_\alpha:\mathbf{R}\rangle\chi_\alpha(\mathbf{R},t) \tag{1.1}$$

where $|\Omega\rangle\!\rangle$ represents the state of the whole system, $|\Psi : \mathbf{R}\rangle$ is the electronic state projected on the nuclear positional eigenstate $|\mathbf{R}\rangle$ as $|\Psi : \mathbf{R}\rangle = \langle\mathbf{R}|\Omega\rangle\!\rangle$ and the αth nuclear wave function $\chi_\alpha(\mathbf{R})$ is the projection of $|\Psi : \mathbf{R}\rangle$ onto the electronic state $|\Phi_\alpha : \mathbf{R}\rangle$. The Schrödinger equation is given as

$$i\hbar\dot{\chi}_\alpha(\mathbf{R},t) = \left[\sum_k \frac{1}{2M_k}\left(\frac{\hbar}{i}\nabla^k - i\hbar\mathbf{X}^k - \frac{Q_k}{c}\mathbf{A}\right)^2_{\alpha\beta} + H^{el}_{\alpha\beta}(\mathbf{R})\right]\chi_\beta(\mathbf{R}) \tag{1.2}$$

Here M_k, Q_k, and $\mathbf{X}^k$ are the mass, charge and derivative coupling matrix[1]($\left(\mathbf{X}^k\right)_{\alpha\beta} \equiv \langle\Phi_\alpha : \mathbf{R}|\nabla^k|\Phi_\beta : \mathbf{R}\rangle$) associated with the kth nucleus.

Static quantum-mechanical states of a molecule near its equilibrium configuration is in many cases well-described using the static approximation on the nuclear degrees of freedom. This approximation was derived by Born and Oppenheimer [2], based on the large mass differences between an electron and a nucleus.

Under moderate conditions, the Born-Oppenheimer approximation can be extended to the adiabatic approximation in explicitly time-dependent problems. The adiabatic approximation reduces the original problem to an effective nuclear dynamical problem on a single adiabatic electronic potential energy surface (PES). In such process, the electronic dynamics does not take part in explicitly as it is fixed as electronic ground state. Dropping all but a single state α in Eq. (1.2), the adiabatic dynamics is described by a single component nuclear equation

$$i\hbar\dot{\chi}(\mathbf{R}) = \left[\sum_k \frac{1}{2M_k}\left(\frac{\hbar}{i}\nabla^k - \frac{Q_k}{c}\mathbf{A}\right)^2 + \mathcal{E}_\alpha(\mathbf{R})\right]\chi(\mathbf{R}). \tag{1.3}$$

In general, the validity condition for the adiabatic approximation is, for a set of adiabatic states α and β, $\hbar\dot{\mathbf{R}}\cdot\mathbf{X}_{\alpha\beta}/(\mathcal{E}_\alpha - \mathcal{E}_\beta) \ll 1$. The adiabatic approximation hence breaks down in processes where the derivative coupling between a pair of states become non-negligible compared to the difference of the corresponding adiabatic energies, which typically occurs in the following situations; (1) two or more PESs avoid-cross or come close to each other (2) the nuclear wavepacket velocity (in a semiclassical sense) is large (3) the system is exposed in strong external perturbation. The resultant dynamics, which is referred to as nonadiabatic dynamics, includes multiple PESs and non-trivial correlations (entanglements) between electronic and nuclear states, as is seen in full-size expansion of Eq. (1.2).

---

[1] A practical method of analytical calculation of derivative couplings was established Ref. [22], which was also reviewed in Ref. [89]. For completeness, essential points and related references are also reviewed in Appendix E.

Here we further note that, in many cases in the field-free nonadiabatic dynamics, breakdown of the adiabatic approximation is actually limited in space and time, and the adiabatic condition recovers in the asymptotic region. This is an implicit assumption in 'non-' adiabatic dynamics.

Developments in the theory of nonadiabatic dynamics Study of nonadiabatic dynamics dates back as early as 1932, when Landau [9] and Zener [10] (LZ) independently derived the nonadiabatic transition probability in a linearized two-state model. It was soon followed by more refined treatment by Stueckelberg [11] where he incorporated phase effects arising from the curve-crossing and nuclear propagation between crossings (this is indeed a large step forward from LZ's treatment to incorporate electron-nucleus correlation within one-dimensional model). The one-dimensional linearized curve-crossing problem thus established was further studied until Zhu and Nakamura reached complete solution [12]. These theories are remarkable in that it gives analytical solution, which includes a minimal number of parameters in such a manner that elucidates the essential physics of nonadiabatic transitions [2]. On the other hand, due to the drastic simplification in the model construction, it certainly lacks quantitative accuracy when the results are compared to the experimental observables. These are categorized as 'classic' approaches.

Modern approaches are contrasted with the 'classic' ones by intensive use of *ab initio* calculations, which, within some limitations arise from finite-size numerical computation, faithfully reproduce the true molecular properties such as the potential energy surfaces(PES) and relevant matrix elements. Another important difference is the nuclear degrees of freedom, which has much larger dimensionality and closely correlated to the electronic degrees of freedom. Earlier works include surface hopping [13], classical mapping [14] and mean-field approaches [15, 16]. Besides with refinement of the algorithm, these early version of methods have been revised reflecting the progress in computational technology and the development in the *ab initio* calculation techniques including efficient basis sets [17], refined post Hartree-Fock calculation algorithms [18, 19], efficient analytical gradient methods [20]. Methods that are favorably used in recent studies include the surface hopping [21], modern version of semiclassical Ehrenfest theory (SET) [22], mean-field theory supplemented by "natural

[2] For example, the exponential dependence on the system parameters of LZ formula reflects the fact that the result is obtained by an asymptotic analysis rather than a perturbative analysis. The LZ exponent also has correct limiting behavior both in the diabatic and the adiabatic limit.

decay" algorithm [23], spawning methods [24], branching algorithms [25].

Except for full-quantum approach, however, all these practical computational schemes include a number of approximations and/or even some 'prescriptions', which have little justification except for numerical evidences. Additionally, many of these methods have been designed to work best on field-free chemical reaction problems. In order to apply them to unknown phenomena such as reactions in strong laser field, one has to at least re-examine their validity from the first principle or even reformulate it so as to best-describe the underlying physics [3]. We will thus going to seek for reformulation of nonadiabatic dynamics that is appropriate for our needs in current view of interest.

Current state of the nonadiabatic dynamics In order to further clarify the requirements for a "new" theory, we review the current state of this study field [26]. The scope of nonadiabatic dynamics has much expanded from that in the early days. Dominant roles of nonadiabatic transitions have been found in systems with vanishing level spacings including metal surfaces [27], highly excited atomic/molecular states near continuums [28]. There have also been renewed interests in its role in biological systems, chemical system with electronic transfers [29] or nanoscale devices (in the form of inelastic tunneling) [30, 31]. Reviewing the whole theory is thus far beyond our current scope. We therefore concentrate on our major interest, dynamics in intense laser field and related phenomena.

Developments in the laser technology and nonadiabatic dynamics Dynamics of our interest occurs in timescale shorter than relevant nuclear vibrational periods, which typically range from 10^0 to 10^3fs. Such ultrafast dynamics has become direct observable as the experimental probe realized sub-ps resolution [3]. Sub-ps pulse was achieved in mid 1970's using mode-locked dye lasers [32], which was successively followed by achievements of even shorter pulse of femto-second duration in 1980's. Real-time spectroscopy of nuclear wavepacket dynamics was pioneered by Zewail [3, 33, 34]. In Ref. [33], he established pump-probe technique using the Nd:YAG-pumped pulsed dye amplifier and the molecular beam technique to achieve real-time observation of slow wavepacket oscillation in NaI [33]. Here

[3] Take, for example, the surface hopping algorithm [21] and consider its application to the field-induced dynamics. The effectiveness of the stochastic approach is doubted when it is applied on the problem with successive small bifurcations including their interferences. Moreover, the validity of stochastic hopping is questioned when one is to calculate field-matter interaction including the quantum-mechanical phase. Use of adiabatic basis may be inappropriate in quasiperiodic background.

the vibrational period of the excited state of NaI was around 1 ps whereas the pulse width used for pump and probe was around 100 fs. The experiment has been a landmark in the study of nonadiabatic dynamics in that it realized the first experimental observation of the curve-crossing dynamics, which was the starting point in the theory of nonadiabatic dynamics. Many theoretical calculations followed to reproduce the experimental results [35], to predict details of outcomes such as angle-resolved dissociation probabilities [36]. Moreover, it has been one of the strongest motivation for the development in advanced calculation schemes [21, 22, 24].

Another important impact of the laser technology on atomic/molecular physics came from its large field amplitude that is comparable to the intrinsic nuclear Coulomb field, which lead to a variety of multiphoton effects. Multiphoton effects, which will be discussed in more detail in PartII, are first studied in the field of atomic physics. As the development of high-power laser achieved intensity of 'non-perturbative regime', which is typically $\gtrsim 10^{14}$ W/cm^2, there have been observed a number of multiphoton effects, including the above threshold ionization (ATI) [37] and High-harmonic generation [38, 39]. It is also to be noted that in those early days of the research, there have been important progress in the theory of multiphoton ionization starting from Keldysh's work [40–44]. From late 1980's, study of high-field phenomena has diverged to include molecules, where there have been found molecular analog of ATI [45] and HHG [5, 46, 47]. Moreover, it has been found that the additional nuclear degrees of freedom provides richer variety of physics including enhanced ionization [48, 49], orientation effects [50], dissociation dynamics with bond softening [51–53]/hardening [54, 55], Coulomb explosions [56–58]. These molecular multiphoton phenomena are characterized by field-electron coupled states and nuclear dynamics driven by thus created unconventional electronic states.

These effects clearly indicate the capacity of intense laser field of (a) inducing a high-energy electronic response, HHG, which serves a time-resolved probe of dynamical electronic states (b) inducing electronic dynamics that alters chemical bonds. Below we discuss these two intriguing phenomena.

a. Probing the electronic dynamics through HHG

In order for a direct observation of time-dependent changes in the electronic state, one needs resolution of 10^0fs or even shorter[4] . Generation of pulses with sub-femto duration, which is

[4] here we assume a typical value of level spacing is 10^{-1} eV or larger, which correspond to 40fs in the

shorter than a typical optical period of visible light ($\lambda = 780$nm field of Ti:Sapphire laser has $T \approx 2.6$fs), requires some sub-cycle mechanisms. High harmonic generation (HHG), whose emission is restricted in a limited range of the (pumping) laser cycle [59, 60], is a source of such short pulse. Isolated attosecond pulses are generated by restricting effective pumpings to a single (or less) optical cycle. There have been developed several techniques to achieve this to successfully generate pulses of duration 10^2as [61] or less. However, due to the low intensity of thus genrated pulse, attosecond pump-probe experiments have not been fully established yet.

Another use of HHG is to directly extract electronic state informations on the source molecules; its intensity profile (harmonic order dependence of intensity) and the recombination phase reflects the channel-dependent ionization potentials whereas the angular distribution reflects the distribution of the Dyson orbital in the source molecules. These points are reviewed in Appendix A. Experimental measurement of these quantities was demonstrated in Ref. [62] where they identified contributions from multiple ionization channels in the HHG from a CO_2 molecule. Reference [63] monitors the progress of a dissociation process in a Br_2 molecule by observing the time-dependent interference pattern of HHG to probe the internuclear distance dependent ionization potential. The advantages of HHG as a probe of electronic state includes attosecond time-resolution, nanometer spatial resolution[5], direct relation to the electronic (Dyson) orbitals which includes potentially rich information such as angular distribution. On the other hand, these experiments require a number of advanced experimental techniques including phase measurement, and also theoretical calculations for interpretation. The fact leaves possibility of wrong or biased interpretation, whereas, taken optimistically, there are also possibility that advanced theoretical analysis may extract more detailed information from these measurements.

b. Reaction engineering

The capacity of the high-intensity (typically $\gtrsim 10^{13}$W/cm^2), short pulse($\sim 10^2$fs) field[6] on changing chemical reaction has stimulated the study of reaction engineering [64–66]. Up to date the most successful reaction control theory is the variational optimization theory proposed by Rabitz and coworkers [66]. Their theory is distinguished from others in that they

oscillation period, and required the pulse duration to be an order or more shorter

[5] 20 th harmonic of a typical Ti:Sapphire laser has period 0.13 fs, wavelength 39 nm, whereas the de Brogile wavelength of the corresponding colliding electron is around 4 Bohr.

[6] the shortness of pulse, equal to or shorter than relevant nuclear vibration periods is again important to produce some transient states like trapped state on an light-induced PES

also propose a learning algorithm [67] to experimentally realize the optimization. Experimental realization of their theory has achieved branching ratio control of field-dissociation of inorganic/organic molecules [68–70] and induction of a rearrangement reaction (reaction to yield $C_6H_5CH_3$ from $C_6H_5COCH_3$). Laser pulses used in these studies are Ti:Sapphire laser pulses of $\lambda \approx 800$nm, intensity around 10^{13} to 10^{14} W/cm^2, pulse duration 60 to 100 fs with optimized substructures.

These experiments are remarkable in that they actually demonstrated the reaction control, which otherwise had been highly hypothetical. Their current success partly owes to independence on numerical calculations, which can be limited in accuracy. Instead, pulse shapes are 'automatically' optimized using the feedback mechanism. On the other hand, lack of theoretical reasoning leaves us a doubt in the "quality" of optimization in larger parameter space; there is little reason to believe the obtained pulse shape is still close to optimal if the available parameter ranges were expanded, or more qualitatively different options, such as the second laser field, were added. There need theoretical estimates for designing these experimental settings before detailed optimization process. Establishing a method of such estimate is one of the strongest motivation for this study.

Apart from Rabitz's scheme, we also note on the work of Stolow [71], where he proposed and demonstrated much simpler way of reaction control. His proposal, the dynamical Stark control (DSC), controlles the shape of PESs and the velocity of the nuclear wavepacket at the nonadiabatic crossing point to control the branching ratio. His theory was demonstrated in field-dissociation experiment of IBr, which has two dissociation channels that couples by spin-orbit (as well as the nonadiabatic) coupling but not by the direct dipole coupling. Application of 'control pulse' achieved branching ratio control over several factors.

His study was carefully arranged so as to exclude direct contribution of dipole coupling. The success of this control therefore suggest the importance of kinematic nonadiabatic coupling in field-induced dissociation problems. However, it is more natural to consider that the kinematic nonadiabatic coupling, which is undoubtedly key factor in field-free nonadiabatic dynamics, may be of *fundamental* importance, even in dipole-coupled problems. We will later consider fully nonadiabatic theory of laser-induced dynamics that incorporates field-induced (dipole) transitions, nonadiabatic transition induced by nuclear motion, and nonadiabatic transitions (among Floquet state) due to the change of laser parameters.

More recent attempts

Before concluding, we also note on more recent works on reaction engineering that uses

carrier-envelope phase controlled few-cycle pulses. The mechanism of these experiments are, according Ref. [72], high-energy electronic processes including recollisions and subsequent double-ionizations. Although being intriguing as new methodology for reaction engineering, we do not discuss them further as it is beyond our current scope. This work concentrates longer timescale dynamics that extends over several cycles or more.

Scope and organization of this work From above observations on the new trends in the study of nonadiabatic electron-nucleus coupled dynamics, we saw following requirements for new theoretical approach.

(i) Accurate reproduction of quantum-mechanical electron (or electron-field coupled) dynamics : In the new types of dynamics including field-induced ones, unconventional dynamical electronic states play key roles. Quantum-mechanically accurate description of electron dynamics, free of empirical prescriptions, is therefore indispensable for analysis.

(ii) Appropriate description of nuclear dynamics that couples to the electronic dynamics : Nuclear dynamics should correctly reflect the above-calculated electronic state. It should also correctly reproduce possible bifurcations in the electronic state.

(iii) Applicability to a certain variety of molecules : In order to deduce chemically meaningful results, its applicability should not be limited to the simplest molecules, but should include diatomics with different types of bond properties (ionic or covalent) and those with higher degrees of freedom; triatomics or more.

(iv) Clear description of the underlying physics : It should provide clear insights into the underlying physics that was not obtained in other approaches.

We hence start from reconstruction (re-derivation starting from exact quantum-mechanical theory) of the mixed quantum-classical (MQC) formulation of nonadiabatic dynamical theory. We then discuss several key problems arising from quantum-classical conflict including wavepacket bifurcation. In doing so, we also seek for a practical implementation or numerical computation method of such theory. We next apply it to the field-induced dynamics, and develop a Floquet-based analysis that would provide accurate as well as conceptually clear description of the phenomena. We also show some numerical results in order to show accuracy of the theory in simple problems where accurate results are available through quantum wavepacket method. Application of thus established theory to larger size molecules (with different implementation) is also discussed but much is left for future work.

This work consists of two parts. We work on the reconstructing the mixed quantum

classical formulation in Part I and its application to the laser-induced dissociation problem in Part II. Each part is self-contained with brief introduction and concluding remarks.

APPENDIX A: DERIVATION OF RELEVAMT QUANTITIES FOR INTERPRETATION OF HHG EXPERIMENTS

Representation of (1;N-1) system We first neglect double or more ionizations. Then all N particle electronic states can be expanded using $N-1$ particle bound state as

$$|\Psi_t\rangle = \sum_a |[f_t^{(a)}, \Phi_a]\rangle \tag{A.1}$$

where Φ_a represents $N-1$ particle electronic bound state (ionic state), $|[\cdot,\cdot]\rangle$ represents antisymmetrized electronic state, whereas $f_t^{(a)}$ represents single particle states subject to normalization $\sum_a \|f_t\|^2 = 1$, the associated single particle wavefunctions are denoted as $f_t(\mathbf{r})$ and are subject to $\sum_a \int d^3\mathbf{r}|f_t(\mathbf{r})|^2 = 1$. In order for the expansion to be unique, we first define a set of bound-state orbitals $\mathcal{B} = \{\phi_k\}_{k=1,...,L}$ with their associated annihilation operators $\{\hat{c}_k\}_{k=1,...,L}$ and assume that the $N-1$ particle bound states can be expanded by the Slater determinants $\{S_a\}$, $|S_a\rangle \equiv \hat{c}^\dagger_{a_{N-1}}...\hat{c}^\dagger_{a_1}|0\rangle$ where $a_1,...,a_{N-1}$ is aligned in increasing order. Any N particle state that consist of $N-1$ those orbitals and one more (not necessarily bound) orbital is then uniquely identified in the form of Eq. (A.1) by choosing the first component, $f_t^{(a)}$ to be either orthogonal to all $\mathcal{B}$ or those with the largest index (i.e. HOMO).

Single-particle reduced Schrödinger Equation The Schrödinger equation

$$i\hbar\partial_t|\Psi_t\rangle = H|\Psi_t\rangle \tag{A.2}$$

is then converted into an effective single-particle equation by applying $\langle^P\Phi_b|\hat{\psi}(\mathbf{r})$ from the left, where $\hat{\psi}(\mathbf{r})$ is the electronic annihilation operator and $\langle^P\Phi_b|$ is a $N-1$ particle state obtained from the Slater determinant expansion of state $\langle\Phi_b| = \sum_k \langle S_k|C_b^k$, by replacing each S_k by $\langle^P S_k| \equiv \langle 0|\left[\prod_{j=1}^{k_{N-1}}(1-n_j)\right]\hat{c}_{k_1}\hat{c}_{k_2}...\hat{c}_{k_{N-1}}$. We then have

$$i\hbar\partial_t f_t^{(b)}(\mathbf{r}) = \langle\langle^P\Phi_b|\hat{\psi}(\mathbf{r})H\sum_a |||[f_t^{(a)}, \Phi_a]\rangle. \tag{A.3}$$

In order to obtain intuitive understanding, we show its orbital expansion assuming that each state consist of a single Slater determinant: $\Phi_b \approx S_b$.

$$i\hbar\partial_t f_t^{(b)}(\mathbf{r}) = \left(\mathcal{E}_b^{N-1} + \hat{h} + W_{HF}^{bb}(\mathbf{r})\right) f_t^{(b)}(\mathbf{r}) + (1-\delta_{b,a})\langle S_b|\hat{h}|S_a\rangle f^{(a)}(\mathbf{r}) + \sum_k \hat{h}\phi_{a_k}\langle S_b|[f^{(a)}, S_a^{\backslash a_k}]\rangle + \sum_k \langle S_b|\hat{h}|[f^{(a)}, S_a^{\backslash a_k}]\rangle\phi_{a_k}(\mathbf{r}) + R^{ab} \tag{A.4}$$

where $\hat{h}$ is the single-electron term in the electronic Hamiltonian; $\hat{h} = \frac{-\hbar^2}{2m}\Delta - \boldsymbol{\mu}\cdot\mathbf{E} + U(\mathbf{r})$ with $U(\mathbf{r})$ being the nuclear Coulomb potential, $\mathcal{E}_b^{N-1} = \langle S_b|H|S_b\rangle$ is the ionic energy, $W_{HF}^{bb}(\mathbf{r})$ is the Hartree-Fock potential of the ionic state b and the rest of off-diagonal electronic repulsion terms are represented as R^{ab}. Each term in Eq. (A.4) hence has the following meaning; The second term represents ionic excitation.

The third term represents the exchange contribution of single-particle operator $\hat{h}$, which becomes large if (f^a is ond of the bound state orbital and) $|[f^{(a)}, S_a^{\backslash a_k}]\rangle$ equals $|S_b\rangle$, which is important for the ionization of inner orbital a_k.

The fourth term also represents the exchange contribution, which becomes large if $S_a^{\backslash a_k}$ equals $N-2$ of S_b, important for recombination of f to inner orbital.

Tunneling problem We next restrict Eq. (A.3) to single channel and derive tunneling solution. The effective single-particle equation is rewritten as

$$i\hbar\partial_t f_t^{(b)}(\mathbf{r}) = \left[\mathcal{E}_b^{N-1} + \hat{h} + W_{HF}^{bb}(\mathbf{r})\right] f_t^{(b)}(\mathbf{r}) \tag{A.5}$$

The tunneling amplitude to a final state outside the potential barrier with momentum $\hbar\mathbf{k}$ is derived, using the first order perturbation expansion of path-integral,

$$f_t^{(b)}(\mathbf{p}) = \int d^3\mathbf{r} e^{-i\mathbf{k}\cdot\mathbf{r}} \frac{1}{i\hbar}\int dt' \int d^3\mathbf{r}' \exp[\frac{i}{\hbar}S^{(0)}(\mathbf{r},t;\mathbf{r}',t')]V(\mathbf{r}',t')u^{(b)}(\mathbf{r}',t') \tag{A.6}$$

where we take the starting point $\mathbf{r}'$ inside deep in the barrier where the atomic potential is negligible compared to the field. Within the weak field approximation, $u^{(b)}(\mathbf{r},t') \approx u^{(b)}(\mathbf{r})e^{-i\varepsilon t'/\hbar}$ where $u^{(b)}(\mathbf{r})$ constitutes a bound state and ε is the minus of ionization potential in this channel. Here we take the radiation gauge; $\hat{h} = \frac{1}{2m}\left(\hat{\mathbf{p}} - \frac{q}{c}\mathbf{A}\right)^2$, and the zeroth order propagator $\exp\left[\frac{i}{\hbar}S^{(0)}(\mathbf{r},t;\mathbf{r}',t')\right]$ is expanded as $\int d\mathbf{p} e^{i\mathbf{p}\cdot(\mathbf{r}-\mathbf{r}')}e^{-\frac{i}{\hbar}\int_{t'}^{t} d\tau \frac{1}{2m}\left(\mathbf{p}-\frac{q}{c}\mathbf{A}_\tau\right)^2}$. The stationary phase condition $\mathbf{r}$ gives $\mathbf{p} = \hbar\mathbf{k}$, while that for t' gives

$$\frac{1}{2m}\left(\mathbf{p} - \frac{q}{c}\mathbf{A}_{t'}\right)^2 = \varepsilon \tag{A.7}$$

which fixes the starting time $t' = \frac{i}{\omega}\,\mathrm{arcsinh}(\gamma - i\eta)$ where $\gamma \equiv \sqrt{2m|\varepsilon|}\frac{c}{q|\mathbf{A}|}$ and $\eta \equiv \hbar k_z/(qA/c)$, which is assumed to be small $\eta \ll 1$. The exponential damping factor is given as $\frac{-1}{\hbar\omega}\left[\left(\frac{1}{2m}\mathbf{p}_\perp^2 + |\varepsilon| + U_p\right)\mathrm{arcsinh}(\gamma) - U_p\gamma\sqrt{1+\gamma} + U_p\eta\omega/\sqrt{1+\gamma^2}\right]$. which gives exponential dependence on the channel-dependent ionization potential $|\varepsilon| = I_p^{(b)}$.

Recollision and recombination phase We temporarily neglect inter-channel terms and rewrite the Schrödinger equation as

$$i\hbar\dot{f}_t^{(b)} = \left[\mathcal{E}_b^{N-1} + \hat{h}\right] f_t^{(b)} \tag{A.8}$$

expanding the single electron wavefunction as

$$\int d^3\boldsymbol{\pi}(\mathbf{r}|\boldsymbol{\pi})a_{\boldsymbol{\pi}} + \sum_i (\mathbf{r}|b_i)c_i \tag{A.9}$$

where $\boldsymbol{\pi}$ is meant to represent 'kinetic momentum' in the dipole gauge, ket $|\boldsymbol{\pi})$ represents the momentum eigenstate ($(\mathbf{r}|\boldsymbol{\pi}) \equiv \frac{1}{\sqrt{2\pi}^3}e^{i\boldsymbol{\pi}\cdot\mathbf{r}/\hbar}$), whereas $|b_i)$ is the ith bound state, and $\{a_{\boldsymbol{\pi}}\}$, $\{c_i\}$ are the continuum state and the bound-state expansion coefficients, respectively. The Fourier transformation of single particle Schrödinger equation becomes

$$i\hbar\dot{a}_{\boldsymbol{\pi}} = \left[\mathcal{E}_b^{N-1} + \frac{1}{2m}\boldsymbol{\pi}^2 - i\hbar q_e\mathbf{F}\cdot\frac{\partial}{\partial\boldsymbol{\pi}}\right]a_{\boldsymbol{\pi}} - \sum_i (\boldsymbol{\pi}|\boldsymbol{\mu}|b_i)\cdot\mathbf{F}_t c_i \tag{A.10}$$

$$i\hbar\dot{c}_i = \left[\left(\mathcal{E}_b^{N-1} + \varepsilon_i\right)\delta_{ij} - \boldsymbol{\mu}_{ij}\cdot\mathbf{F}_t\right]c_j - \int d^3\boldsymbol{\pi}'(i|\boldsymbol{\mu}|\boldsymbol{\pi}')a_{\boldsymbol{\pi}'}\cdot\mathbf{F}_t \tag{A.11}$$

If the ground state depletion is negligible, we can assume the ground state coefficient to be unity $c_i(0) = \delta_{i0}$ at time $t = 0$ and use the first order perturbative expansion to obtain

$$a_{\boldsymbol{\pi}}(t) = \int_0^t dt' \frac{-(\boldsymbol{\pi}_{t'}|\boldsymbol{\mu}|b_0)\cdot\mathbf{F}_{t'}}{i\hbar}\exp\left[-\frac{i}{\hbar}\int_{t'}^t d\tau\left\{\left(\mathbf{p} - \frac{q}{c}\mathbf{A}_\tau\right)^2/2m\right\}\right]\exp[-\frac{i}{\hbar}\varepsilon_0 t'] \tag{A.12}$$

where $\mathbf{p} = \boldsymbol{\pi}_t + \frac{q}{c}\mathbf{A}_t$ is the canonical momentum. The recombination matrix element is thus obtained as

$$\begin{aligned}\bar{\boldsymbol{\mu}}_t = \int \frac{d^3\mathbf{p}}{(2\pi)^3}\int_0^t dt'(b_0|\boldsymbol{\mu}|\mathbf{p} - \frac{q}{c}\mathbf{A}_t)\exp\left[-\frac{i}{\hbar}\int_{t'}^t d\tau\left\{\left(\mathbf{p} - \frac{q}{c}\mathbf{A}_\tau\right)^2/2m - \varepsilon_0\right\}\right] \\ \times\frac{1}{i\hbar}(\mathbf{p} - \frac{q}{c}\mathbf{A}_{t'}| - \boldsymbol{\mu}|b_0)\cdot\mathbf{F}_{t'}.\end{aligned} \tag{A.13}$$

here the single-particle energy ε_0 is to be understood as the minus of the ionization potential $I_p^{(b)}$ of channel b. The stationary phase approximation on $\mathbf{p}$ gives $\int_{t'}^t d\tau\left(\mathbf{p} - \frac{q}{c}\mathbf{A}_\tau\right)/m = 0$, which means that the classical returning at time t. Taking account of the fact $(\mathbf{p} - \frac{q}{c}\mathbf{A}_{t'}| - \boldsymbol{\mu}|b_0)$ takes nonzero value at $\mathbf{p} - \frac{q}{c}\mathbf{A}_{t'} = 0$, the classical returning condition is to be solved

with the initial condition $\mathbf{p} - \frac{q}{c}\mathbf{A}_{t'} = 0$ to give recombination time $t_r(t')$. The recombination phase in this approximation $-\frac{i}{\hbar}\int_{t'}^{t} d\tau \left\{ \left(\mathbf{p} - \frac{q}{c}\mathbf{A}_\tau\right)^2 / 2m + I_p^{(b)} \right\}$ depends on the ionization potential as $I_p^{(b)}(t_r(t') - t')$.

Part I

Mixed quantum classical representation of electron-nucleus coupled nonadiabatic dynamics

1. INTRODUCTION

In Part I, we reformulate electron-nucleus coupled nonadiabatic dynamics with special emphasis on the mixed quantum-classical representation. The mixed quantum-classical (MQC) approximation refers to the approximation of quantum dynamics where the fast (electronic) dynamical variables are treated in the quantum mechanical manner while the slow (nuclear) ones are treated in a trajectory-type approximation. The most remarkable virtue of this approximation is its low computational cost. Rough estimate of required memory gives, $\left[\prod_{j=1}^{f} L_j\right] \times N_{\mathcal{H}}$ for the full quantum (FQ) calculations, $f^{\alpha} + N_{\mathcal{H}}$ for a 'typical' semiclassical (SC) calculations and $f + N_{\mathcal{H}}$ for the MQC approximation, where f, $N_{\mathcal{H}}$ and L_j denotes the number of independent nuclear degrees of freedom, the electronic Hilbert space dimension, and the number of spatial grid in the jth spatial direction, whereas α denotes a methodology-dependent exponent [7] It also follows from the point-like treatment that one does not need the knowledge of global potential energy surface (PES) and the electronic matrix elements in advance of the calculation; one can instead perform on-the-fly calculations at each timeslice during the calculation. Such drastic reduction of computational cost makes it a virtually indispensable technique for calculations of large molecular systems.

On the other hand, there are a number of difficulties arising from the contradicting nature of quantum and classical mechanics. The most obvious ones being the absence of purely quantum mechanical effects such as tunneling and interference effects, which we consider as unavoidable and will not discuss further. There still remains a number of controversial points in its implementation which severely affects the outcomes. Among all, we concentrate our discussions on the following two difficulties.

[7] Multiplication factors are ignored. In fact classical and semiclassical calculations often require a large number of sampling over initial conditions. Possible wavepacket branching would also increase the cost by a multiplication factor

(1) Derivation of an effective nuclear dynamics in the presence of multiple interacting PESs : If one introduces the adiabatic approximation, there remains only a single PES, and the problem is trivially resolved ; the effective nuclear dynamics should be the Newtonian dynamics driven by the gradient of PES.

The problem is no longer trivial in the presence of multiple adiabatic states; the Semiclassical Ehrenfest theory (SET) derives an effective force as the electronic wavepacket average of the Helmann-Feynmann force, $\mathbf{F} = \langle\psi_t| - \nabla H^{ele}|\psi_t\rangle$ (hereafter referred to as the "state-averaged force", whereas the surface hopping algorithms use the gradient force of a single PES but introduces stochastic hopping across multiple PESs.

In a typical scattering or reaction problem, the state-average approach becomes clearly unphysical when the system evolves into the asymptotic region. The hopping approach, on the other hand, has to introduce effective stochastic transitions that apparently contradicts the quantum-mechanical principle. It also has to introduce discontinuous change of momentum at each hop so as to conserve energy of the whole state. There are also variants of SET where correlation between the different asymptotic states are forced to diminish at the end [23, 73, 74], however, there need some artificial "decoherence" terms which are absent in the original Hamiltonian. For later convenience, those include "decoherence" terms are hereafter referred to as natural decay of mixing (NDM) approaches, although there are several versions of this type of approaches.

(2) Classical representation of quantum-mechanical wavepacket bifurcations: As for this problem, SET gives no answer as it keeps single nuclear trajectory, whereas surface hop and NDM gives an effective representation within their own algorithm. Neither of them, however, deal with quantum mechanical bifurcation of nuclear wavepackets; the surface hop converts the problem to a semiclassical stochastic one which somewhat gives a reasonable solution to the original problem through ensemble average, whereas NDM introduces an artificial term of 'decoherence', which does not exist in the original Hamiltonian, and eliminate 'undesired' components.

These difficulties are also characteristic to nonadiabatic dynamics as it does not arise in the adiabatic dynamics. In order to discuss them on the firm ground, we reformulate the MQC representation of electron-nucleus coupled dynamics from the first principle quantum mechanical path integral.

2. FORMULATION

Notation: In Part I, we consider an electron-nucleus coupled system with N_n nuclei and N_e electrons. The mass, coordinate, and charge of the jth nucleus is denoted as M_j, $\mathbf{R}^j$ and Q_j, respectively. Each component of $\mathbf{R}^j$ is denoted as $R^{(j,a)}$ where a denotes either of three dimensional component, $a \in \{x, y, z\}$. We also use Greek indices to represent combined indices in the sense $\mu = (j, a)$. The electronic state is expanded in $\mathbf{R}$-dependent N_e body electronic basis set $\{|\phi_a : \mathbf{R}\rangle\}$ which satisfies the orthonormal condition $\langle\phi_a : \mathbf{R}|\phi_b : \mathbf{R}\rangle = \delta_{ab}$.

2-1. Formulation of MQC path integral

A path integral formulation of coupled slow and fast dynamical variables was established by Pechukas[75]. One of the greatest feature of his formalism is that a classical-like equation of motion can be derived in a systematic manner from the exact quantum-mechanical description. The resultant equation of motion is NOT an Ehrenfest-type dynamics driven by some expectation value of the quantum system, but reflects quantum mechanical entanglement, which is just what we are interested in. On the other hand, Pechukas did not give an explicit expression of the electronic path integral, whereas we need an electronic equation of motion including the nonadiabatic coupling terms. We resolve this problem using the coherent state representation [76, 77]. Another missing point in this formulation is that he did not show higher order expansion over the stationary phase approximation (SPA). The point will be discussed separately in Sec. 6.

i. Integration by step

We consider the transition amplitude of the system from a state $\{\mathbf{R}_i, \xi_i(\mathbf{R}_i)\}$ at time t_i to a state $\{\mathbf{R}_f, \xi_f(\mathbf{R}_f)\}$ at time t_f. We discretize the time interval t_i to t_f into N equally spaced time slices. Each time interval is $\epsilon = \frac{t_f - t_i}{N}$, $N + 1$ time points are denoted as $\{t_n\}$, with $t_n = t_i + \epsilon n$. The nuclear coordinate at each time point t_n is denoted as $\mathbf{R}_n$, which satisfies, on either of the boundaries, $\mathbf{R}_0 = \mathbf{R}_i$ and $\mathbf{R}_N = \mathbf{R}_f$, respectively. The propagator

for the total system is represented, up to the first order in ϵ, as

$$\begin{aligned}
&\mathcal{K}(\mathbf{R}_f, \xi_f(\mathbf{R}_f), t_f; \mathbf{R}_i, \xi_i(\mathbf{R}_i), t_i) \\
&= \int d\,\mathbf{R}_{N-1} d\,\mathbf{R}_{N-2} \cdots d\,\mathbf{R}_1 \sum_{a_N} \sum_{a_{N-1}} \cdots \sum_{a_1} \sum_{a_0} \langle \xi_f : \mathbf{R}_f | \phi_{a_N} : \mathbf{R}_N \rangle \\
&\times \prod_{j=0}^{N-1} \left\langle \mathbf{R}_{j+1} \middle| \langle \phi_{a_{j+1}} : \mathbf{R}_{j+1} | e^{-\frac{i}{\hbar}\epsilon \mathcal{H}} | \phi_{a_j} : \mathbf{R}_j \rangle \middle| \mathbf{R}_j \right\rangle \langle \phi_{a_0} : \mathbf{R}_0 | \xi_i : \mathbf{R}_i \rangle. \qquad (2.1)
\end{aligned}$$

This expression is equivalent in the sense of the path integration to

$$\begin{aligned}
&\mathcal{K}(\mathbf{R}_f, \xi_f(\mathbf{R}_f), t_f; \mathbf{R}_i, \xi_i(\mathbf{R}_i), t_i) \\
&= \int d\,\mathbf{R}_{N-1} \cdots d\,\mathbf{R}_1 \sum_{a_N} \sum_{a_{N-1}} \cdots \sum_{a_1} \sum_{a_0} \langle \xi_f : \mathbf{R}_f | \phi_{a_N} : \mathbf{R}_N \rangle \langle \phi_{a_0} : \mathbf{R}_0 | \xi_i : \mathbf{R}_i \rangle \\
&\times \prod_{n=0}^{N-1} \left(\exp \left[\frac{i}{\hbar} \left(\sum_j \frac{M_j (\mathbf{R}_{n+1}^j - \mathbf{R}_n^j)^2}{2\epsilon} - U_{nuc}(\mathbf{R}_n)\epsilon \right) \right] \langle \phi_{a_{n+1}} : \mathbf{R}_{n+1} | e^{-\frac{i}{\hbar}\epsilon \mathcal{H}^{el}(\mathbf{R}_n)} | \phi_{a_n} : \mathbf{R}_n \rangle \right), \qquad (2.2)
\end{aligned}$$

which is further rewritten as

$$\begin{aligned}
&\mathcal{K}(\mathbf{R}_f, \xi_f(\mathbf{R}_f), t_f; \mathbf{R}_i, \xi_i(\mathbf{R}_i), t_i) \\
&= \int \prod_{n=1}^{N-1} d\mathbf{R}_n \exp \left[\frac{i}{\hbar} S_{nuc}(\{\mathbf{R}\}) + \frac{i}{\hbar} S_{eff}(\{\mathbf{R}\} : \xi_f(\mathbf{R}_f), t_f; \xi_i(\mathbf{R}_i), t_i) \right], \qquad (2.3)
\end{aligned}$$

where the nuclear coordinate integrals $\int d\,\mathbf{R}_{N-1} d\,\mathbf{R}_{N-2} \cdots d\,\mathbf{R}_1$ is to be performed with an appropriate normalization factor in what follows. Details of the Trotter decomposition in Eq. (2.1) is summarized in Appendix A. The nuclear action $S_{nuc}(\{\mathbf{R}\})$ in Eq. (2.3) is defined as

$$S_{nuc}(\{\mathbf{R}\}) = \sum_n \left(\sum_j \frac{M_j (\mathbf{R}_{n+1}^j - \mathbf{R}_n^j)^2}{2\epsilon} - U_{nuc}(\mathbf{R}_n)\epsilon \right). \qquad (2.4)$$

The effective action $S_{eff}(\{\mathbf{R}\} : \xi_f(\mathbf{R}_f), t_f; \xi_i(\mathbf{R}_i), t_i)$ arising from the electronic part is defined as

$$S_{eff}(\{\mathbf{R}\} : \xi_f(\mathbf{R}_f), t_f; \xi_i(\mathbf{R}_i), t_i) = \frac{\hbar}{i} \ln \mathcal{K}^{el}(\{\mathbf{R}\} : \xi_f(\mathbf{R}_f), t_f; \xi_i(\mathbf{R}_i), t_i), \qquad (2.5)$$

where the electronic propagator $\mathcal{K}^{el}$ is defined as

$$\begin{aligned}
\mathcal{K}^{el}(\{\mathbf{R}\} : \xi_f(\mathbf{R}_f), t_f; \xi_i(\mathbf{R}_i), t_i) &= \sum_{a_N} \sum_{a_{N-1}} \cdots \sum_{a_1} \sum_{a_0} \langle \xi_f : \mathbf{R}_f | \phi_{a_N} : \mathbf{R}_N \rangle \\
&\times \left[\prod_{n=0}^{N-1} \langle \phi_{a_{n+1}} : \mathbf{R}_{n+1} | e^{-\frac{i}{\hbar}\epsilon \mathcal{H}^{el}(\mathbf{R}_n)} | \phi_{a_n} : \mathbf{R}_n \rangle \right] \langle \phi_{a_0} : \mathbf{R}_0 | \xi_i : \mathbf{R}_i \rangle. \qquad (2.6)
\end{aligned}$$

In the next step, rather than directly evaluating the path integral itself, we derive the equation of motion of the most probable path using the stationary phase approximation. In this course, we will further have to write down the path integral in an appropriate manner for our purpose. This is because the result of such stationary phase approximation does depend on the representation, even though the exact result would be independent of representation.

ii. The electronic path integral

The electronic path integral is expanded in the Hilbert space of electronic many-body states dependent on the nuclear configuration. This choice of representation, which is never an only choice[78], matches the (configuration interaction (CI) theory of) current *ab initio* electronic state calculation, and crucial for deriving an electronic time evolution which is exact within this calculation. We first consider general properties of the path-integral expanded on the nuclear-configuration dependent basis, then we introduce the coherent state expansion in order to write down the action in the coefficient space.

Evaluation of overlaps

We expand Eq. (2.6) up to the first order in time interval ϵ. Since it includes the electronic matrix elements between the state vectors of two different nuclear configurations $\mathbf{R}$, the overlap products, expanded up to the second order in nuclear coordinate difference $\mathbf{R}_{n+1}-\mathbf{R}_n$, becomes

$$\begin{aligned}\langle \phi_a : \mathbf{R}_{n+1} | \phi_b : \mathbf{R}_n \rangle = \delta_{a,b} &- \sum_{\mu} (R^{\mu}_{n+1} - R^{\mu}_{n}) X^{\mu}_{ab}(\mathbf{R}_{n+1/2}) \\ &+ \frac{1}{2} \sum_{\mu,\nu} (R^{\mu}_{n+1} - R^{\mu}_{n})(R^{\nu}_{n+1} - R^{\nu}_{n}) \mathcal{Y}^{\mu,\nu}_{ab}(\mathbf{R}_{n+1/2}). \end{aligned} \tag{2.7}$$

Here we have introduced the first and the second order derivative coupling matrices X^{μ} and $\mathcal{Y}^{\mu,\nu}$, whose matrix elements are defined as

$$X^{\mu}_{ab}(\mathbf{R}) = \left\langle \phi_a : \mathbf{R} \middle| \frac{\partial \phi_b}{\partial R^{\mu}} : \mathbf{R} \right\rangle, \tag{2.8}$$

and

$$\begin{aligned}\mathcal{Y}^{\mu,\nu}(\mathbf{R}) = \frac{1}{4} \Bigg(&\left\langle \frac{\partial^2 \phi_a}{\partial R^{\mu} \partial R^{\nu}} : \mathbf{R} \middle| \phi_b : \mathbf{R} \right\rangle - \left\langle \frac{\partial \phi_a}{\partial R^{\mu}} : \mathbf{R} \middle| \frac{\partial \phi_b}{\partial R^{\nu}} : \mathbf{R} \right\rangle \\ &- \left\langle \frac{\partial \phi_a}{\partial R^{\nu}} : \mathbf{R} \middle| \frac{\partial \phi_b}{\partial R^{\mu}} : \mathbf{R} \right\rangle + \left\langle \phi_a : \mathbf{R} \middle| \frac{\partial^2 \phi_b}{\partial R^{\mu} \partial R^{\nu}} : \mathbf{R} \right\rangle \Bigg). \end{aligned} \tag{2.9}$$

We have also introduced the notation $\mathbf{R}_{n+1/2}$ in Eq. (2.7), which denotes the middle point of $\mathbf{R}_n$ and $\mathbf{R}_{n+1}$, that is, $\mathbf{R}_{n+1/2} = \dfrac{\mathbf{R}_n + \mathbf{R}_{n+1}}{2}$. Nuclear coordinate derivatives that arise from

overlaps of electronic brakets belonging to different nuclear coordinates, $\mathbf{R}_{n+1}$ and $\mathbf{R}_n$, are to be evaluated at the 'mid-point' $\mathbf{R}_{n+1/2}$. This rule is widely referred to as 'mid-point rule' [79], and we adopt it in what follows unless otherwise noted. For notational convenience, we also use three-component (x, y, z) vector notation for X, $\mathbf{X}_{ab}(\mathbf{R}) = \langle\phi_a : \mathbf{R}|\nabla^j|\phi_b : \mathbf{R}\rangle$, and three-component summed-up form of $\mathcal{Y}$, defined as $\mathcal{Y}^j(\mathbf{R}) = \sum_{a=x,y,z}\mathcal{Y}^{(j,a),(j,a)}(\mathbf{R})$. Symbols with a hat denote the 'operator forms' of the corresponding quantities in the manner $\hat{\mathcal{O}}(\mathbf{R}) = \sum_{a,b}|\phi_a : \mathbf{R}\rangle\mathcal{O}_{ab}(\mathbf{R})\langle\phi_b : \mathbf{R}|$, where $\mathcal{O}$ is either $\mathcal{Y}^{\mu,\nu}$, X^μ, or $\mathcal{Y}^j$. Derivation of Eq. (2.9) is given in Appendix B.

We then make several assumptions on nuclear paths so that we can identify the terms that contribute to the first order in ϵ. (i) In discretized representation of paths $\{\mathbf{R}\}$, $|\mathbf{R}_{n+1} - \mathbf{R}_n|$ is an $O(\epsilon)$ quantity, and $|\mathbf{R}_{n+1} + \mathbf{R}_{n-1} - 2\mathbf{R}_n|$ is an $O(\epsilon^2)$ quantity. (ii) Each point $\mathbf{R}_n$ in discretized paths is to be integrated with an appropriate Gaussian kernel. We assume, up to the first order in ϵ, that

$$\int d\,\mathbf{R}_{N-1}\cdots d\,\mathbf{R}_1 e^{\frac{i}{\hbar}S_{nuc}}(R_{n+1}^{(j,a)} - R_n^{(j,a)})(R_{n+1}^{(k,b)} - R_n^{(k,b)}) = \delta_{j,k}\delta_{a,b}\frac{i\hbar\epsilon}{M_j} \quad \text{for } \forall\ n. \tag{2.10}$$

These assumptions are satisfied if the nuclear action of the system is given as Eq. (2.4). We thus obtain, up to the first order in ϵ,

$$\begin{aligned}
&\langle\phi_{a_{n+1}} : \mathbf{R}_{n+1}|e^{-\frac{i}{\hbar}\epsilon\mathcal{H}^{el}(\mathbf{R}_n)}|\phi_{a_n} : \mathbf{R}_n\rangle \\
&= \exp\left(-\frac{i}{\hbar}\epsilon\mathcal{H}^{el}_{a_{n+1},a_n}(\mathbf{R}_n) + \sum_\mu \epsilon\dot{R}_n^\mu X^\mu(\mathbf{R}_{n+1/2})\right. \\
&\quad \left. + \frac{1}{2}\sum_{\mu,\nu}(R_{n+1}^\mu - R_n^\mu)(R_{n+1}^\nu - R_n^\nu)\mathcal{Y}^{\mu,\nu}(\mathbf{R}_{n+1/2})\right),
\end{aligned} \tag{2.11}$$

where $\dot{R}_n^\mu\epsilon = R_{n+1}^\mu - R_n^\mu$.

Coherent state path integral

Here we discuss the path integral in coefficient space; the electronic degrees of freedom is represented by coefficients over a specific many-body basis set. We denote the Ith base state by $|I : \mathbf{R}\rangle$, which satisfies the orthonormal condition $\langle I : \mathbf{R}|J : \mathbf{R}\rangle = \delta_{IJ}$. The coherent state is then defined as its superposition

$$|\tilde{c} : \mathbf{R}\rangle \equiv \sum_I \tilde{c}_I|I : \mathbf{R}\rangle, \tag{2.12}$$

which is NOT normalized. For later convenience, we also introduce an normalized notation $|c : \mathbf{R}\rangle \equiv \sum_I c_I|I : \mathbf{R}\rangle$, where $c_I = \tilde{c}_I/\sqrt{\sum_J |c_J|^2}$. The closure is given as

$$1 = \int d[\tilde{c}, \tilde{c}^*]|\tilde{c} : \mathbf{R}\rangle\langle\tilde{c} : \mathbf{R}|. \tag{2.13}$$

where the integration $\int d[\tilde{c}, \tilde{c}^*]$ is defined as

$$\int d[\tilde{c}, \tilde{c}^*] = \int_{-\infty}^{\infty} \prod_I \frac{d\,\tilde{a}^I\, d\,\tilde{b}^I}{2\pi} e^{-\sum_J |\tilde{c}^J|^2} \tag{2.14}$$

where $\tilde{a}^I$ and $\tilde{b}^I$ are real and imaginary degrees of freedom of $\tilde{c}^I$ defined as $\tilde{a}^I = \frac{1}{\sqrt{2}}(\tilde{c}^I + \tilde{c}^{*I})$ and $\tilde{b}^I = \frac{1}{i\sqrt{2}}(\tilde{c}^I - \tilde{c}^{*I})$, respectively.

With this set of bases, the electronic propagator becomes

$$\begin{aligned}
&\mathcal{K}^{el}(\{\mathbf{R}\} : \xi_f(\mathbf{R}_f), t_f; \xi_i(\mathbf{R}_i), t_i) = \\
&\times \int d[\tilde{c}_N, \tilde{c}_N^*] \langle \xi_f : \mathbf{R}_f | \tilde{c}_N : \mathbf{R}_f \rangle d[\tilde{c}_0, \tilde{c}_0^*] \langle \tilde{c}_0 : \mathbf{R}_i | \xi_i : \mathbf{R}_i \rangle \\
&\times \prod_{n=1}^{N-1} d\,[\tilde{c}_n, \tilde{c}_n^*] \langle \tilde{c}_{n+1} : \mathbf{R}_{n+1} | e^{-\frac{i}{\hbar}\epsilon \mathcal{H}^{el}(\mathbf{R}_n)} | \tilde{c}_n : \mathbf{R}_n \rangle.
\end{aligned} \tag{2.15}$$

Applying the same procedure as we derived Eq. (2.11), we obtain

$$\begin{aligned}
&\mathcal{K}^{el}(\{\mathbf{R}\} : \xi_f(\mathbf{R}_f), t_f; \xi_i(\mathbf{R}_i), t_i) \\
&= \int \left(d[\tilde{c}_N, \tilde{c}_N^*] \langle \tilde{c}_N : \mathbf{R}_N | \tilde{c}_N : \mathbf{R}_N \rangle \sum_J \xi_f^{J*} \tilde{c}_N^J \right) \left(d[\tilde{c}_0, \tilde{c}_0^*] \langle \tilde{c}_0 : \mathbf{R}_0 | \tilde{c}_0 : \mathbf{R}_0 \rangle \sum_K \tilde{c}_0^{K*} \xi_i^K \right) \\
&\times \prod_{n=1}^{N-1} d\,[\tilde{c}_n, \tilde{c}_n^*] \langle \tilde{c}_n : \mathbf{R}_n | \tilde{c}_n : \mathbf{R}_n \rangle \exp\left(\frac{i}{\hbar} \sum_{I,J} \left(i\hbar c_{n+1}^{*I} (c_{n+1}^I - c_n^I) \delta_{IJ} - c_{n+1}^{*I} \left(\mathcal{H}^{el}(\mathbf{R}_n)_{IJ} \epsilon - i\hbar \dot{\mathbf{R}}_n \cdot \mathbf{X}_{IJ} \epsilon \right. \right. \right. \right. \\
&\left. \left. \left. \left. - \frac{i\hbar}{2} \sum_{\mu,\nu} (R_{n+1}^\mu - R_n^\mu)(R_{n+1}^\nu - R_n^\nu) \mathcal{Y}_{IJ}^{\mu,\nu} \right) c_n^J \right) \right).
\end{aligned} \tag{2.16}$$

In what follows, the integral measure $d\,[\tilde{c}_n, \tilde{c}_n^*] \langle \tilde{c}_n : \mathbf{R}_n | \tilde{c}_n : \mathbf{R}_n \rangle$ is simply denoted as $d\,[c_n, c_n^*]$ by a redefinition of the notation. We also simplify the notation $|\tilde{c} : \mathbf{R}\rangle$ as $|c : \mathbf{R}\rangle$.

The electronic equation of Motion Differentiation of Eq. (2.16) with respect to c_{n+1}^{*I} gives the stationary phase condition for the electronic state as

$$i\hbar \dot{c}_n^I = \sum_J \left(\mathcal{H}^{el}(\mathbf{R}_n)_{IJ} - i\hbar \dot{\mathbf{R}}_n \cdot \mathbf{X}_{IJ} + \frac{i\hbar}{2} \sum_{\mu,\nu} (R_{n+1}^\mu - R_n^\mu)(R_{n+1}^\nu - R_n^\nu) \mathcal{Y}_{IJ}^{\mu,\nu} \right) c_n^J, \tag{2.17}$$

with $\dot{c}_n^I \epsilon = c_{n+1}^I - c_n^I$ in the discretized notation.

The last term in Eq. (2.17) has a subtle effect; although it is of the second order in nuclear displacement, if we perform the path integral of the nuclear coordinates, or apply the steepest descent method, it yields a contribution of an order $O(\epsilon)$ as in Eq. (2.10). The physical origin of this $O(\epsilon)$ contribution is the quantal fluctuation of nuclear coordinates. If we apply the stationary phase approximation for the nuclear degrees of freedom in the same level of

approximation, the last term in Eq. (2.17), that is, $\frac{i\hbar}{2}\sum_{\mu,\nu}(R^{\mu}_{n+1}-R^{\mu}_{n})(R^{\nu}_{n+1}-R^{\nu}_{n})\mathcal{Y}^{\mu,\nu}_{IJ}$ is replaced with $\sum_j \frac{\hbar^2}{2M_j}\mathcal{Y}^{j}_{IJ}$ [8] , and thus we obtain

$$i\hbar\dot{c}^{I}_{n}=\sum_{J}(\mathcal{H}^{el}(\mathbf{R}_n)_{IJ}-i\hbar\dot{\mathbf{R}}_n\cdot\mathbf{X}_{IJ}-\sum_j\frac{\hbar^2}{2M_j}\mathcal{Y}^{j}_{IJ})c^{J}_{n}. \tag{2.18}$$

It is interesting that the term $\mathcal{Y}^{j}_{IJ}$ in Eq. (2.18), defined in Eq. (2.9) is manifestly Hermitian, where the derivatives are evaluated at the mid-point $\mathbf{R}_{n+1/2}$. A less symmetric expression is obtained through 'end-point' derivative as

$$i\hbar\dot{c}^{I}_{n}=\sum_{J}(\mathcal{H}^{el}(\mathbf{R}_n)_{IJ}-i\hbar\dot{\mathbf{R}}_n\cdot\mathbf{X}_{IJ}-\sum_j\frac{\hbar^2}{2M_j}Y^{j}_{IJ})c^{J}_{n}, \tag{2.19}$$

with

$$Y^{j}_{IJ}=\left\langle I:\mathbf{R}\left|\sum_a\frac{\partial^2}{\partial R^{(j,a)\,2}}\right|J:\mathbf{R}\right\rangle. \tag{2.20}$$

The last term in Eq. (2.19) is the same as the second order derivative coupling Y^{k}_{IJ} in Eq. (8) of Ref. [82]. (More precisely, our Y^{j}_{IJ} corresponds to the sum of Y^{k}_{IJ} of Ref. [82] over all the coordinate indices k that belong to the jth nucleus.) Apparent non-Hermicity of this matrix; $Y^{j}_{IJ}\neq Y^{j\,*}_{JI}$ will be discussed in the Appendix C. The effect of this second order derivative coupling is in fact not thoroughly discussed; the diagonal elements (in terms of the adiabatic representation) of Y^{j} have been known as an energy correction arising from the non-Born-Oppenheimer effect [83], however, the (nonadiabatic) effects of the off-diagonal elements are not well known and are often dropped in practical calculations[21–23].

Basis set appropriate for nonadiabatic dynamical calculations

Although discussions in this section do not depend on the choice of basis set, a set of configuration state functions (CSF) basis may be one of the best choices. CSF-based nonadiabatic dynamical calculations was studied in Ref. [22], where they have established several core computational techniques including calculation of derivative coupling matrix elements and methodology for keeping smooth 'connection' of basis sets over adjacent timesteps. Then it has been confirmed, through many subsequent applications of these techniques [80], that the CSF-based derivative couplings often behaves moderately (almost free of singularity) as functions of nuclear configuration $\mathbf{R}$. This is in contrast to the adiabatic-based counterpart,

[8] In our formulation, the path integrations over the nuclear coordinates have to be performed after the electronic path integrals. Thus, strictly speaking, the replacement of $\frac{i\hbar}{2}\sum_{\mu,\nu}(R^{\mu}_{n+1}-R^{\mu}_{n})(R^{\nu}_{n+1}-R^{\nu}_{n})\mathcal{Y}^{\mu,\nu}_{IJ}$ to $\sum_j\frac{\hbar^2}{2M_j}\mathcal{Y}^{j}_{IJ}$ effectively violates the order. Nevertheless, we adopt Eq. (2.18) on the ground that it gives physically reasonable equations of motion.

which often become large near the avoided crossings. Absence of singularity is particularly important in numerical calculations. Although there is no general proof that the CSF basis is an approximate diabatic basis, there are several reasons to expect this. In diatomics, for example, in small nuclear separation, where correlation effects are small, the ground state is well-approximated by a single Slater determinant, whereas in larger nuclear separation, the adiabatic state becomes a superposition of CSFs reflecting the correlation effects. Then it is the coordinate derivative of these coefficients, rather than the derivative of CSFs that exhibit singular behavior near the avoided-crossings.

iii. The nuclear path integral

Having formulated the electronic path integral, we can now evaluate the nuclear path integral using $S_{eff} \equiv \frac{\hbar}{i} \ln K^{el}$. We seek for the stationary phase condition with respect to R_n^μ as

$$\begin{aligned}
&\frac{\partial}{\partial R_n^\mu} \left(S_{nuc}[\{\mathbf{R}\}] + S_{eff}[\{\mathbf{R}\}] \right) \\
&= -M\ddot{R}_n^\mu \epsilon - \frac{\partial}{\partial R_n^\mu} \left(U_{nuc}\epsilon - \frac{\hbar}{i} \ln \mathcal{K}^{el}(\{\mathbf{R}\} : \xi_f(\mathbf{R}_f), t_f; \xi_i(\mathbf{R}_i), t_i) \right) \\
&= 0,
\end{aligned} \tag{2.21}$$

where

$$\ddot{R}_n^\mu \epsilon^2 = R_{n+1}^\mu + R_{n-1}^\mu - 2R_n^\mu. \tag{2.22}$$

Thus we obtain the equation of motion for nuclei as

$$M_j \ddot{R}_n^{(j,a)} = -\frac{\partial}{\partial R_n^\mu} U_{nuc} + \mathcal{F}_n^{(j,a)}|_{[\xi_f(\mathbf{R}_f), t_f; \xi_i(\mathbf{R}_i), t_i]}. \tag{2.23}$$

The quantity $\mathcal{F}$ in this expression is defined as

$$\begin{aligned}
\mathcal{F}_n^\mu|_{[\xi_f(\mathbf{R}_f), t_f; \xi_i(\mathbf{R}_i), t_i]} &= -\frac{\partial}{\partial R_n^\mu} \left(-\frac{\hbar}{i\epsilon} \ln \mathcal{K}^{el}(\{\mathbf{R}\} : \xi_f(\mathbf{R}_f), t_f; \xi_i(\mathbf{R}_i), t_i) \right) \\
&= \overline{\langle c_{n+1} : \mathbf{R}_{n+1} | \hat{\mathcal{F}}_n^\mu | c_n : \mathbf{R}_n \rangle}_{[\xi_f(\mathbf{R}_f), t_f; \xi_i(\mathbf{R}_i), t_i]},
\end{aligned} \tag{2.24}$$

where the operator $\hat{\mathcal{F}}_n^\mu$ is defined as

$$\begin{aligned}
\hat{\mathcal{F}}_n^\mu = \mathcal{H}^{el}(\mathbf{R}_n)\hat{X}^\mu - \hat{X}^\mu \mathcal{H}^{el}(\mathbf{R}_n) - \sum_{I,J} |I : \mathbf{R}_n\rangle \frac{\partial}{\partial R_n^\mu} \langle I : \mathbf{R}_n | \mathcal{H}^{el}(\mathbf{R}_n) | J : \mathbf{R}_n \rangle \langle J : \mathbf{R}_n | \\
+ i\hbar \dot{R}_n^\nu \left(\hat{X}^\mu \hat{X}^\nu - \hat{X}^\nu \hat{X}^\mu \right) + \sum_\nu i\hbar \dot{R}^\nu \left(\frac{\partial X^\nu}{\partial R^\mu} - \frac{\partial X^\mu}{\partial R^\nu} \right).
\end{aligned} \tag{2.25}$$

Here we have introduced an 'expectation value over an electronic path', which is defined, for an arbitrary operator $\hat{A}$ as

$$\overline{A}_{n\,[\xi_f(\mathbf{R}_f),t_f;\xi_i(\mathbf{R}_i),t_i]} = \frac{1}{\mathcal{K}^{el}(\{\mathbf{R}\}:\xi_f(\mathbf{R}_f),t_f;\xi_i(\mathbf{R}_i),t_i)} \int d\,[c_N,c_N^*]\langle\xi_f:\mathbf{R}_f|c_N:\mathbf{R}_N\rangle$$
$$\prod_{\ell=n+1}^{N-1}\Big\{d\,[c_\ell,c_\ell^*]\langle c_{\ell+1}:\mathbf{R}_{\ell+1}|e^{-\frac{i}{\hbar}\epsilon\mathcal{H}^{el}(\mathbf{R}_\ell)}|c_\ell:\mathbf{R}_\ell\rangle\Big\}$$
$$\times\, d\,[c_n,c_n^*]\langle c_{n+1}:\mathbf{R}_{n+1}|e^{-\frac{i}{\hbar}\epsilon\mathcal{H}^{el}(\mathbf{R}_n)}\hat{A}|c_n:\mathbf{R}_n\rangle$$
$$\times\prod_{\ell=0}^{n-1}\Big\{d\,[c_\ell,c_\ell^*]\langle c_{\ell+1}:\mathbf{R}_{\ell+1}|e^{-\frac{i}{\hbar}\epsilon\mathcal{H}^{el}(\mathbf{R}_\ell)}|c_\ell:\mathbf{R}_\ell\rangle\Big\}\times\langle c_0:\mathbf{R}_0|\xi_i:\mathbf{R}_i\rangle, \tag{2.26}$$

where rather lengthy subscripts represents the path, and recalls that the value is dependent on the electronic as well as nuclear time evolution.

If we restrict the nuclear coordinate to be real, $\mathcal{F}_n^\mu|_{[\xi_f(\mathbf{R}_f),t_f;\xi_i(\mathbf{R}_i),t_i]}$ in Eq. (2.23) should be replaced by its real part

$$\mathcal{F}_n^\mu|_{[\xi_f(\mathbf{R}_f),t_f;\xi_i(\mathbf{R}_i),t_i]} = \mathrm{Re}\,\overline{\langle c_{n+1}:\mathbf{R}_{n+1}|\hat{\mathcal{F}}_n^\mu|c_n:\mathbf{R}_n\rangle}_{[\xi_f(\mathbf{R}_f),t_f;\xi_i(\mathbf{R}_i),t_i]}. \tag{2.27}$$

Equation (2.23) using the force in Eq. (2.27), which will be referred to as 'Pechukas Force', is equivalent to Pechukas' result. Restriction to real part is discussed in Appendix D

The operator $\hat{\mathcal{F}}$ is referred to as 'Force Matrix' in what follows. It is equivalent to the operator form of the force matrix formerly defined in Eq. (28) of Ref. [25]. We also note that it is formally equivalent to the operator form of the Hellman-Feynman force $-\partial H^{el}/\partial R^\mu$ although in practical calculation within finite basis expansion, Eq. (2.25), based on derivative calculation techniques [20] is known to give more accurate result rather than directly evaluating the Hellman-Feynman force. The quantity $\mathcal{F}^\mu$ in Eq. (2.24) is called 'Force Form', which is a c-number quantity corresponding to an evaluation of the force matrix along a "path" in $[\{\mathbf{R}\};\xi_f(\mathbf{R}_f),t_f;\xi_i(\mathbf{R}_i),t_i]$.

The nature of the electron-nucleus coupled equations of motion

Thus we have obtained a coupled equations of motion for the electrons (Eq. (2.18)) as well as for the nuclei (Eq. (2.23)). Being dependent on the 'future' as well as the past trajectory, the coupled equation does not have explicit solution. Coupled dynamics that would be derived from the coupled equation will be referred to as 'Pechukas dynamics', which has hypothetical nature in the sense that there is no practical computational method to realize it except for mapping approach proposed by Mayer-Miller-Thoss[14, 84]. In the following section, we will explore a practical method that somehow avoids the difficulty. On the other hand, this

difficulty, being manifestation of quantum mechanical entanglement of the two system, itself worth studying and will be detailed in Subsec. 4-1.

2-2. Path branching and split path integral

As is clear from the nuclear equation of motion Eq. (2.23), the (electronic) path dependence of the Force results in multiple trajectories, which is the origin of path bifurcation.

For example, in a typical chemical reaction problem with single initial state and multiple final state(channel)s, each channel should yield a different nuclear trajectory due to the final state dependence of the effective Force. In practice, however, there has been no established way of reproducing branching trajectories in a self-consistent manner. Here we consider a way to explicitly introduce (a possible) path branching in arbitrary time point

Consider an identical transformation of path integral by inserting the identity operator $1 = \sum_{p\in\Lambda} |\lambda_p\rangle\langle\lambda_p|$ at some fixed time t_S [9], where t_S lies in between t_i and t_f ($t_i \le t_S \le t_f$), and $\{\lambda_p\}_{p\in\Lambda}$ is a complete basis set which satisfies the orthonormal relation, $\langle\lambda_{p'}|\lambda_p\rangle = \delta_{p',p}$. The choice of $\{\lambda_p\}_{p\in\Lambda}$ is otherwise arbitrary, and we specify it later on to meet our convenience on a physical ground. We obtain, as an identical transformation of Eq. (2.2),

$$
\begin{aligned}
&\mathcal{K}(\mathbf{R}_f, \xi_f(\mathbf{R}_f), t_f; \mathbf{R}_i, \xi_i(\mathbf{R}_i), t_i) \\
&= \int d\,\mathbf{R}_{N-1} \cdots d\,\mathbf{R}_1 e^{\frac{i}{\hbar} S_{nuc}(\{\mathbf{R}_n\})} \\
&\times \sum_p \mathcal{K}^{el}(\{\mathbf{R}\} : \xi_f(\mathbf{R}_f), t_f; \lambda_p, t_S) \mathcal{K}^{el}(\{\mathbf{R}\} : \lambda_p, t_S; \xi_i(\mathbf{R}_i), t_i) \\
&= \sum_p \int d\,\mathbf{R}_{N-1} \cdots d\,\mathbf{R}_1 e^{\frac{i}{\hbar} S_{nuc}[\{\mathbf{R}_n\}]} \\
&\times \mathcal{K}^{el}(\{\mathbf{R}\} : \xi_f(\mathbf{R}_f), t_f; \lambda_p, t_S) \mathcal{K}^{el}(\{\mathbf{R}\} : \lambda_p, t_S; \xi_i(\mathbf{R}_i), t_i) \\
&= \sum_p \int d\,\mathbf{R}_{N-1} \cdots d\,\mathbf{R}_1 \exp\left(\frac{i}{\hbar} S_{nuc}\left(\{\mathbf{R}\}\right)\right) \exp\left(\frac{i}{\hbar} S_{eff}^{(\xi_f;\lambda_p)}\left(\{\mathbf{R}\}\right) + \frac{i}{\hbar} S_{eff}^{(\lambda_p;\xi_i)}\left(\{\mathbf{R}\}\right)\right).
\end{aligned}
\tag{2.28}
$$

As is seen in Eq. (2.28), the propagator is split, and each propagator has a state projection $|\lambda_p\rangle\langle\lambda_p|$ at the time point t_S. The effective action $S_{eff}^{(\xi_f;\lambda_p)}\left(\{\mathbf{R}\}\right)$ in this expression is defined

[9] Here, we do not specify the nuclear coordinate $\mathbf{R}$. When we perform the electronic path integral, we fix the nuclear position $\mathbf{R}$ at time points $\{t_n\}$, thus if t_S coincides with one of t_ns, the nuclear coordinate is $\mathbf{R}_n$, otherwise, the nuclear coordinate takes some intermediate value.

as

$$S_{eff}^{(\xi_f;\lambda_p)}(\{\mathbf{R}\}) = \frac{\hbar}{i}\ln\left(\mathcal{K}^{el}(\{\mathbf{R}\}:\xi_f(\mathbf{R}_f),t_f;\lambda_p,t_S)\right). \tag{2.29}$$

Equation (2.28) is an identical transformation, provided that the integrations are performed exactly. Nevertheless it gives a different result if we apply the stationary phase approximation; each split amplitude gives different stationary phase condition or nuclear path. We will see that this transformation is indeed closely related to a practical path branching algorithm.

We emphasize that this procedure does not justify "decoupling" treatment on each branches. In order for electronic dynamics to be correct, each split amplitude must be coherently summed over. In practice, however, almost all existing algorithms introduce decoupling approximation between branches. We will come back to this problem later on in Subsec. 4-2.

3. REDERIVATION OF PRACTICAL CALCULATION METHODS BY THE PATH INTEGRAL FORMALISM

Having established the formal theory of electron-nucleus coupled dynamics, we will discuss the central two problems stated in the introduction, by considering two practical calculation algorithms.

3-1. Semiclassical Ehrenfest theory (SET)

We first consider the Semiclassical Ehrenfest theory (SET). To be specific, we consider the formulation in Ref. [22], which we consider as a highly generalized and practical computational method in the modern context of nonadiabatic dynamics.

We start from the formal coupled equation of motion Eq. (2.23), and Eq. (2.18), which does not allow explicit solution due to the future time dependence of the Force form. It is found, however, the difficulty is completely removed by two additional assumptions; (1) Existence of single nuclear path, and (2) Assumption that the final electronic state is given by a unitary electronic time evolution along such single nuclear path;

$$|\xi_f:\mathbf{R}_f\rangle = \prod e^{-\frac{i}{\hbar}\epsilon H(\mathbf{R}_n)}|\xi_i:\mathbf{R}_i\rangle \times e^{i\gamma}, \tag{3.1}$$

where each $\mathbf{R}_n$ is the nuclear coordinate at time t_n which should be determined self-consistently, and $e^{i\gamma}$ is a possible phase factor, which shall be canceled out in the final

result. These assumptions drastically simplifies the Force form to give

$$\begin{aligned}\mathcal{F}_n^{\mu}|_{[\xi_f(\mathbf{R}_f),t_f;\xi_i(\mathbf{R}_i),t_i]} &= \sum_{I,J} \frac{\mathcal{K}^{el}(\{\mathbf{R}\}:\xi_f(\mathbf{R}_f),t_f;I,t_n)\mathcal{F}_{IJ}^{\mu}\mathcal{K}^{el}(\{\mathbf{R}\}:J,t_n;\xi_i(\mathbf{R}_i),t_i)}{\mathcal{K}^{el}(\{\mathbf{R}\}:\xi_f(\mathbf{R}_f),t_f;\xi_i(\mathbf{R}_i),t_i)} \\ &= \sum_{I,J} \frac{\langle\xi_i:\mathbf{R}_i|e^{\frac{i}{\hbar}\mathcal{H}(t_f-t_n)}|I:\mathbf{R}_n\rangle\mathcal{F}_{IJ}^{\mu}\langle J:\mathbf{R}_n|e^{-\frac{i}{\hbar}\mathcal{H}(t_n-t_i)}|\xi_i:\mathbf{R}_i\rangle}{1} \\ &= \sum_{I,J} c_n^{I\,*}\mathcal{F}_{IJ}^{\mu}c_n^J. \end{aligned} \tag{3.2}$$

Substitution of Eq. (3.2) to Eq. (2.23) yields the nuclear equation of motion, which is to be solved self-consistently with Eq. (2.18) to reproduce the SET formulated in Ref.[22] (note the second order derivative coupling is dropped).

Thus we can conclude that the SET is reasonable method provided that there is no nuclear path bifurcation. It is indeed numerically confirmed that the electronic transition probability estimated with SET is quite accurate in many cases with moderately large nuclear translational energies [25]. On the other hand, it would be almost useless in cases with path bifurcation. It is indeed known to give unphysical nuclear path in the asymptotic region where two adiabatic states should take independent trajectory.

3-2. Method of phase-space averaging and natural branching (PSANB)

We next turn to a path branching algorithm. Here we consider the method of phase-space averaging and natural branching (PSANB), proposed in Ref.[25], whose accuracy has been numerically confirmed in Refs. [25, 85], and now is being applied to a number of important problems[86]. Its algorithm is first derived using the variational principle in the Schrödinger picture [25] and is summarized as follows;
(1) Let $|\lambda_p\rangle$ be an eigenvector of force matrix along the system's moving direction $\hat{\mathcal{F}}^{\parallel} \equiv \mathbf{n}\cdot\boldsymbol{\mathcal{F}}$, where $\mathbf{n} \equiv \dot{\mathbf{R}}/|\dot{\mathbf{R}}|$. Branches of electronic state vector $|\Psi_t\rangle$ are derived as the projection to these eigenstates with weight $w_p = |\langle\lambda_p|\Psi_t\rangle|^2$. (2) The nuclear coordinate of each branch is propagated using the corresponding Force $\mathbf{n}f_p + \langle\lambda_p|\hat{\mathcal{F}} - \mathbf{n}\hat{\mathcal{F}}^{\parallel}|\lambda_p\rangle$ (3) **[averaging]** If the 'branching criterion' does not apply, the displacements $\Delta\mathbf{R}$ and $\Delta\mathbf{P}$ are averaged over branches (with weight w_p) to give a single branch. **[branching]** On the other hand, if the criterion applies, the displacements are not averaged and branches are propagated independently.

A simplest branching criterion is to branch at the time points where the nonadiabatic coupling between states $|\mathbf{v}\cdot\mathbf{X}|_{pq}$ decrease to get smaller than a predetermined value X_{thr}.

The criterion is, however, not unique and different criteria have been proposed in recent researches. We will back to the discussion of these criteria later in Secs. 4 and 5, but here we follow the simplest approach and examine if the above procedure can be explained using the path-integral formulation.

The application of split path integral using the Force Matrix ($\hat{\mathcal{F}}^{\parallel}$) eigenstates yields the multiple branches whose Force form, in its moving direction $\mathbf{n} \equiv \dot{\mathbf{R}}/|\mathbf{R}|$, evaluated as

$$\frac{\langle \xi | e^{-\frac{i}{\hbar}\epsilon H^{el}} \hat{\mathcal{F}}^{\parallel} | \lambda_p \rangle}{\langle \xi | e^{-\frac{i}{\hbar}\epsilon H^{el}} | \lambda_p \rangle} = f_p, \tag{3.3}$$

where the electronic state after the short time propagation is temporarily represented as $|\xi\rangle$. Because of the eigenstate property, (3.3) holds independent of $|\xi\rangle$, and gives correct Force form for the short time. Forces in the other directions, $\mathbf{F}^{\perp}$ may be well approximated by its equal time expectation value, $\langle \lambda_p | \mathbf{F}^{\perp} | \lambda_p \rangle$.

On the other hand, the path integral formulation does not justify the procedure of 'averaging'. The procedure should be therefore understood as a 'prescription' to avoid infinite number of branching. It is then required that such prescriptions are to be optimized using formal theory as a guiding principle. In the next section, formal theory is reexamined in order to seek for requirements for practical algorithms.

4. REQUIREMENTS FOR MQC DYNAMICS

4-1. Conservation laws for branching paths

In spite of practical difficulties, Pechukas dynamics satisfies a set of important conservation laws, which are often violated in practical calculation methods. Consider an energy-like quantity defined as

$$\mathcal{E}(t) \equiv \frac{1}{2}\sum_j M_j \left(\dot{\mathbf{R}}^j\right)^2 + \mathrm{Re}\,\frac{\langle \beta | \hat{U}(t'',t) H^{el} \hat{U}(t,t') | \alpha \rangle}{\langle \beta | \hat{U}(t'',t') | \alpha \rangle}. \tag{4.1}$$

Assuming no explicit time-dependence in H^{el}, the quantity $\mathcal{E}(t)$ can be easily proven to be conserved under the Pechukas dynamics. Although $\mathcal{E}(t)$ is not an energy in the strict sense and there is no reason to believe that the quantity should be conserved during the time-evolution, it becomes a true energy (in the sense of MQC) when $\mathbf{R}$ asymptotes to the stationary configuration $\mathbf{R}_i$ and $\mathbf{R}_f$ where we assume that α and β are the Energy eigenstates

of eigenvalue $E_\alpha(\mathbf{R}_i)$ and $E_\beta(\mathbf{R}_f)$, respectively[10];

$$\mathcal{E}(t'') = \frac{1}{2}\sum_j M_j \dot{\mathbf{R}}^j{}^2_{t''} + E_\beta(\mathbf{R}_f) \tag{4.2}$$

$$\mathcal{E}(t') = \frac{1}{2}\sum_j M_j \dot{\mathbf{R}}^j{}^2_{t'} + E_\alpha(\mathbf{R}_i), \tag{4.3}$$

where t'' and the minus of t' are assumed to be positive large number. The conservation of $\mathcal{E}(t)$ then lead to a physically meaningful relation

$$\frac{1}{2}\sum_j M_j \dot{\mathbf{R}}^j_{t''}{}^2 + E_\beta(\mathbf{R}_f) = \frac{1}{2}\sum_j M_j \dot{\mathbf{R}}^j_{t'}{}^2 + E_\alpha(\mathbf{R}_i). \tag{4.4}$$

Considering the same type of relations for all possible final states from the same initial state, we see that the energy is conserved for each asymptotic channel. This conservation law is physically correct and also crucial in some experimental techniques including time of flight measurements[87].

In a central symmetric system, conservation of the angular momenta can also be discussed in the same manner using the quantity defined as

$$J(t) \equiv \sum_j M_j \mathbf{R}^j \times \dot{\mathbf{R}}^j + \mathrm{Re}\,\frac{\langle\beta|\hat{U}(t'',t)\mathcal{J}^{el}\hat{U}(t,t')|\alpha\rangle}{\langle\beta|\hat{U}(t'',t')|\alpha\rangle} \tag{4.5}$$

where $\mathcal{J}^{el} \equiv \mathcal{J}^{tot} - \sum_j M_j \mathbf{R}^j \times \dot{\mathbf{R}}^j$ is the angular momentum operator for the internal degrees of freedom.

These simple conservation laws are nevertheless not assured, in fact they are sometimes even severely violated, in many of existing calculation methods including mean-field methods like the Semiclassical Ehrenfest theory (SET). In some calculation methods including the surface hopping[13, 21] method and the multiple spawning method[24], the problem is circumvented by adjusting the linear momenta of nuclei on hopping or spawning. We will revisit the point in the next subsection.

In case of SET, what is explicitly conserved is a different type of quantity, namely, state-averaged quantities such as

$$\overline{\mathcal{E}}(t) \equiv \frac{1}{2}\sum_j M_j \dot{\mathbf{R}}^j{}^2 + \langle\alpha|\hat{U}(t',t)H^{el}\hat{U}(t,t')|\alpha\rangle \tag{4.6}$$

[10] Here, for simplicity, we assume the situation where the nonadiabatic transitions asymptotes to zero in the limit $t \to \pm\infty$.

for the energy and

$$\overline{\mathbf{J}}(t) \equiv \sum_j M_j \mathbf{R}^j \times \dot{\mathbf{R}}^j + \langle\alpha|\hat{U}(t',t)\mathcal{J}^{el}\hat{U}(t,t')|\alpha\rangle \tag{4.7}$$

for the angular momentum. This conservation law is reasonable up to where there is no clear wavepacket bifurcation. Moreover, it can be clearly shown that the mutual exchange of these conserved quantities between the electronic and nuclear subsystems can be described using the 'work' and 'torque' of the Force Form, respectively[88].

On the other hand, it leads to unphysical result in case there is clear branching to distinct asymptotic states. For example, the Energy conservation law in such case indicates that the nuclear kinetic energy is given as $K^{ave} = E_{tot} - \sum w_\beta E_\beta(\mathbf{R}_f)$, where w_β is the branching weight of each asymptotic state.

A truly challenging issue is then for a branching algorithms like PSANB, which adopts mean-field like scheme in the strongly interacting region and does not introduce discontinuous momentum shift, to reproduce this conservation laws in 'natural' manner. The requirement is that each branch, whose asymptotic electronic energy is $E_\beta(\mathbf{R}_f)$, asymptotically acquires the kinetic energy $K_\beta = E_{tot} - E_\beta(\mathbf{R}_f)$. It is clearly insufficient to apply a single branching procedure at the endpoint of interacting region, which would give results close to K^{ave}, irrespective to channel. Clearly one would have to apply multiple branching inside the interacting region to reflect the channel dependence on the wavepacket motion.

4-2. Requirements for branching algorithm

Based on the above discussion, we propose the following two requirements for a branching algorithm.

(1) Reproduction of correct electron dynamics: Calculation should reproduce the correct quantum-mechanical (nonadiabatic) time evolution of the electronic state.

(2) Reproduction of the correct nuclear wavepacket velocity in the asymptotic region. The requirement is, for each asymptotic channel,

$$E_{tot} = \sum_j \frac{M_j}{2}\left(\dot{\mathbf{R}}^i\right)^2 + E_\beta(\mathbf{R}_f) \tag{4.8}$$

where E_{tot} is the total energy of the system and $E_\beta(\mathbf{R}_f)$ is the electronic energy in the asymptotic configuration $\mathbf{R}_f$. The conservation rule is, however, required in the asymptotic region and does not restrict occurrence of 'classically forbidden' hops [91].

Another point to be taken into account is that almost all known MQC implementation of branching introduce decoupling between branches.

It is then obvious that the two requirements contradicts each other. As we have discussed before, in order to satisfy the requirement (2), there have to be multiple branchings in the region where nonadiabatic transitions still exist. On the other hand, however, decouplings introduced by the branching would generally lead to wrong electron dynamics. In more practical sense, the resultant electronic dynamics would deviate from SET, which is known to give relatively accurate result with respect to the electronic dynamics.

These observation, suggests a need for an improved treatment of branches that includes corrections over the decoupling treatment, together with that for correct treatment of "Force", which, through multiple branchings, somewhat reproduce the correct conservation law, Eq. (4.8).

5. GENERAL DISCUSSIONS ON BRANCHING CRITERIA

This section is meant to discuss the problem from more general standpoint. We do not necessarily stick to the path-integral formulation but examine other known implementation in broader perspective. A central problem is to find out hints for better branching algorithm, in particular, criteria for when one should actually introduce branching.

5-1. Sketch of the problem

We start by recalling the Schrödinger picture full-quantum description. The exact decomposition of the electron-nucleus coupled state, and the corresponding Schrödinger equation are given in Eq. (1.2). In this viewpoint, our problem is (1) to find out the best approximation of the wavefunctions $\chi_I(\mathbf{R},t)$ as a superposition of a small number of localized wavepackets $\{\chi_k\}$. One may further add an additional condition that (2) the time evolution of these wavepackets are uniquely derived from an effective equation of motion, which is either some semiclassical time-evolution equation or the classical equation of motion of the position $\mathbf{Q}_k(t)$ and the momentum $\mathbf{P}_k(t)$ associated with the center of the wavepacket χ_k.

We first consider an intuitive description of the problem. We temporary consider an electronic state expansion and write its short time evolution in Trotter form

$$\chi_I(\mathbf{R},t+\epsilon)=\int d\mathbf{R}'\left(e^{-\frac{i}{\hbar}\epsilon K'}\right)_{IJ}\langle\mathbf{R}|e^{-\frac{i}{\hbar}\epsilon\left(\hat{T}+H_{JJ}\right)}|\mathbf{R}'\rangle\chi_J(\mathbf{R}',t) \tag{5.1}$$

where $\hat{T}$ is the kinetic operator, $K'_{IJ} = H_{IJ} - \sum_j i\hbar \mathbf{X}^j \cdot \frac{\hbar}{iM_j}\nabla^j - \sum_j \frac{\hbar^2}{2M_j}\Delta^j$ includes all off-diagonal terms. The first operator is electronic state diagonal but in general change the position; it is known to be well-described by the frozen Gaussian approximation on the wavepacket, which is equivalent to the gradient dynamics on a single potential energy surface. whereas the second operator is position diagonal but state off-diagonal. On the other hand, however, if one of the summation in the third term, for example, J is dominant, the peak position of χ_I should be the same as that of χ_J. SET is constructed on the assumption that all peak positions of nonadiabatically coupled states should be the same.

Based on the observations, the simplest scheme would be as follows.

• unbiased expansion

Expand the true wavefunctions $\chi_I(\mathbf{R}, t)$ by $\tilde{\chi}_I(\mathbf{R}, t)$, which assumes the form $\tilde{\chi}_I(\mathbf{R}, t) = \sum_k c_I^k g(\mathbf{R}; \mathbf{\Gamma}_k(t))$ with standard normalized Gaussian $g(\mathbf{R}; \mathbf{\Gamma}) \equiv \sqrt[4]{\det\left(\frac{2\gamma}{\pi}\right)} \exp\left[\frac{i}{\hbar}\left[\mathbf{P}\cdot(\mathbf{R}-\mathbf{Q}(t)) + i\hbar(R^a - Q^a(t))\gamma_{ab}(R^b - Q^b(t))\right]\right]$. Parameters are set so that it minimizes the squared deviation at time $t = 0$;

$$\int d\mathbf{R}\, |\chi_I(\mathbf{R}, 0) - \tilde{\chi}_I(\mathbf{R}, 0)|^2 \tag{5.2a}$$

$$\int d\mathbf{R}\, \left|\dot{\chi}_I(\mathbf{R}, t) - \dot{\tilde{\chi}}_I(\mathbf{R}, t)\right|^2 \tag{5.2b}$$

where in the second line, $\dot{\chi}_I$ is given by the Schrödinger equation.

For a given set of expansion parameters at $t = 0$, $\{\Gamma_k(0)\}$, optimization of coefficients c_I^k and its time-derivatives gives

$$(g_I^j|\chi_I) = \sum_k S_I^{jk} c_I^k \tag{5.3a}$$

$$i\hbar \sum_k S_I^{jk} c_I^k = \sum_k \left(\hat{T} + H_{II} - i\hbar\partial_t\right)^{jk} c_I^k + \left(K'_{IJ}\right)^{j\ell} c_J^\ell, \tag{5.3b}$$

where the inner products are defined as $(g_I^j|O|g_J^\ell) \equiv \int d\mathbf{R} g_I^j(\mathbf{R})^* O(\mathbf{R}) g_J^\ell(\mathbf{R})$ and matrices are denoted as $(O_{IJ})^{j\ell} \equiv (g_I^j|O|g_J^\ell)$ and $S_I^{jk} \equiv (g_I^j|g_I^k)$. Eqs. (5.3a), (5.3b) are usual derivation of the expansion coefficients and (an expansion of) the Schrödinger equation.

On the other hand, optimization of Gaussian parameters $\{\Gamma_k\}$ requires another set of variational equations. If these equations were solved, it would give an 'unbiased description' of the dynamics and gives a definite branching criterion.

• The multiple spawning method

Equations (5.3a), (5.3b) are are similar to those appears in the formulation of the multiple

spawning method [24]. In fact 'full-numerical' version of the spawning method can be seen as Gaussian expansion of the exact Schrödinger equation. On the other hand, as for the Gaussian parameters, the multiple spawning method does not apply variational optimization; the Gaussian width is fixed In the multiple spawning method, however, Gaussian parameters, (wavepacket center momentum and position, and Gaussian width) are not variationary optimized. the Gaussian width γ is fixed at a predetermined value, the wavepacket center positions $\mathbf{Q}_t$ and momenta $\mathbf{P}_t$ are fixed by the classical equation of motion. Moreover, extra basis sets needed for branched wavepackets are generated in an analogous manner to the surface hopping method. It may be necessary to make the method practical but would certainly 'bias' the result. Interestingly, in Ref. [89], the spawning method is not considered as Gaussian expansion of the Schrödinger equation but frozen-Gaussian modification of the surface hopping approach.

- Semiclassical approach

Miller and George [90] generalized the Stueckelberg's formulation to propose a semiclassical theory of nonadiabatic transition of nuclear wavepackets. The original Stueckelberg's theory solves one-dimensional two-state problem by the asymptotic, or equivalently, semiclassical analysis. In his formulation, the coupled (diabatic) Schrödinger equation for the original two-state problem

$$-\frac{\hbar^2}{2M}u_1'' + W_1 u_1 + V u_2 = E u_1 \tag{5.4a}$$

$$-\frac{\hbar^2}{2M}u_2'' + W_2 u_2 + V u_1 = E u_2 \tag{5.4b}$$

is reduced to a single component quartic differential equation,

$$u_2 = \left(u_1'' + p_1^2 u_1\right)/\alpha \tag{5.5a}$$

$$u_1^{IV} + \frac{-2\alpha'}{\alpha}u_1^{III} + \left(p_1^2 + p_2^2 - \frac{\alpha''}{\alpha} + 2\left(\frac{\alpha'}{\alpha}\right)^2\right)u_1^{II} + \left(2(p_1^2)' - 2\frac{\alpha'}{\alpha}p_1^2\right)u_1' + \left((p_1^2)'' - 2\frac{\alpha'}{\alpha}(p_1^2)' + \left[-\frac{\alpha''}{\alpha} + 2(\frac{\alpha'}{\alpha})^2\right]p_1^2\right)u_1 = 0. \tag{5.5b}$$

where $p_i = \sqrt{2M(E - W_i)}/\hbar$ are the 'diabatic' wavenumbers, $\alpha = 2MV/\hbar^2$ is the reduced diabatic coupling.

The asymptotic behavior of the solution of the quartic equation, in the lowest order of $\hbar$, is 'adiabatic solution'; $\exp[\pm\frac{i}{\hbar}\int \nu_\pm dr]$ with $\nu_\pm^2 \equiv (p_1^2 + p_2^2)/2 \pm \sqrt{(p_1^2 - p_2^2)^2/4 + \alpha^2}$. In the complex r plane, there is a cut associated to the root in the equation of $\nu_\pm^2$ along $\mathrm{Re}\, r = 0$ connecting the two points (r_* and its complex conjugate), where two adiabatic wavenumbers

$\nu_\pm$ degenerate. The solution to the left of crossing point $r = 0$ is therefore connected to the solution to the right by a contour integral around the cut. Hence it gains an exponential factor $\mathrm{Im}\int_0^{r_*}(\nu_+ - \nu_-)\,dt$, which would give the Landau-Zener (LZ) exponent $\pi\frac{V^2}{|F_1-F_2|\hbar v}$ if the assumptions in the LZ model were to be applied.

Miller's idea is to generalize the argument to higher dimension and describe the nonadiabatic transition of the nuclear degrees of freedom by the complex contour integral connecting the avoided-crossing point of the original PES $\mathbf{R}_c$, complex crossing point $\mathbf{R}_*$ and the point on another PES where all component of R except that of the reaction coordinate becomes real.

The approach is remarkable in that it 'analytically' derives non-classical motion of the wavepacket center. It may give practical guideline for deriving an appropriate branching point or time. On the other hand, it is not clear that this approach is truly mathematically correct; the Stueckelberg's theory is based on the WKB asymptotic expansion, which have no established higher-order generalization. Moreover, introducing complex-valued $\mathbf{R}$ in the electronic Hamiltonian may violate the Hermicity of $H^{el}(\mathbf{R})$. We thus see that full implementation of this approach, if any, may not be suited for our purpose.

• Meyer-Miller implementation of the Pechukas Dynamics

Pechukas dynamics, in formal sense, satisfies the both requirements. However, as we have emphasized before, its numerical implementation is not simple. One implementation is to change the equation of Force form, Eq. (2.24), by an equal-time expectation value

$$\mathcal{F}_t = \langle\psi_t^{\xi_f,\xi_i}|\left(-\frac{\partial H}{\partial \mathbf{R}}\right)|\psi_t^{\xi_f,\xi_i}\rangle \tag{5.6}$$

but requires that the electronic state to evolve smoothly from a given initial state $|\xi_i\rangle$ to the specified final state $|\xi_f\rangle$ (up to the phase). This actually requires solution of double boundary problem from $\{\mathbf{R}_i, \mathbf{P}_i, |\xi_i\rangle\}$ to $\{\mathbf{R}_f, \mathbf{P}_f, |\xi_f\rangle\}$. Such problem has never solved in the original form, but becomes solvable if one applies a mapping procedure and converts into an effective classical problem [14]. The double boundary problem is then solvable to reproduce Pechukas dynamics.

• Other implementation of the Pechukas Dynamics

In fact the Pechukas dynamics does not necesarrily requires the quantum state to evolve from $|\xi_i\rangle$ to $|\xi_f\rangle$. The fact suggests unnecessity of the electronic double boundary problem. The equation of the Force form, Eq. (2.24), with an explicit real-value projection, is rewritten as

follows

$$\boldsymbol{\mathcal{F}}_n = \mathrm{Re}\left(\frac{\langle \xi_f^{(B)}(t)| \left(-\frac{\partial H}{\partial \mathbf{R}}\right) |\xi_i^{(F)}(t)\rangle}{\langle \xi_f^{(B)}(t)|\xi_i^{(F)}(t)\rangle} \right) \tag{5.7}$$

where 'backward-propagated' bra vector $\langle \xi_f^{(B)}(t)|$ and 'forward-propagated' ket vector $|\xi_i^{(F)}(t)\rangle$ are defined as

$$\langle \xi_f^{(B)}(t)| \equiv \langle \xi_f|\hat{U}(t_f, t) \tag{5.8}$$

$$|\xi_i^{(F)}(t)\rangle = \hat{U}(t, t_i)|\xi_i\rangle \tag{5.9}$$

where the time-evolution operator $\hat{U}$ implicitly depend on the nuclear path. In fact these two do not have to be mutually conjugate to each other. We can therefore consider multiple final states (branches) and propagate backward to obtain branch-dependent Force form from Eq. (2.24). Numerical implementation of such dynamics is under development. In stead of double boundary problem, we now have to seek for self-consistent solutions for implicit problem. Possible outcomes of this study is to be reported elsewhere.

Summary Seeking hints for branching algorithm, we have examined three types of possibilities, each related with an existing approach. We first examined possible "unbiased" expansion in Gaussian wavepackets, where we saw a certain difficulty in optimization of Gaussian parameters (the centers of wavepackets). This approach actually shares two of the core equations with the multiple spawning method, although in the multiple spawning method, addition of new basis functions ('spawning') is governed by an algorithm similar to the Surface Hopping approach, thereby introducing a certain "biases". We can then suggest that modification of this process may answer our question of when to introduce branching.

We next examined semiclassical approach with imaginary trajectories where we saw that, at least in simplest case, the branching path can be uniquely drawn by imaginary path. This would give us a definite branching criterion. However, it is far from obvious how to introduce imaginary $\mathbf{R}$ coordinate in a consistent manner to the electron-nucleus coupled dynamics in general dimension.

Finally we discussed possible implementations of Pechukas dynamics. We saw that there is no known algorithm to solve a coupled double boundary problem except for classical mapping approach. However, we have pointed out that such 'double boundary problem' may not be necessary to realize Pechukas dynamics.

6. HIGHER ORDER EXPANSION

We discuss higher order expansion beyond the stationary phase approximation. It is well known that higher order approximation of path-integral can be obtained from Gaussian integrals using the second order expansion of the action around the stationary phase path. In case of ordinary path-integrals in an external potential, the Gaussian kernel is given by the second order derivative of potential energy function. In case of path-integrals with a coupled degrees (electron-nucleus) of freedom, on the other hand, there is nontrivial contribution from functional derivative of different time point in the form of a special correlation function. We will then see that inclusion of such correlation function in the pre-exponential factor is crucial for obtaining the correct path-integral of coupled dynamics, in particular near the caustic singularity.

Notation In this section, in order for simplicity, the second derivative of nuclear potential U_{nuc} is denoted as $U'^{\mu\nu}_{nuc} \equiv \dfrac{\partial^2 U_{nuc}}{\partial R^\mu \partial R^\nu}$.

6-1. General procedures

We start from the formal nuclear path integral Eq. (2.3). We expand the action in Eq. (2.3) around the stationary phase solution (or "classical" solution) $\mathbf{R}^{SP}$. Using the fluctuation variable $\mathbf{Y}_t \equiv \mathbf{R}_t - \mathbf{R}_t^{SP}$, which is subject to the Dirichlet boundary condition $\mathbf{Y}_{t_i} = \mathbf{Y}_{t_f} = 0$

$$S = S^{SP} + \frac{1}{2}\delta S^{(2)}[\mathbf{Y}_t] + \delta S'[\mathbf{Y}_t] \tag{6.1}$$

where S^{SP}, $\delta S^{(2)}$ and $\delta S'$ denotes the stationary phase action, the second order expansion, and higher order expansion, respectively. The second order expansion is rewritten as $\delta S^{(2)} = \int dt \int dt' Y_t^\mu \, \mathcal{G}^{-1}{}_{\mu\nu}(t,s) Y_s^\nu$ where the kernel is defined as $\mathcal{G}^{-1}{}_{\mu\nu}(t,s) \equiv \frac{\delta^2 S}{\delta R_t^\mu \delta R_s^\nu}$. The path-integral becomes

$$\begin{aligned} K &= e^{\frac{i}{\hbar}S^{SP}} \int \mathscr{D}\mathbf{Y}_t e^{\frac{i}{2\hbar}\delta S^{(2)}[\mathbf{Y}_t]} \sum_{n=0}^{\infty} \frac{1}{n!} \left(\frac{i}{\hbar}\delta S'\right)^n \\ &= e^{\frac{i}{\hbar}S^{SP}} \sqrt{\prod_\mu \frac{M_\mu}{2\pi i\hbar T}} \left(\det \mathcal{G}^{-1}\right)^{-1/2} \langle \sum_{n=0}^{\infty} \frac{1}{n!} \left(\frac{i}{\hbar}\delta S'\right)^n \rangle_{\mathcal{G}^{-1}} \end{aligned} \tag{6.2}$$

where the average $\langle \cdots \rangle_{\mathcal{G}^{-1}}$ denotes the average using Gaussian kernel ;

$$\langle O \rangle_{\mathcal{G}^{-1}} \equiv \int \mathscr{D}\mathbf{Y}_t e^{\frac{i}{2\hbar}\int ds \int ds' Y^\mu(s)\, \mathcal{G}^{-1}{}_{\mu\nu}(s,s') Y^\nu(s')} O \Big/ \int \mathscr{D}\mathbf{Y}_t e^{\frac{i}{2\hbar}\int ds \int ds' Y^\mu(s)\, \mathcal{G}^{-1}{}_{\mu\nu}(s,s') Y^\nu(s')} \tag{6.3}$$

The higher order terms are to be decomposed into pairs of Y^μs and evaluated according to $\langle Y_t^\mu Y_s^\nu \rangle_{\mathcal{G}^{-1}} = i\hbar \mathcal{G}_{\mu\nu}(t,s)$. An order estimate of such fluctuation is, in analogy to the harmonic oscillator, $\langle Y_t^\mu Y_s^\nu \rangle_{\mathcal{G}^{-1}} \sim \frac{\hbar}{\bar{M}\bar{\omega}}$ where $\bar{M}$, $\bar{\omega}$ is a typical value of nuclear mass and its eigenmode frequency. The $2n$th order expansion terms are thus estimated as, denoting the $2n$th order derivative of potential as $U_{nuc}^{(2n)}$, $\frac{1}{\hbar}U_{nuc}^{(2n)}\left(\frac{\hbar}{\bar{M}\bar{\omega}}\right)^n$. We can hence regard these terms as small because of the difference of electronic length scale and nuclear fluctuation length scale, however, this estimate does not take into account of singularity which may occur at some special value of t and s.

We now discuss the singularity, which is, as we see below, enhancement of fluctuation in the parameter space where the second order fluctuation kernel takes zero mode. In 'ordinary' path-integrals in an external potential with Lagrangean $\mathcal{L} = \frac{M_\mu}{2}\dot{X}^\mu{}^2 - U_{nuc}$, the second order fluctuation kernel is ${\mathcal{G}^{-1}}_{\mu\nu}(t,s) = \delta(t-s)\left(-M_\mu \frac{d^2}{dt^2} - U_{nuc}^{,\mu\nu}\right)$. The derivative of classical path X^μ with respect to the initial momentum p_i^α, $\frac{\partial X^\mu}{\partial p_i^\alpha}$ formally satisfies

$$\int ds \sum_\nu {\mathcal{G}^{-1}}_{\mu\nu}(t,s)\frac{\partial X^\nu}{\partial p_i^\alpha} = 0. \tag{6.4}$$

It therefore becomes a zero-mode, i.e. zero-eigenvalue mode of the second order fluctuation kernel, if it satisfies the Dirichlet boundary condition. Here $\left.\frac{\partial X^\mu}{\partial p_i^\alpha}\right|_{t=t_i} = 0$ is obvious whereas the other condition

$$\left.\frac{\partial X^\mu}{\partial p_i^\alpha}\right|_{t=t_f} = 0 \tag{6.5}$$

is satisfied if and only if the point $(\mathbf{X}_f, t_f)$ is a caustic point. It then follows that the singularity occurrence of S_{cl} at the caustics should be consistent to that of the pre-exponential factor $\left(\det \mathcal{G}^{-1}\right)^{-1/2}$ due to the emergence of a zero-mode. The simplest example can be found in the harmonic oscillator path integral; $\lim_{t_f \to \frac{\pi N}{\omega}} \sqrt{\frac{m\omega}{2\pi i\hbar \sin\omega t_f}} e^{\frac{i}{\hbar}S_{cl}(x_f,t_f;x_i,0)} = \delta(x_f - x_i)$.

In fact Pechukas considered the term to be negligible. Rewriting his discussion in Ref. [75], he considered that the term

$$\langle \xi_f | \delta\hat{U}(t_f,t)\delta H(t)\hat{U}(t,t_i)|\xi_i\rangle, \tag{6.6}$$

mainly arises from the phase fluctuation of the time-evolution operator $\delta\hat{U}(t_f,t)$, which is symbolically written as $\delta\hat{U}(t_f,t) \approx \hat{U}(t_f,t)\delta\phi_t$. And considered this to be irrelevant for the second order fluctuation of his action; $\mathrm{Im}\left(\hbar \ln K_{fi}^{el}\right)$. On the other hand, in our formulation,

the second order fluctuation Eq. (6.6) is evaluated as

$$\int dt' \langle \xi_f | \hat{U}(t_f, t') \left(-\frac{i}{\hbar} \frac{\partial H^{el}(\mathbf{R}_{t'})}{\partial R^{\mu}_{t'}} \right) \delta R^{\mu}_{t'} \hat{U}(t', t) \left(\frac{\partial H^{el}(\mathbf{R}_t)}{\partial R^{\nu}_t} \right) \delta R^{\nu}_t \hat{U}(t, t_i) | \xi_i \rangle$$
$$= - \int dt' \sum_{\mu\nu} \frac{\hbar}{i} W^{\mu\nu}(t', t) \delta R^{\mu}_{t'} \delta R^{\nu}_t. \tag{6.7}$$

6-2. Correlation function of force

The second order derivative of the effective action (Eq. (2.5)) is given as

$$W^{\mu\nu}(t, t') = \frac{i}{\hbar} \frac{\langle \xi_f | \hat{U}(t_f, t_> : \mathbf{R}_\tau) \left(-\frac{\partial H^{el}}{\partial R^{\mu}} \right) |_{t_>} \hat{U}(t_>, t_< : \mathbf{R}_\tau) \left(-\frac{\partial H^{el}}{\partial R^{\nu}} \right) |_{t_<} \hat{U}(t_<, t_i : \mathbf{R}_\tau) | \xi_i \rangle}{K^{el}(\xi_f, \xi_i; \mathbf{R}_\tau)}$$
$$- \frac{i}{\hbar} \mathcal{F}^{\mu}(t) \mathcal{F}^{\nu}(t'), \tag{6.8}$$

where $t_>$ and $t_<$ indicate the larger and smaller one of t and t', respectively, and $(\cdot)\,|_t$ indicates that the dynamical variables in the bracket should be fixed at corresponding value at time t. Symbols $\mathcal{F}^{\mu}(t)$ indicate the continuous time representation of force form, which is dependent on the system's time-evolution. The quantity in Eq. (6.8), divided by factor $\frac{i}{\hbar}$, is the correlation function of the force operator, and will be referred to as 'force-force correlation function'.

We now evaluate the second order derivative of the action and obtain

$$\delta S^{(2)}[\widetilde{\mathbf{Y}}_t] = \int dt \int dt' \sum_{\mu\nu} \widetilde{Y}^{\mu}_t \left[\left(-\delta_{\mu\nu} \frac{d^2}{dt^2} - \widetilde{U}^{,\mu\nu}_{nuc} \right) \delta(t - t') - \widetilde{W}_{\mu\nu}(t, t') \right] \widetilde{Y}^{\nu}_{t'}, \tag{6.9}$$

where we have adopted mass-weighted representation $\widetilde{Y}^{\mu}_t \equiv \sqrt{M^{\mu}} Y^{\mu}_t$ and associated derivative are denoted as $\widetilde{U}^{,\mu\nu}_{nuc} \equiv \frac{\partial^2 U_{nuc}}{\partial \widetilde{Y}^{\mu} \partial \widetilde{Y}^{\nu}}$ and $\widetilde{W}_{\mu\nu}(t, t') \equiv \frac{\delta^2 S^{eff}}{\delta \widetilde{Y}^{\mu}(t) \delta \widetilde{Y}^{\nu}(t')}$ Because of the Dirichlet boundary condition $\widetilde{Y}^{\mu}_{\tau=T} = \widetilde{Y}^{\mu}_{\tau=0} = 0$, time-dependent fluctuation coordinates can be expanded in the Fourier sine series $\sqrt{\frac{2}{T}} \sin \nu_n t$, with discrete frequencies $\nu_n := \frac{n\pi}{T}$. The second order action becomes

$$\delta S^{(2)}[\{C^{\mu}_k\}] = \sum_{\mu,\nu} \sum_{k,\ell} C^{\mu}_k \left(\nu^2_k \delta_{k,\ell} - \left(\widetilde{U}^{,\mu\nu}_{nuc} \right)_{k,\ell} - \widetilde{W}^{\mu\nu}_{k,\ell} \right) C^{\nu}_{\ell} \tag{6.10}$$

where $\{C^{\mu}_k\}$ are the Fourier sine expansion coefficients of the fluctuation $\widetilde{Y}^{\mu}_\tau$, while $\left(\widetilde{U}^{,\mu\nu}_{nuc} \right)_{k,\ell}$ and $\widetilde{W}^{\mu\nu}_{k,\ell}$ are the Fourier sine expansions of $\widetilde{U}^{,\mu\nu}_{nuc}(t)$ and $\widetilde{W}^{\mu\nu}(t, t')$, respectively. The formal path integral, corresponding to Eq. (6.2) is given as

$$\int \prod dC^{\mu}_k e^{\frac{i}{2\hbar} \delta S^{(2)}[\{C^{\mu}_k\}]} \left\{ \sum_{p=0}^{\infty} \frac{1}{p!} \left(\frac{i}{\hbar} S'[\{C^{\mu}_k\}] \right)^p \right\}. \tag{6.11}$$

The kernel now has non-trivial correlations over different time points because of the force-force correlation. Our major interest is then how this kernel behaves and how this affects to the transition amplitudes. We rewrite the action as follows

$$\delta S^{(2)}[\{C_k^\mu\}] = \sum_{\mu,\nu}\sum_{k,\ell} C_k^\mu \left(\left(g_0^{-1}\right)_{k,\ell}^{\mu\nu} - \widetilde{W}_{k,\ell}^{\mu\nu} \right) C_\ell^\nu = \sum_{\mu,\nu}\sum_{k,\ell} C_k^\mu \left(\mathcal{G}^{-1}\right)_{k,\ell}^{\mu\nu} C_\ell^\nu \tag{6.12}$$

where g_0^{-1} is 'zero-th order kernel' whose component is $_{k\ell}^{\mu\nu}$th component is $\nu_k^2\delta_{k,\ell} - \left(\widetilde{U}_{nuc}^{,\mu\nu}\right)_{k\ell}$, whereas $\mathcal{G}^{-1}$ is the full kernel $\mathcal{G}^{-1} = g_0^{-1} - W$. By extension of the discussion given before, a caustics (of coupled dynamics) occur when there is a zero-mode of the kernel $\mathcal{G}^{-1}$, ξ_k^ν with the correct Dirichlet boundary condition. It hence means $\det\left(\mathcal{G}^{-1}\right) = \det\left(g_0^{-1}\left(1 - g_0 W\right)\right) = 0$. Assuming that such zero-mode is different from that of original g_0^{-1}, a zero mode emerges at the point an eigenvalue of $g_0 W$ equals unity so that $\det\left(1 - g_0 W\right) = 0$. Only the correct prefactor, which is given as $\sqrt{\frac{1}{2\pi i\hbar}}^N \left(\det G^{-1}\right)^{-1/2}$, has singularity at the same point, whereas uncorrected prefactor $\sqrt{\frac{1}{2\pi i\hbar}}^N \left(\det g^{-1}\right)^{-1/2}$ would have singularities at wrong point. We can thus conclude that inclusion of the force-force correlation recovers the correct prefactor, which is crucial near the caustics of the electron-nucleus coupled mode.

In fact a perturbative expansion is possible using the form Eq. (6.12).

$$\begin{aligned}
\det\left(g_0^{-1} - \widetilde{W}\right) &= \exp\left[\mathrm{tr}\ln\left(g_0^{-1} - \widetilde{W}\right)\right] \\
&= \det\left(g_0^{-1}\right)\exp\left[\mathrm{tr}\ln\left(1 - g_0\widetilde{W}\right)\right] \\
&= \det\left(g_0^{-1}\right)\exp\left[-\sum_{n=1}^{\infty}\frac{1}{n}\left(g_0\widetilde{W}\right)^n\right]
\end{aligned} \tag{6.13}$$

It does not give the correct pole unless one can perform the infinite summation, however, it clearly suggests the existence of singularity at $\det(1 - g_0\widetilde{W}) = 0$.

6-3. Model studies

In order to illustrate the effect of force-force correlation, we study simplified models based on coupled harmonic oscillators. Although it does not correspond to any realistic electron-nucleus coupled system, singularities are clear.

In this section, we temporarily consider the following model problem

$$H = \sum_\mu \left[\frac{P_\mu^2}{2M_\mu} + \frac{M_\mu}{2}\Omega_\mu^2 X_\mu^2\right] + \sum_r \left[\frac{p_r^2}{2m_r} + \frac{m_r}{2}\omega_r^2 x_r^2\right] - \sum_{\mu,r} g_{\mu,r} X_\mu x_r, \tag{6.14}$$

where $\{X_\mu\}$ and $\{x_r\}$ denote coordinates of quantum-mechanical oscillators whose mode frequencies are $\{\Omega_\mu\}$ and $\{\omega_r\}$, respectively. These are linearly coupled by coupling constants $g_{\mu,r}$. The subscripts μ and r runs through 1 to N_n and 1 to N_e, respectively. Although the problem is symmetric, we refer to variables $\{P_\mu, X_\mu\}$ as 'nuclear' while variables $\{p_r, x_r\}$ as 'electronic'. We first observe that the whole problem can be decomposed into $N_n + N_e$ independent modes with their eigenfrequencies obtained by diagonalizing We first observe that the whole problem can be decomposed into $N_n + N_e$ independent modes with their eigenfrequencies obtained by diagonalizing

$$\underline{\Omega}_{tot} \equiv \begin{pmatrix} \Omega_1^2 & & ... & & \widetilde{g}_{11} & \widetilde{g}_{12} & ... & \widetilde{g}_{1N_e} \\ & \Omega_2^2 & ... & & \widetilde{g}_{21} & \widetilde{g}_{22} & ... & \widetilde{g}_{2N_e} \\ & & ... & & & & ... & \\ & & ... & \Omega_{N_n}^2 & \widetilde{g}_{N_n1} & \widetilde{g}_{N_n2} & ... & \widetilde{g}_{N_nN_e} \\ \widetilde{g}_{11} & \widetilde{g}_{21} & ... & \widetilde{g}_{N_n1} & \omega_1^2 & & ... & \\ \widetilde{g}_{12} & \widetilde{g}_{22} & ... & \widetilde{g}_{N_n2} & & \omega_2^2 & ... & \\ & & ... & & & & ... & \\ \widetilde{g}_{1N_e} & \widetilde{g}_{2N_e} & ... & \widetilde{g}_{N_nN_e} & & & ... & \omega_{N_e}^2 \end{pmatrix}, \tag{6.15}$$

where $\widetilde{g}_{\mu,r} \equiv \frac{g_{\mu,r}}{\sqrt{M_\mu m_r}}$. The eigenvalues of the matrix $\underline{\Omega}_{tot}$ is denoted as $\{\lambda_\alpha^2\}$, $\alpha = 1, 2, ..., N_n + N_e$. for simplicity, we assume all the frequencies, $\{\Omega\}$, $\{\omega\}$, as well as $\{\lambda\}$ to be real-valued, which is indeed the case at sufficiently weak coupling. The propagator becomes

$$\sqrt{\prod_\mu M_\mu \prod_r m_r} \sqrt{\prod_\alpha \frac{\lambda_\alpha}{2\pi i \sin \lambda_a T}} e^{\frac{i}{\hbar} S_c(\{X_f\},\{x_f\},t_f;\{X_i\},\{x_i\},t_i)}. \tag{6.16}$$

We next consider the same problem using the stepwise path integral The electronic propagator becomes

$$\mathcal{K}^{el} = \sqrt{\prod_r \frac{m_r \omega_r}{2\pi i \sin \omega_r T}} e^{\frac{i}{\hbar} \sum_r S_{J_r}(x_{rf},t_f;x_{ri},t_i)} \tag{6.17}$$

where $S_{J_r}(x_f, t_f; x_i, t_i)$ is the action integral of forced oscillator

$$\begin{aligned} S_{J_r}(x_{rf}, t_f; x_{ri}, t_i) = \frac{m_r\omega_r}{2\sin\omega T} \Big[& (x_{rf}^2 + x_{ri}^2)\cos\omega T - 2x_{rf}x_{ri} \\ & + \frac{2x_{rf}}{m_r\omega_r} \int_{t_i}^{t_f} dt \sin\omega_r(t - t_i) J_r(t) + \frac{2x_{ri}}{m_r\omega_r} \int_{t_i}^{t_f} dt \sin\omega_r(t_f - t) J_r(t) \\ & - \frac{2}{m_r^2\omega_r^2} \int_{t_i}^{t_f} dt \int_{t_i}^{t} dt' J_r(t) \sin\omega_r(t_f - t) J_r(t') \sin\omega_r(t' - t_i) \Big] \end{aligned} \tag{6.18}$$

hence we have $S^{eff} = \sum_r S_{\sum_\mu g_{\mu,r} X_\mu} + \frac{\hbar}{i} \ln \left[\sqrt{\prod_r \frac{m_r \omega_r}{2\pi i \sin \omega_r T}} \right]$. The force-force correlation function is thus obtained as

$$\sum_r \frac{\partial^2 S_{J_r}}{\partial X_\mu(t) \partial X_\nu(t')} = \sum_r \frac{\partial g_{\mu,r} x_r(t)}{\partial X_\nu(t')} = -\sum_r g_{\mu,r} g_{\nu,r} \frac{\sin(\omega_r t_<) \sin \omega_r (T - t_>)}{\omega_r \sin \omega T} \tag{6.19}$$

which forms, except for a constant factor, the inverse of the Matrix form of the integration kernel in the sense

$$\left[-\frac{d^2}{dt^2} - \omega_r^2 \right] \frac{\sin(\omega_r t_<) \sin \omega_r (T - t_>)}{\omega_r \sin \omega T} = \delta(t - t'). \tag{6.20}$$

Hence we have, in the Fourier series representation,

$$S^{(2)} = \frac{1}{2} \sum_n \mathbf{C}_n^\dagger \left[\nu_n^2 1 - \underline{\Omega_n} - \underline{\widetilde{g}} \left(\nu_n^2 1 - \underline{\omega_e} \right)^{-1} \underline{\widetilde{g}}^t \right] \mathbf{C}_n, \tag{6.21}$$

where 1 is the unit matrix and $\underline{\Omega_n}[\ \underline{\omega_e}\ ]$ is a diagonal matrix with its μ $[r]$ th diagonal element Ω_μ^2 $[\omega_r^2]$, and $\underline{\widetilde{g}}$ is a $N_n \times N_e$ matrix composed of $\widetilde{g}_{\mu,r}$. The kernel, what is in the square bracket $[\cdots]$ is denoted as M_n^P. We define, in a similar manner, M^{el} as the electronic kernel $\omega_n^2 1 - \underline{\omega_e}$, M^{tot} as the total kernel $\nu_n^2 1 - \underline{\Omega_{tot}}$. These kernels indeed satisfy

$$\det M_n^P \det {M^{el}}_n = \det {M^{tot}}_n \tag{6.22}$$

hence the total propagator becomes

$$\begin{aligned} \left(\prod_n \det M_n^P \right)^{-\frac{1}{2}} \sqrt{\prod_r \frac{m_r \omega_r}{2\pi i \sin \omega_r' T}} e^{\frac{i}{\hbar} S_{tot}} &= \left(\prod_n \det M_n^P \right)^{-\frac{1}{2}} \left(\prod_n \det {M^{el}}_n \right)^{-\frac{1}{2}} e^{\frac{i}{\hbar} S_{tot}} \\ &= \frac{1}{\sqrt{\det M^{tot}}} e^{\frac{i}{\hbar} S_{tot}} \end{aligned} \tag{6.23}$$

Hence the inclusion of force-force correlation term in the second order fluctuation integral here reproduces the correct preexponential factor including mode coupling effects between the 'nuclear' and 'electronic' subsystems. It can be seen as another manifest of nonadiabaticity, or the fact that electron-nucleus coupled dynamics can *not* be simply reduced to classical nuclear dynamics on a fixed PES.

There is another model problem hinted by study of frame conversion in Ref. [92], which further indicates the close relation to mode coupling. The assumptions and discussions leading to the conclusion is almost prarell to the above example and will be given in Appendix H.

7. CONCLUDING REMARKS

In Part I, we have reformulated the electron-nucleus coupled nonadiabatic dynamics in MQC representation, seeking for a reliable theory that is free from empirical prescriptions so as to applicable to unconventional dynamics such as that in an intense optical field. We have first pointed out two major difficulties in MQC description of nonadiabatic dynamics, which arises from conflict of quantum and classical logics; (1) derivation of an effective nuclear dynamics in the presence of multiple interacting PESs (2) classical representation of quantum-mechanical wavepacket bifurcations. We started our discussion from the exact full quantum-mechanical path integral and reduced it in form of MQC equations of motion through a systematic applications of the stationary phase approximations. The resultant formal theory of MQC dynamics, free from empirical prescriptions, was close to the Pechukas' theory with several modifications. Several favorable properties of this formal theory was further confirmed through conservation laws. A formal solution for the first difficulty (1) was thus found to be an effective classical dynamics driven by the 'force form', which is a path-dependent average of the Hellmann-Feynman force operator. It also solves the second one (2); branching solutions of nuclear path should arise from path-dependence of the force form. These formal solutions, however, is not very practical since derivation of the exact force form requires self-consistent solutions of implicit equations of motion for which there have been known no established approaches. In seek for more practical approach, we proposed split path integrals to explicitly introduce branching. Standing on this formal framework, we further examined practical computational methods. We have found that SET can be obtained by an additional assumption of 'single path', which accounts for several favorable behaviors of this method in problems with no nuclear path bifurcations as well as a catastrophic fault in presence of branchings. We have also found that a key idea in PSANB is accountable using the split path integral technique but there remains several prescriptions unproven; most notably, its 'branching criteria'.

In an attempt to fix the remaining part, we have clarified central requirements for branching and have further discussed possible branching algorithms. Further discussions as well as numerical tests are left for future work.

In Sec. 6, we have discussed a slightly different type of problem, concerning to the higher order expansion of the path integral. We have pointed out that higher order expansion of the nuclear dynamics on PES requires evaluation of the force-force correlations. Here

the difference from an 'external potential', which is assumed in many textbook examples of path integrals, is in the fact that what represented by PES originates from electron-nucleus interactions. Inclusion of force-force correlation term is essential for correctly account for mode-mode couplings.

APPENDIX A: DETAILS OF THE TROTTER DECOMPOSITION

Here we prove the validity of the Trotter decomposition in Eq. (2.1). We first decompose the total Hamiltonian into nuclear position diagonal terms and off-diagonal terms

$$\mathcal{H} = \mathcal{T}_{nuc} + U_{nuc} + \mathcal{H}^{el}, \tag{A.1}$$

where $\mathcal{T}_{nuc}$, U_{nuc} and $\mathcal{H}^{el}$ are the nuclear kinetic energy terms, nuclear Coulombic interaction, and the electronic Hamiltonian, respectively. Thus the infinitesimal propagator turns out, up to the first order in ϵ, to be

$$\begin{aligned}
&\left\langle \mathbf{R}_{n+1}\right|\langle\phi_{a_{n+1}} : \mathbf{R}_{n+1}|e^{-\frac{i}{\hbar}\epsilon\mathcal{T}_{nuc}}e^{-\frac{i}{\hbar}\epsilon\left(U_{nuc}+\mathcal{H}^{el}\right)}|\phi_{a_n} : \mathbf{R}_n\rangle\left|\mathbf{R}_n\right\rangle \\
&\quad = \left\langle \mathbf{R}_{n+1}\right|\langle\phi_{a_{n+1}} : \mathbf{R}_{n+1}|\sum_{\alpha}|\alpha\rangle\langle\alpha| \\
&\times \int d\,\mathbf{P}\left|\mathbf{P}\right\rangle\left\langle\mathbf{P}\right|\exp\left[-\frac{i}{\hbar}\epsilon\mathcal{T}_{nuc}\right]\exp\left[-\frac{i}{\hbar}\epsilon\left(U_{nuc}(\mathbf{R}_n)+\mathcal{H}^{el}(\mathbf{R}_n)\right)\right]|\phi_{a_n} : \mathbf{R}_n\rangle\left|\mathbf{R}_n\right\rangle \\
&\quad = \int d\,\mathbf{P}\left\langle \mathbf{R}_{n+1}\right|\left.\mathbf{P}\right\rangle\exp\left[-\frac{i}{\hbar}\epsilon\sum_j\frac{\mathbf{P}_j^2}{2M_j}\right]\left\langle\mathbf{P}\right|\left.\mathbf{R}_n\right\rangle\exp\left[-\frac{i}{\hbar}\epsilon U_{nuc}(\mathbf{R}_n)\right] \\
&\times\sum_{\alpha}\langle\phi_{a_{n+1}} : \mathbf{R}_{n+1}|\alpha\rangle\langle\alpha|e^{-\frac{i}{\hbar}\epsilon\mathcal{H}^{el}(\mathbf{R}_n)}|\phi_{a_n} : \mathbf{R}_n\rangle \\
&\quad = \int d\,\mathbf{P}\exp\left[\frac{i}{\hbar}\mathbf{P}\cdot(\mathbf{R}_{n+1}-\mathbf{R}_n)-\frac{i}{\hbar}\epsilon\sum_j\frac{\mathbf{P}_j^2}{2M_j}-\frac{i}{\hbar}\epsilon U_{nuc}(\mathbf{R}_n)\right] \\
&\times\sum_{\alpha}\langle\phi_{a_{n+1}} : \mathbf{R}_{n+1}|\alpha\rangle\langle\alpha|e^{-\frac{i}{\hbar}\epsilon\mathcal{H}^{el}(\mathbf{R}_n)}|\phi_{a_n} : \mathbf{R}_n\rangle \\
&\quad = \exp\left[\frac{i}{\hbar}\left(\sum_j\frac{M_j\left(\mathbf{R}_{n+1}^j-\mathbf{R}_n^j\right)^2}{2\epsilon}-U_{nuc}(\mathbf{R}_n)\epsilon\right)\right]\langle\phi_{a_{n+1}} : \mathbf{R}_{n+1}|e^{-\frac{i}{\hbar}\epsilon\mathcal{H}^{el}(\mathbf{R}_n)}|\phi_{a_n} : \mathbf{R}_n\rangle.
\end{aligned} \tag{A.2}$$

Here, $|\mathbf{P}\rangle$ is the momentum eigenstate of the nuclear system, and $\int d\mathbf{P} = \int\prod_j\frac{d^3\mathbf{P}_j}{(2\pi\hbar)^3}$ is the momentum integral. $\{|\alpha\rangle\}$ is a complete set of electronic basis that is *independent* of nuclear position.

APPENDIX B: DERIVATION OF OVERLAP PRODUCT

We here derive Eq. (2.9). We evaluate the overlap product of state vectors of different nuclear positions, $\langle\phi_a : \mathbf{R}_{n+1}|\phi_b : \mathbf{R}_n\rangle$. The 'ket' vector $|\phi_b : \mathbf{R}_n\rangle$ is expanded around $\mathbf{R}_{n+1/2}$ up to the second order in coordinate difference $\mathbf{R}_{n+1} - \mathbf{R}_n$ as

$$\begin{aligned}|\phi_b : \mathbf{R}_n\rangle = |\phi_b : \mathbf{R}_{n+1/2}\rangle - \sum_\mu \frac{(R^\mu_{n+1} - R^\mu_n)}{2}\partial_\mu|\phi_b : \mathbf{R}_{n+1/2}\rangle \\ - \frac{1}{2}\sum_\mu\sum_\nu \frac{(R^\mu_{n+1} - R^\mu_n)}{2}\frac{(R^\nu_{n+1} - R^\nu_n)}{2}\partial_\mu\partial_\nu|\phi_b : \mathbf{R}_{n+1/2}\rangle \\ + O(|\mathbf{R}_{n+1} - \mathbf{R}_n|^3),\end{aligned} \tag{B.1}$$

where ∂_μ indicates $\frac{\partial}{\partial R^\mu}$. The 'bra' vector $\langle\phi_a : \mathbf{R}_{n+1}|$ is also expanded in the similar manner. Hence the product becomes

$$\begin{aligned}\langle\phi_a : \mathbf{R}_{n+1}|\phi_b : \mathbf{R}_n\rangle = \delta_{a,b} - \sum_\mu (R^\mu_{n+1} - R^\mu_n)X^\mu(\mathbf{R}_{n+1/2}) \\ + \frac{1}{2}(R_{n+1} - R_n)^\mu(R_{n+1} - R_n)^\nu\sum_\mu\sum_\nu \mathcal{Y}^{\mu,\nu}.\end{aligned} \tag{B.2}$$

In the first line, we used the relation

$$\langle\phi_a : \mathbf{R}|\partial_\mu\phi_b : \mathbf{R}\rangle + \langle\partial_\mu\phi_a : \mathbf{R}|\phi_b : \mathbf{R}\rangle = 0, \tag{B.3}$$

which is obtained by differentiating the orthonormal relation $\langle\phi_a : \mathbf{R}|\phi_b : \mathbf{R}\rangle = \delta_{ab}$. Thus we obtain Eq. (2.9). Yet a different expression is obtained if we evaluate the derivative at the end point as follows

$$\begin{aligned}&\langle\phi_a : \mathbf{R}_{n+1}|\phi_b : \mathbf{R}_n\rangle = \delta_{a,b} - \sum_\mu (R^\mu_{n+1} - R^\mu_n)\Big(X^\mu(\mathbf{R}_n) + \sum_\nu \frac{(R^\nu_{n+1} - R^\nu_n)}{2}\partial_\nu X^\nu(\mathbf{R}_n)\Big) \\ &\quad + \frac{1}{2}(R_{n+1} - R_n)^\mu(R_{n+1} - R_n)^\nu\sum_\mu\sum_\nu \mathcal{Y}^{\mu,\nu}(\mathbf{R}_{n+1/2}) \\ &= \delta_{a,b} - \sum_\mu (R^\mu_{n+1} - R^\mu_n)X^\mu(\mathbf{R}_n) \\ &\quad + \frac{1}{2}\sum_\mu\sum_\nu (R_{n+1} - R_n)^\mu(R_{n+1} - R_n)^\nu\langle\phi_a : \mathbf{R}_n|\partial_\mu\partial_\nu\phi_b : \mathbf{R}_n\rangle.\end{aligned} \tag{B.4}$$

Here, terms with the third order or higher in $\mathbf{R}_{n+1} - \mathbf{R}_n$ has been neglected, because they vanish or give $O(\epsilon^2)$ contribution to the path integral after the Gaussian integration. We have also used the following relation obtained by the second derivative of the orthonormal

relation $\langle \phi_a : \mathbf{R} | \phi_b : \mathbf{R} \rangle = \delta_{ab}$

$$\begin{aligned} &\langle \partial_\mu \partial_\nu \phi_a : \mathbf{R} | \phi_b : \mathbf{R} \rangle + \langle \partial_\mu \phi_a : \mathbf{R} | \partial_\nu \phi_b : \mathbf{R} \rangle \\ &+ \langle \partial_\nu \phi_a : \mathbf{R} | \partial_\mu \phi_b : \mathbf{R} \rangle + \langle \phi_a : \mathbf{R} | \partial_\mu \partial_\nu \phi_b : \mathbf{R} \rangle = 0. \end{aligned} \tag{B.5}$$

APPENDIX C: THE SECOND ORDER DERIVATIVE COUPLING AND NON-HERMICITY

Here we discuss the origin of apparent non-Hermicity of the second order derivative term. We first reconsider the full-quantum formulation, Eq. (1.2). We rewrite the RHS of Eq. (1.2) with slight different form with external vector field dropped,

$$\langle\langle \Omega | H^{tot} | \Omega \rangle\rangle = \int d\mathbf{R} \chi^*_\alpha(\mathbf{R}) \left[\sum_k \frac{1}{2M_k} \left(\frac{\hbar}{i} \nabla_k - i\hbar \mathbf{X}^k \right)^2_{\alpha\beta} + H^{el}_{\alpha\beta}(\mathbf{R}) \right] \chi_\beta(\mathbf{R}). \tag{C.1}$$

Using the relation $\nabla_k \mathbf{X}^k + \mathbf{X}^k \cdot \mathbf{X}^k = Y^k$, the RHS is rewritten as

$$\langle\langle \Omega | H^{tot} | \Omega \rangle\rangle = \int d\mathbf{R} \chi^*_\alpha(\mathbf{R}) \left[\sum_k \frac{-\hbar^2}{2M_k} \left(\Delta_k + 2\mathbf{X}^k \cdot \nabla_k + Y^k \right)^2_{\alpha\beta} + H^{el}_{\alpha\beta}(\mathbf{R}) \right] \chi_\beta(\mathbf{R}). \tag{C.2}$$

Although $Y^k_{\alpha\beta}$ being non-Hermitian, Eq. (C.2) is still its Hermitian because this can be rewritten as

$$\begin{aligned} \langle\langle \Omega | H^{tot} | \Omega \rangle\rangle &= \int d\mathbf{R} \chi_\beta(\mathbf{R}) \left[\sum_k \frac{-\hbar^2}{2M_k} \left(\Delta_k + 2 \left(\nabla_k \cdot \mathbf{X}^k_{\alpha\beta} + \mathbf{X}^k_{\alpha\beta} \cdot \nabla_k \right) + Y^k_{\alpha\beta} \right) + H^{el\,*}_{\beta\alpha}(\mathbf{R}) \right] \chi^*_\alpha(\mathbf{R}) \\ &= \int d\mathbf{R} \chi_\beta(\mathbf{R}) \left\{ \left[\sum_k \frac{-\hbar^2}{2M_k} \left(\Delta_k + 2\mathbf{X}^k \cdot \nabla_k + Y^k \right)_{\beta\alpha} + H^{el}_{\beta\alpha}(\mathbf{R}) \right] \chi^*_\alpha(\mathbf{R}) \right\}^* \end{aligned} \tag{C.3}$$

where we used the relation $Y^k_{\alpha\beta} - 2\nabla_k \mathbf{X}^k{}_{\alpha\beta} = Y^k_{\beta\alpha}$, which can be obtained from the derivative of $\mathbf{X}^k_{\alpha\beta} + \mathbf{X}^k_{\beta\alpha} = 0$.

The key for the Hermicity is in the term $\mathbf{X}^k_{\alpha\beta} \cdot \nabla_k$, whose Hermitian conjugate is $\nabla_k \cdot \mathbf{X}^k_{\beta\alpha} + \mathbf{X}^k_{\beta\alpha} \cdot \nabla_k$, whereas in MQC correspondence of Eq. (C.2), ∇_k is replaced by $i\mathbf{P}_k/\hbar$ and the Hermicity is lost.

In Schrödinger picture, we can construct the expansion that is free from the second order derivative. In stead of the expansion Eq. (1.1), we consider an approximate expansion, assuming that the nuclear wavefunction written in the superposition of time-dependent wavepackets centered at $\mathbf{Q}_t$,

$$|\Omega\rangle\rangle \approx \sum_\lambda |\mathbf{R}\rangle |\Psi : \mathbf{Q}^\lambda_t\rangle \chi^\lambda_I(\mathbf{R}; \mathbf{Q}^\lambda_t) \tag{C.4}$$

Neglecting all overlap integrals of wavepackets with different center coordinate $\mathbf{Q}_t^\lambda$, the corresponding Schrödinger equation becomes,

$$i\hbar\dot{\chi}_\alpha(\mathbf{R};\mathbf{Q}_t) = \left[\sum_k \frac{1}{2M_k}\left(\frac{\hbar}{i}\nabla_k\right)^2 \delta_{\alpha\beta} + \tilde{H}^{el}_{\alpha\beta}(\mathbf{R}) - i\hbar\dot{\mathbf{Q}}_t^k \cdot \langle\Phi_\alpha:\mathbf{Q}_t|\frac{\partial}{\partial\mathbf{Q}^k}|\Phi_\alpha:\mathbf{Q}_t\rangle\right]\chi_\beta(\mathbf{R}), \tag{C.5}$$

where $\tilde{H}^{el}_{\alpha\beta}(\mathbf{R}) = \langle\Phi_\alpha:\mathbf{Q}_t^\lambda|H(\mathbf{R})|\Phi_\beta:\mathbf{Q}_t^\lambda\rangle$. Taking the small width limit of the wavepacket, however, Eq. (C.5) looks as equally appealing as Eq. (1.2).

APPENDIX D: RESTRICTION TO REAL-VALUED TRAJECTORIES

As we mentioned in the main text, Pechukas modified the straightforward SPA result Eq. (2.24) by projecting to the real part to define what is now referred to as the Pechukas Force. Eq. (2.27). Although taking the real part should be necessary to produce a strictly real-valued trajectory, there is, up to author's knowledge, no concrete justification for this procedure. Mathematically, in order for the asymptotic expansion to be valid (i.e. the expansion series damps as the power series of $\hbar$), the first order derivative term of the action should be zero, or if any, should be small as $S_{,a} \sim \hbar$. Then we have to show that the neglected imaginary contribution to be of order $\hbar$, up to our knowledge, no proof has been ever known.

On the other hand there is a possibility of constructing meaningful complex-valued trajectory. As we see in Sec. 5, Miller and George [90] proposed a complex trajectory scheme as an generalization of Stueckelberg's nonadiabatic transition theory. Recalling that we are discussing some effective representation of nuclear motion, there is no reason to restrict $\mathbf{R}$ to be real-valued as long as it gives some consistent description.

In practice, however, introducing complex $\mathbf{R}$ in our problem introduces further complications including the Hermicity of the electronic equation of motion. There seems to be no general complex representation to achieve this.

From these consideration, we keep unprojected formula, Eq. (2.24) as formal result. We do use this in the context of SET and PSANB where the evaluation of Force form do yield the real solution. On the other hand, in general procedure, we are forced to use real-projected force form unless we can establish a consistent complex trajectory representation.

APPENDIX E: CALCULATION OF DERIVATIVE COUPLING

Here we show an analytic calculation of the derivative coupling [93]. The set of atomic and molecular orbitals are denoted as $\{\chi_\mu(\mathbf{r})\}$ and $\{u_\ell(\mathbf{r})\}$, respectively. The overlap of AOs are denoted as $S_{\mu\nu}$ whereas MOs are assumed to be mutually orthonormal. The inner product is defined in an obvious manner as $(u_\ell|A|u_m) \equiv \int d\mathbf{r} u_\ell(\mathbf{r}) A(\mathbf{r}) u_m(\mathbf{r})$. AO expansion of MOs are denoted as $u_\ell(\mathbf{r}) = \sum_\mu \chi_\mu(\mathbf{r}) C_\ell^\mu$.

What we need for our calculation is $\langle\Phi_I|\frac{\partial}{\partial R^a}|\Phi_J\rangle$ for an arbitrary pair (I,J) of N-body basis set $\{|\Phi_I\rangle\}$.

$$\begin{aligned}\int d\mathbf{r}\langle\Phi_I|\hat{\psi}^\dagger(\mathbf{r})\frac{\partial}{\partial R^a}\hat{\psi}(\mathbf{r})|\Phi_J\rangle &= \int d\mathbf{r}\langle\Phi_I|\hat{C}_\ell^\dagger u_\ell(\mathbf{r})\frac{\partial}{\partial R^a}u_m(\mathbf{r})\hat{C}_m|\Phi_J\rangle \\ &= a_{\ell m}^{IJ}(u_\ell|\frac{\partial}{\partial R^a}|u_m) \end{aligned} \tag{E.1}$$

where $a_{\ell m}^{IJ} \equiv \langle\Phi_I|\hat{C}_\ell^\dagger\hat{C}_m|\Phi_J\rangle$ is $\mathbf{R}$-independent "occupation number" for the pair (I,J).

We next evaluate the inner product

$$(u_\ell|\frac{\partial}{\partial R^a}|u_m) = \int d\mathbf{r} u_\ell(\mathbf{r})\frac{\partial}{\partial R^a}\left(\sum_\mu \chi_\mu(\mathbf{r})C_m^\mu\right) = S_{\ell m}^{a(R)} + U_{\ell m}^a \tag{E.2}$$

where $U_{\ell m}^a \equiv \sum_{\mu\nu} C_\ell^\mu S_{\mu\nu}\frac{\partial C_m^\nu}{\partial R^a}$ is the MO rotation matrix, whereas derivative overlaps $S_{\ell m}^{a(R)}$ are defined as $S_{\ell m}^{a(R)} \equiv \sum_{\mu\nu} C_\ell^\mu C_m^\nu \int d\mathbf{r}\chi_\mu(\mathbf{r})\frac{\partial}{\partial R^a}\chi_\nu(\mathbf{r})$. Equation (E.2), together with Eq. (E.1) gives the desired derivative coupling matrix element. We can further simplify the result using the relation

$$U_{\ell m}^a + U_{m\ell}^a + S_{\ell m}^a = 0 \tag{E.3}$$

where the (full) derivative overlap is defined as $S_{\ell m}^a \equiv \sum_{\mu\nu} C_\ell^\mu C_m^\nu \frac{\partial S_{\mu\nu}}{\partial R^a}$, which satisfies $S_{\ell m}^a = S_{\ell m}^{a(R)} + S_{m\ell}^{a(R)}$.

If the MOs are obtained in the Hartree-Fock calculation, orbital rotation matrix is obtained by the Coupled Perturbed Hartree-Fock method [94]. The orbital rotation matrices for occupied-occupied or virtual-virtual pairs are symmetric and given as $U_{\ell m}^a = U_{m\ell}^a = -S_{\ell m}^a/2$, whereas those for occupied-virtual pairs satisfy

$$S_{m\ell}^{a(R)} + U_{m\ell}^a = S_{m\ell}^{a(R)} - U_{\ell m}^a - S_{\ell m}^a = -S_{\ell m}^{a(R)} - U_{\ell m}^a, \tag{E.4}$$

hence we have

$$\langle\Phi_I|\frac{\partial}{\partial R^a}|\Phi_J\rangle = \sum_{\substack{\ell,m\in ocp.\\ \ell,m\in virt.}} a_{\ell m}^{IJ}\left(S_{\ell m}^{a(R)} - S_{m\ell}^{a(R)}\right) + \sum_{\ell\in ocp.}\sum_{m\in virt.}\left(a_{\ell m}^{IJ} - a_{m\ell}^{IJ}\right)\left(U_{\ell m}^a + S_{\ell m}^{a(R)}\right). \tag{E.5}$$

APPENDIX F: MOLECULAR VIBRATION

In MQC implementation of nonadiabatic dynamics, treatment of low-energy vibration mode, in particular the zero-point vibration mode introduce subtle problems, which are regarded as another manifestation of quantum-classical conflict.

In MQC simulation of chemical reaction problems, the initial nuclear coordinates/velocities are set so that they correspond to classical oscillations around the equilibrium point with zero-point energy. These classical analogue of "zero point vibrations", however, induce spurious electronic state transitions through the nonadiabatic coupling term $-i\hbar\dot{\mathbf{R}} \cdot \mathbf{X}_{IJ}$ (the nonadiabatic term with $\dot{\mathbf{R}}$ substituted the vibrational velocity induce electronic transition). The problem arises due to the absence of quantization in the classically represented vibrations. It does not always lead to severe problem if the vibration frequency is far smaller than the electronic transitions, and/or the collisional energy, or the translational energy in reaction coordinate, is large enough for this transition to be relatively negligible. On the other hand, it does cause problem if one deals with low energy problem, especially those with low-lying electronic excitation levels.

APPENDIX G: OTHER REQUIREMENTS TO BE CONSIDERED

In the main text, we discussed the requirements for "correct" MQC dynamics based on the conservation laws. The subject has also been a long dispute in literatures. Here we review and discuss some of these arguments.

Tully in Ref. [95] points out following two problems as the deficiencies of SET;

SET-1. Absence of correlation: driving 'Force' for the wavepackets belonging to different electronic states should not be averaged but different.

SET-2. Absence of microscopic reversibility: he considers that, in weak nonadiabaticity, an wavepacket started as state 1 but branched to the state 2 would be driven by the PES of 2 in backward process.

He also discuss other problems of SET in Ref. [26] as

SET-3. Absence of decoherence : he discusses that the spatially separated wavepackets should lose coherence.

SET-4. Lack of detailed balance : if the system is coupled to a finite temperature (classical) bath, the quantum system evolves into infinite temperature

SET-1. was thoroughly discussed in the main text, whereas we do not completely agree with **SET-2.**; in the described situation, if one propagates back the 'mixed' state wavepacket, it should be track back to the initial state.

As for **SET-3.**, the "decoherence problem", we have completely different views. We first point out that there do exist coherence between nuclear wavepackets as is seen in the Stueckelberg oscillation. Secondly, most importantly, what is often called "decoherence" in this type of discussion, which is described, for example in the NDM approach [73], is not a decoherence in the standard terminology; the term decoherence should refer to the statistical process where the off-diagonal elements of the density matrix diminishes through coupling to some random perturbations by thermal bath or impurities. There should be no decoherence in pure ensemble dynamics with no external perturbation, and the population of wavepacket, which belongs to the diagonal part of density matrix, should not diminish by decoherence. Thirdly, we can see that quantum wavepacket calculation do reproduce the correct dynamics without any decoherence. Problems in approximate methods should be attributed to incompleteness of the method. Fourth, one should be much careful in introducing terms that is absent in the original Hamiltonian (possibly never), for it would limit the applicability to unknown problems.

SET-4. deals with statistics and is beyond our curent scope.

Truhlar, on the other hand, also discusses the "decoherence" problem, but he also points out that the branched wavepacket, if any, should converge to a pure adiabatic state. The point is important, as an inappropriate branching may end in some mixed state in the asymptotic region, but it is not of large problem since in the asymptotic region, another branching is enough to decouple uncorrelated states.

He also points out following defects of surface hopping scheme:

SH-1 Representation dependence: The result is known to be representation (either adiabatic or diabatic) dependent.

SH-2 Discontinuous jump in the momentum and the effective potential on the hop

We do not fully agree with **SH-1**, since representation dependence is not a fatal defect in approximate methods although there should be definite prescription (as well as reasoning) on which representation to be adopted. PSANB adopts Force matrix eigenstate with clear reasoning while SET is known to be representation independent.

SH-2 was among motivations in the "natural" branching approach [25]. In addition, the

Pechukas dynamics, if possible, would reproduce the correct velocity of each branch with no discontinuity. On the other hand, there is no strong reason to believe that the wavepacket velocity should be continuous. We have also seen that in the imaginary time approach, the trajectory goes into imaginary time and emerges on the other surface with shifted momentum.

We can also see that the Pechukas dynamics is almost free from these problems; We first exclude **SET-3.** and **SET-4.** for above-stated reasons. What is called "correlation", or the channel dependence of nuclear driving force is reproduced by the path dependence of the Force form. The electronic path integral is fully covariant with respect to representation choice

APPENDIX H: FRAME CONVERSION

We next discuss a different type of problem. Up to here we have used the notion of electronic Hamiltonian $H^{ele}(\mathbf{X}_t)$ in the form exactly equal to that in the frozen nucleus model. Although it is quite common in the literature, however, as has recently been pointed out by Sutcliffe [92], an exact analysis of Lagrangean yields mass-polarization terms due to the kinematic coupling of electronic and nuclear degrees of freedom. Sutcliffe [92] further pointed out that, the correct (infinitesimal) electronic time-evolution operator, or the "correct electronic Hamiltonian" should include terms of the form $p_j p_k|_{j\neq k}$, which we hereafter refer to as the momentum-momentum coupling term, with small but nonzero coefficients (typically of order $\frac{m_e}{M_n}$, where M_n represents a typical nuclear mass).

Here we show that in the path-integral formalism, the electronic Hamiltonian can be defined without the electronic momentum-momentum coupling term, but with nuclear velocity that couples to the electronic term in the form of the gauge coupling. The electronic problem here is simplified than that of the Hamiltonian formalism in the sense the interaction terms (momentum-momentum coupling terms) are replaced by the couplings to "an external field", $\mathbf{V}$. We argue that, on the other hand, the remaining nuclear path integral, including the result of the first path integral as an effective action, should recover the correct momentum-momentum coupling effects to give the equivalent result as those obtained from the Hamiltonian formalism. We will show the equality in a simple model, although general proof is left for future study.

We consider the electronic coordinate relative to the center of mass (COM) of the nuclear subsystem. As we have formulated in Sec. 2 , we first 'fix' the nuclear variables and calculate

the electronic path integral as a functional of those nuclear variables. Here we set nuclear COM velocity V_τ and other nuclear coordinates as $\mathbf{X}_J$. The Lagrangian for the electronic part is written as

$$\mathcal{L}^{el} = \frac{1}{2}\sum_j m_e \left(\dot{\boldsymbol{\xi}}_j + \mathbf{V}_\tau\right)^2 - V_{ee}(\boldsymbol{\xi}) - U_{eN}(\boldsymbol{\xi}, \mathbf{X}_\tau). \tag{H.1}$$

Since the nuclear quantities are regarded as purely external fields, the Lagrangian transforms into the following Hamiltonian

$$\mathcal{H}^{el}(\mathbf{V}_\tau, \mathbf{X}_\tau) = \frac{1}{2m_e}\sum_j (\mathbf{p}_j - m_e\mathbf{V}_\tau)^2 + V_{ee}(\boldsymbol{\xi}) + U_{eN}(\boldsymbol{\xi}, \mathbf{X}_\tau) - \sum_j \frac{1}{2} m_e \mathbf{V}_\tau^2, \tag{H.2}$$

which includes a "vector potential" $m_e\mathbf{V}_\tau$, but is (at least formally) free of momentum-momentum couplings. The electronic transition amplitude is calculated as

$$\mathcal{K}_2(\xi_F, \xi_I : \mathbf{X}_\tau, \mathbf{V}_\tau) = \langle \xi_F | \lim_{N\to\infty} \prod_j e^{-\frac{i}{\hbar}\epsilon H^{el}(\mathbf{X},\mathbf{V})} | \xi_I \rangle, \tag{H.3}$$

which gives the effective action $S^{eff} = \frac{\hbar}{i}\ln \mathcal{K}_2$ as a functional of nuclear variables.

Due to nontrivial functional dependence on V_τ, it is difficult to directly show the equality of two formulation in general case. Below we consider a simple solvable model where S^{eff} is quadratic in V_τ.

Simplified model

Here we consider a model problem where two nuclei and two electrons interact via the harmonic potential on the mass-center of nuclei. We further assume the spatial dimension to be one, although simple extension to higher dimension is almost obvious. The Lagrangian reads

$$\frac{M}{2}\dot{X}^2 + \frac{\mu}{2}\dot{Y}^2 - U_{NN}(Y) + \sum_j \left[\frac{m_e}{2}\dot{x_j}^2 - \frac{1}{2}m_e\omega_j^2(x_j - X)^2\right] \tag{H.4}$$

where X and Y are the nuclear COM and the relative coordinates, respectively, and M and μ are corresponding total mass and reduced mass. The jth electronic coordinate is denoted as x_j. Using the Euler-Lagrange equations, the problem is solved as follows;

Nuclear relative coordinate Y is decoupled and is to be solved separately. The kinetic equations for the remaining nuclear COM coordinate X and the electronic coordinates are obtained as

$$\frac{d}{dt}\left(m_e\dot{x}_j\right) = -m_e\omega_j^2(x_j - X) \tag{H.5}$$

$$\frac{d}{dt}\left(M\dot{X}\right) = -\sum_j m_e\omega_j^2(X - x_j) \tag{H.6}$$

One can see that the total momentum is the constant of motion; $\frac{d}{dt}\left[M\dot{X}+\sum_j m_e\dot{x}_j\right]=0$. Since the potential term is quadratic, the solution for this problem is derived from the standard procedure; transformation to mass-weighted coordinate and diagonalize the potential matrix;

$$\begin{pmatrix} \omega_1^2 & & -\sqrt{\frac{m_e}{M}}\omega_1^2 \\ & \omega_2^2 & -\sqrt{\frac{m_e}{M}}\omega_2^2 \\ -\sqrt{\frac{m_e}{M}}\omega_1^2 & -\sqrt{\frac{m_e}{M}}\omega_2^2 & \sum_j \frac{m_e}{M}\omega_j^2 \end{pmatrix} \tag{H.7}$$

Assuming $\omega_1=\omega_2=\omega$, one obtain the eigen modes (in terms of mass-unweighted coordinate) x_1-x_2 with eigenvalue $\lambda_1^2=\omega^2$, $\sqrt{M}(x_1+x_2)-2\sqrt{m_e}X$ with eigenvalue $\lambda_2^2=(1+2\frac{m_e}{M})\omega$, and $m_ex_1+m_ex_2+MX$ with eigenvalue 0. Path integral with respect to these coordinate yields the total transition amplitude as the direct product of transition amplitude of these modes.

One can, on the other hand, formulate the problem with fixed nuclear COM and relative displacement coordinate of electrons; $\xi_j\equiv x_j-X$ as

$$L^e=\sum_j\left[\frac{1}{2}m_e(\dot{\xi}_j+V_t)^2-\frac{1}{2}m_e\omega_j^2\xi_j^2\right] \tag{H.8}$$

We first treat nuclear COM velocity V_t as external variable and solve the electronic problem influenced by V. Using $\eta_j\equiv m_e(\dot{\xi}_j+V)$, which is the momentum conjugate to ξ_j, one can write the Hamiltonian

$$H^e=\sum_j\left[\frac{1}{2m_e}(\eta_j-m_eV)^2-\frac{m_e}{2}V^2+\frac{m_e}{2}\omega_j^2\xi_j^2\right], \tag{H.9}$$

which is the Harmonic oscillator with external gauge field m_eV_t. The classical action for this problem is $S_J^{cl}(\xi_F,\xi_I,T)$ of the forced HO, with J replaced by the "vector field", $-m_e\dot{V}$. The resulting action S^{cl} is a functional of V, but using the partial integration twice, it can be converted as the functional of X.

One then solves the nuclear path integral with the effective action $S^{cl}[X_\tau]$, functionally dependent on the function X_τ. Here we note that the quadratic part of the functional becomes

In particular, the quadratic term becomes

$$-\sum_j\frac{m_e}{2\omega_j\sin\omega_jT}\left\{\int_0^T d\tau V_\tau^2\sin\omega_jT+\int_0^T d\tau\int_0^T d\tau' V_\tau V_{\tau'}g(\tau,\tau')\right\} \tag{H.10}$$

where $g(\tau,\tau') \equiv -\frac{\sin\omega(T-t_>)\sin\omega t_<}{\omega\sin\omega T}$, which is the Green's function for $m_e\frac{d^2}{dt^2}+m_e\omega^2$. Using the Fourier transformation, the total action for nuclear COM mode becomes

$$S=\frac{1}{2}\sum_n X_n\left[M\nu_n^2-\sum_j m_e\omega_j^4\left(\frac{1}{\nu_n^2-\omega_j^2}+\frac{1}{\omega_j^2}\right)\right]X_n \tag{H.11}$$

where $\nu_n \equiv \frac{n\pi}{T}$ and X_n is the Fourier series expansion coefficient of the fluctuation part of X_t: $X_t = \sum_n \sqrt{\frac{2}{T}}\sin(\nu_n t)X_n$. Just in the analogous way as that in the linearly coupled oscillator model we analyzed in the main text, the matrix kernel inside the bracket in Eq. (H.11) is transformed as

$$D_n = \frac{M\nu_n^2(\nu_n^2-\lambda_1^2)(\nu_n^2-\lambda_2^2)}{(\nu_n^2-\omega_1^2)(\nu_n^2-\omega_2^2)} \tag{H.12}$$

hence the square root inverse of this bracket $\prod_n\sqrt{1/D_n}$ times the 'temporary' prefactor obtained through the electronic path integral $\sqrt{\frac{m_e^2}{(2\pi i)^2\sin\omega_1 T\sin\omega_2 T}}$ yields the correct prefactor $\sqrt{\frac{Mm_e^2}{2\pi i T\sin\lambda_1 T\sin\lambda_2 T}}$.

Part II

Application to dynamics in intense laser fields

1. INTRODUCTION

Notation In this section, we use symbol I and E_0 to represent the laser intensity and the electric field amplitude, respectively. Vectors $\mathbf{A}$ and $\mathbf{E}$ are used to represent the vector field and the electric field, $\boldsymbol{\mu}$ is used for the (total) molecular dipole momentum. Standard notations, m, c, ω and λ are used to represent the electronic mass, the speed of light, the angular frequency and the wavelength of the field, respectively. Symbol q_e is used to represent the electronic charge (-1 in the atomic unit). U_p represents the (nonrelativistic) quiver energy in spatially uniform laser field $U_p \equiv \frac{1}{4m}\left(\frac{q_e}{c}\mathbf{A}\right)^2$. The field-matter interaction term in the Hamiltonian is represented by V_F, which is $V_F = -\boldsymbol{\mu}\cdot\mathbf{E}$ in the dipolar gauge and $V_F = -\frac{q_e}{mc}\mathbf{A}\cdot\mathbf{p} + \frac{1}{2m}\left(\frac{q_e}{c}\mathbf{A}\right)^2$ in the radiation gauge.

1-1. Characterization of strong field

We first characterize the term 'strong field' in order to clearly define the scope of this study.

The electric field amplitude The electric field amplitude E in the atomic unit is the simplest measure of intensity, which is related to the laser field intensity as $I = cE_0^2/8\pi$, which gives $E_0 = 0.1 \times \sqrt{\frac{I[\mathrm{TW/cm^2}]}{351}}$. Assuming that the scale of dipole matrix element to be unity in the atomic unit, it characterizes the strength of field-matter interaction term (in the dipole gauge) $\boldsymbol{\mu}\cdot\mathbf{E}$. It then follows that 3.51TW/cm^2 and 351TW/cm^2 give the value 0.01 and 0.1, respectively. Typical values of atomic field strength in diatomic molecules can be found from the Morse function fit of the ground state PES; which gives 0.037, 0.079 and 0.067 for H_2^+, HCl^+ and LiF[11], hence field strength of 0.1 is strong enough for these molecules to totally change the geometry of their intrinsic PESs.

[11] We first fit the ground state PES by the Morse function $W(R) = K(e^{-2D(R-R_{eq})} - 2e^{-D(R-R_{eq})})$ and estimated the typical value of the gradient force as $F = DK/2$, which is the maximum value of $\left|\frac{dW}{dR}\right|$ in the range $R > R_{eq}$.

Estimate on the field-matter correlation From theoretical point of view, however, the field strength E_0 alone does not determine the behavior of the system independently on the intrinsic properties of the molecule. There need a different measure which directly characterizes field-matter correlation, or the multiphoton-coupled behavior of the wavefunction. In this viewpoint, we characterize the matter (often electron) wavefunctions as showing correlated (multiphoton) behavior if their Fourier series expansion in the laser frequency has non-negligible weights over multiple components. To confirm the validity of this definition, we first consider an electron that interacts only with a classical monochromatic vector field of long wavelength limit; $\mathbf{A}(\mathbf{r},t) = \mathbf{A}_0 \cos\omega t$. The Schrödinger equation in the radiation gauge

$$i\hbar\dot{\Psi} = \frac{1}{2m_e}\left(\mathbf{p} - \frac{q_e}{c}\mathbf{A}\right)^2 \Psi \tag{1.1}$$

has solution (Volkov state) $\Psi_t = e^{i\mathbf{p}\mathbf{x}} \exp\left[-\frac{i}{\hbar}\int^t d\tau \frac{1}{2m}\left(\mathbf{p} - \frac{q_e}{c}\mathbf{A}_\tau\right)^2\right]$. [12]. Its fourier series expansion is given as

$$\Psi_t = e^{-\frac{i}{\hbar}(\varepsilon_{\mathbf{p}}+U_p)t} \sum_{n,k} J_{n-2k}(-q_e \frac{\mathbf{A}\cdot\mathbf{p}}{mc\hbar\omega}) J_k(\frac{U_p}{2\hbar\omega}) e^{-in\omega t}, \tag{1.2}$$

where $J_\ell(x)$ are Bessel functions. This superposition is essential in derivation of non-resonant ionization rate in strong optical field in the Keldysh's pioneering paper[40]. In fact Ref. [40] is based on rather a straightforward time-dependent perturbation theory using the Volkov state as the final state. In Eq. (1.2) the Fourier series typically extends over $\ell \sim \sup\left(|q_e \frac{\mathbf{A}\mathbf{p}}{mc\hbar\omega}|, |\frac{U_p}{\hbar\omega}|\right)$. Then our definition applies if $|q_e \frac{\mathbf{A}\mathbf{p}}{mc\hbar\omega}| \gtrsim 1$ or $|\frac{U_p}{\hbar\omega}| \gtrsim 1$, which states dominance of the scale of field-matter interaction term or that of the quiver energy over the photon energy, respectively.

In order to extend this idea to more general problems in an atomic potential, we recall the Floquet theory, which, in this case, states that the solution of time-dependent Schrödinger equation is given by a (superposition of) eigenstate(s) of the Floquet operator $\mathcal{H} \equiv H - i\hbar\partial_t$;

$$\Psi_t = \sum_\alpha \Phi_\alpha(t) e^{-\frac{i}{\hbar}\lambda_\alpha t} \tag{1.3}$$

where $\Phi_\alpha(t)$ is the eigenstate of the Floquet operator, or Floquet state, with quasi energy λ_α; $\mathcal{H}_t\Phi_\alpha(t) = \lambda_\alpha\Phi_\alpha(t)$. It is a periodic state that represents a 'field-dressed' quastationary

[12] In the length gauge,

$$i\hbar\dot{\Psi} = \left(\frac{1}{2m_e}\mathbf{p}^2 - q_e\mathbf{r}\cdot\mathbf{E}\right)\Psi$$

is solved as $\Psi_t = e^{i\left(\mathbf{p} - \frac{q}{c}\mathbf{A}'_t\right)\cdot\mathbf{x}} \exp\left[-\frac{i}{\hbar}\int d\tau \frac{1}{2m}\left(\mathbf{p} - \frac{q_e}{c}\mathbf{A}'_\tau\right)^2\right]$ with $\mathbf{A}'_t \equiv -c\int^t d\tau \mathbf{E}_\tau$, which is mere a gauge transformation of the previous one

state. Due to the periodicity, Floquet states can be expanded in the Fourier series. We hence have an expansion, using an arbitrary time-independent basis set $\{|I\rangle\}$,

$$|\Phi_\alpha\rangle = \sum_I |I\rangle \sum_n C_\alpha^I[n] e^{-in\omega t} \tag{1.4}$$

For convenience of later discussion, we introduce subvector $\mathbf{C}_\alpha[n]$ which is a column vector of nth Fourier coefficients whose Ith component is $C_\alpha^I[n]$, and submatrix $\mathcal{H}_{n,m}$ which acts on the mth Fourier coefficient vector to give nth Fourier coefficient vector. The definition of multiphoton behavior is characterized as nonnegligible weight distribution over different n subvectors. Such distibution should be governed by the scale of off-diagonal submatrices relative to $\hbar\omega$. The condition for 'multiphoton behavior' is then given as $\mathcal{H}^{off} \gtrsim \hbar\omega$.

In the mean time, we should also be careful of the validity of the Floquet state expansion, in realistic situations, where the perfect periodicity is broken due to the nonperiodic change of pulsed field amplitude. Generalized Floquet anslysis in Sec. 2 will suggest that the sufficient condition is smallness of nonadiabatic coupling terms among the Floquet states relative to the quasienergy differences; $\left|\langle\langle\alpha|i\hbar\dot{\zeta}^\mu \frac{\partial V_F}{\partial \zeta^\mu}|\beta\rangle\rangle\right| \ll |\lambda_\beta - \lambda_\alpha|^2$. A practical requirement for the pulse shape is $\sqrt{\left\|\hbar\dot{A}_0 \frac{\partial V_F}{\partial A_0}\right\|} \ll \inf V_F, \omega$ (in a typical situation where $\omega > V_F/\hbar$, it requires that the time scale of amplitude variation should be longer than the Rabi-cycle).

Relativistic scale as the upper limit Validity of non-relativistic treatment is limited by the condition $\left|q_e \frac{A}{c}\right| \lesssim mc$. For laser wavelength $\lambda = 780$nm, the limit is around 10^{18} W/cm^2. Beyond this scale, one should take into account relativistic effects, including Coulomb field correction, magnetic interaction, pair creation, which are absent our current scope.

Realistic estimates We should also examine a 'realistic' or empirical estimate that takes account of properties of existing molecules and various experimental observations. Refs. [5, 96] suggests the typical lower limit to be 10^{13} W/cm^2. The value matches with experimental reports [55, 69, 71], which suggest that it is a threshold value for causing a significant change in field-induced PES, resulting in the bond hardening in H_2^+ [55]. The field strength of 10^{13} to 10^{14} W/cm^2 is also important scale for moderate reaction engineering [69, 71] which avoids fast ionization. It will also be shown that model calculation of simplest molecule H_2^+, assumed to be perfectly aligned in the polarization axis, dissociates at intensity $I \gtrsim 10^{13}$ W/cm^2.

As for the upper limit, Ref. [5] sets a value $I^{upp} = 10^{18}$ W/cm^2, beyond which, according to Ref. [5], the valence electrons get rapidly strip off and their behavior is dominated by the field rather than the intrinsic atomic field. The condition appears to be empirical but important in the context of chemistry. This I^{upp} corresponds to $E \approx 5$, which may justify the scale as the threshold for molecules to keep its valence electron.

Our scope of strong field is then summarized as follows;

1. Strong non-resonant effects on the electronic potential field, or large deformation of original PES to form field-dependent Quasi Energy Surface (QES). This is characterized by strength of field; $E \gtrsim$ (atomic Coulomb field strength) as well as significant multiphoton behavior; $\|\mathcal{H}^{off}\| \gtrsim \hbar\omega$.

2. The upper limit should be limited by the requirement of small relativistic effect $\frac{q}{c}A \ll mc$. It should also be restricted by some material-specific parameters where the molecule can keep its inner core electrons.

3. For Floquet-type description to be valid, the scale of nonperiodic changes $\|\hbar\frac{d}{dt}\mathcal{H}^{off}\|$ should be limited by the square of a typical quasienergy difference. Furthermore, if one is to exclude ionization processes, the intensity will be further limited by a material-specific value beyond which a significant amount of ionization occur.

These remarks are basically consistent to literatures; in Ref. [5], for example, field intensity is characterized in more intuitive manner using the Rabi frequency $\omega_R \approx |V_F|/\hbar$, and the field is described as 'super' intense if it exceeds ω. The condition is essentially in accord with the above discussions. On the other hand, the Keldysh parameter, which often appears in literature, is irrelevant here since we do not consider ionization.

In practical calculation, one should check relative scale of the optical frequency and the relevant nuclear vibration mode frequency. This is not directly related to field-matter correlation, but related to electron-nucleus correlation. We will come back on this issue later.

1-2. Molecules in intense laser field

We next review two characteristic field-induced phenomena in molecules; field-induced ionization and dissociation. As we have discussed in the General Introduction, these are closely related to the probing (by HHG) and the reaction engineering.

i. Field-induced ionization

Although our current calculation method is not applicable to ionization problems, we briefly review the field-ionization and its effects relevant for our study. Its relevance for our study include drastic effects on the chemical bond and its use as an experimental probe. Moreover, ionization is a fundamental process in the field-induced dynamics in that there can be no definite bound state in presense of an electric field. All field-induced effects therefore occur in competition with the ionization, although in practice, the occurrence of the latter in weak to moderate field is exponentially suppressed.

Perturbation theory The simplest approach to this problem is the time-dependent perturbation theory. Assuming the boundary condition $|\psi_t\rangle \to |\phi_0\rangle$ in the long past $t \to -\infty$ and neglecting any depletion effects in the intermediates, nth order perturbative estimate of n photon absorption is given as

$$|\psi_t^{(n)}\rangle = e^{-\frac{i}{\hbar}(E_0+n\hbar\omega)t} \prod_{k=1}^{n} \left[\frac{1}{E_0 + k\hbar\omega + i0 - \hat{H}_0} \hat{V}_F^+ \right] |\phi_0\rangle, \tag{1.5}$$

where V_F^+ is the 'absorption' part (those propotional to $e^{-i\omega t}$) of the field-matter interaction term. The unit time n-photon ionization probability $d\mathcal{P}_n/dt$ is given as

$$\frac{d\mathcal{P}_n}{dt} = \frac{2\pi}{\hbar} \left| \langle \mathbf{k}_f | V_F^+ | \psi^{(n-1)} \rangle \right|^2 \rho(E_f) \tag{1.6}$$

where E_f is the final state energy $E_f = E_0 + N\hbar\omega > 0$, while $\mathbf{k}_f$ and $\rho(E_f)$ are the momentum and the energy density corresponding E_f. Within this approximation, $dP_n/dt \propto I^n$, which is indeed an appropriate estimate in the weak field limit. Perturbative approach, however, breaks down when the depletion of the ground state becomes non-negligible. Ref. [4] suggests its severe deviation from the reality at around $I \gtrsim 10^{13}$ W/cm^2 in a typical rare gas ionization experiments.

Tunnel ionization in a static field Another approach to this problem is tunneling analysis. The tunneling effect in a static electric field was calculated by Landau [97]. A generalized version for Hydrogen-like atom with nuclear charge Z, angular momentum ℓ in static field of amplitude F, the ionization probability per unit time, in atomic unit, is given as[41, 97]

$$w = \frac{\kappa^2}{2} |C_{\kappa\ell}|^2 (2\ell+1) \left(\frac{2\kappa^3}{F} \right)^{2\lambda-1} e^{-\frac{2}{3F}}, \tag{1.7}$$

where κ is the asymptotic (imaginary) wavenumber corresponding to the bound-state energy as $-\kappa^2/2 = E_b$, and the bound state wave function is assumed to asymptote as $C_{\kappa\ell}\sqrt{\kappa}^3(\kappa r)^{Z-1}e^{-\kappa r}Y_{\ell m}(\theta,\phi)$. Here the exponential dependency with the exponent $-\frac{2}{3F}$ is to be remarked.

Improved perturbation theory using the Volkov state The tunneling ionization theory in optical fields is pioneered by Keldysh[40]. He used time-dependent perturbation theory like those discussed above, but assumed the final state to be the Volkov state (thereby incorporating a part of expansion of Eq. (1.5) in infinite order). In his approach, the first order expansion in the perturbation series is enough to describe multiphoton effects due to the intrinsic multiphoton character in the Volkov state. His result can be expanded in the nondimensional quantity, which is now called the Keldysh parameter, $\gamma \equiv \sqrt{I_p/2U_p}$, more intuitively, $\gamma = \omega\tau_T$, the product of optical frequency and typical 'tunneling time' $\tau_T \equiv I_p/\sqrt{2I_p/m}$. The tunneling limit, in particular, $\gamma \ll 1$ is obtained as an infinite summation over the γ expansion. Later, a similar approach with different form of perturbation expansion is proposed by Perelomov, Popov and Terrent'ev (PPT) [41], which has correct asymptotic behavior in the static limit $\omega \to 0$, which is Eq. (1.7). Their conclusion is applied on Hydrogen-like atomic model by Ammosov, Delone and Krainov (ADK)[42] to derive a tunneling ionization probability formula for general atomic problems, which is now called the ADK formula. The ADK formula has been favorably applied to many experimental situations and its accuracy has been, at least qualitatively, established.

These approaches, however, involve a number of approximations including (a) approximation on the final state as the potential free Volkov state (b) approximation on the initial state as the eigenstate of the field-free atomic Hamiltonian and (c) neglect of higher order effects such as recollisions. Perturbative corrections to the Keldysh's approach has been investigated by Faisal and coworkers [98].

Extension to molecular systems Up to here all the theories assume atomic problems with central symmetry. In particular, in PPT-ADK approach, the initial state, in the asymptotic region with $r \gg 1/\kappa$, was assumed a Coulombic form $C_{n\ell}\left(\frac{Z}{n^*}\right)^{1/2}\left(\frac{Z}{n^* r}\right)^{n^*-1}\exp(-\frac{Z}{n^*}r)Y_{\ell m}(\theta,\phi)$. A molecular extension of ADK approach, which is now called as 'molecular ADK', was formulated in Ref.[99]. In this approach, the HOMO of a given molecule is expanded in central symmetric form with its coefficient $C_{n\ell}$ determined

by numerical calculations to apply the PPT's result. Here an implicit assumption is the correspondence to the atomic problem with the same ionization potential. The correspondence is experimentally observed in some molecular species such as N_2 (correspondence to Ar) and O_2 (Xe), but there have also been found exceptions such as F_2 (Ar)[99]. In addition, large deviation of angular dependence is found in CO_2 [100, 101].

The approximations in MO-ADK, aside with those inherent in the atomic ADK, include (d) neglect of ionization from lower-lying orbital than HOMO and (e) neglect of nuclear configuration dependence beyond the central symmetric expansion. For example, the origin of wrong angular distribution of the CO_2 ionization has been attributed to the assumption (d) [62, 102]; MO-ADK predicts dip of ionization probability in the direction from geometrical property of HOMO, but detailed calculation show that contribution from the second HOMO partly fills the dip. Also, breakdown of the assumption (e) is seen in the enhanced ionization in H_2^+ at the 'critical internuclear distance' R_c [48], which is the point where nuclear potential changes its shape from the single-well structure to the double-well one Due to its simplicity, however, MO-ADK has been accepted as a standard reference. It is then possible to use deviations from the MO-ADK prediction as a clue for the effects neglected in the MO-ADK.

Numerical approaches Numerical approaches to field-ionization problem include numerical integration of the time-dependent Schrödinger equation (TDSE) [103, 104], time-dependent density functional theory (TDDFT) [102, 105]. Among all, TDSE is the most unbiased approach but its direct application is severely limited for multielectron problems. Number of variants have also been proposed in expence of the original exactness [106]. TDDFT [107], which reduces the original problem to an effective single electron problem, is much adapted to large scale multielectron problem, however, its accuracy depend on the choice of exchange-correlation potential [105]. Another possibility is an extension of R-matrix method [108]. There have been proposed R-matrix Floquet theory [109] for periodic problem and time-dependent R-matrix theory [110] for more general problems. The key advantage of these methods is division of the whole space into the 'inner region' where standard bound-orbital expansion is valid and the 'outer region' where reduction to single electron problem is easier. Disadvantages, on the other hand, arise from difficulty of the boundary condition posed on the expansion basis.

ii. Field-induced dissociation

In principle there are two approaches to induce molecular dissociation with an optical field; (a) Inducing electronic (dipole) transition to non-bonding orbital and/or (b) exciting nuclear vibration mode. Field effect on a nucleus is, in general, estimated to be far smaller than that on an electron because of smaller specific charge. Exception occurs in the case the optical frequency is close to the nuclear vibrational frequency, where dominance of nuclear excitation is observed from numerical calculations assuming $\lambda \gtrsim 2000\mu$m [111, 112].

Here we have to reconsider the relative scale of optical frequency and relevant vibrational mode frequency. If the latter is small enough, we can first combine the In what follows, however, we assume the optical frequency to be much larger than relevant nuclear vibrational frequencies and concentrate on the electronic excitation scenario.

Quasiclassical analysis based on the field-induced PES Slow nuclear dynamics in quasiperiodic optical field can be understood as nonadiabatic dynamics on the field-induced PES or what we will call the quasienergy surface (QES) in later sections. In this description, deformation of the field-induced PESs from those in the zero-field limit, describes the field-matter coupled effects. From an analogy to the standard field-free nonadiabatic dynamics, maximum deformation of order $|V_F^+|$ occurs near resonance points.

In view of chemical bond, there can be two possibilities; bond softening due to lowering barrier height or bond hardening due to nuclear wavepacket trapping (to be strict, bonds are referred to be hardened if the unit time dissociation probability decreases with increasing field strength). Theoretical analyses using Floquet analysis [53, 54] predict occurrence of both effects in continuous wave (CW) laser. In practice, however, details of wavepacket dynamics do depend on time-dependent raise and fall of pulsed field strength [113] (see also our discussion in the numerical part).

On application of this type of theory, however, much care has to be payed on the possibility of ionization, which is beyond this analysis. As we have discussed before, field-induced dynamics always accompany possible ionizations, which often lead to fast dissociation with higher energy ionic fragments (in case of H_2^+, ionization causes a Coulomb explosion). In practice, however, due to exponential dependence on the field strength, ionization probability can be suppressed in weak to moderate field intensities (for example, Ref. [49] suggests the threshold intensity of the ionization of H_2^+ to be 8×10^{14} W/cm^2 or more). In some

cases, ionic fragments generated by Coulomb explosions can be distinguishable by their large kinetic energy release [114], but other numerical study [115] suggests significant mixture of its contribution to other processes.

Experimental Observations We next review experimental studies. Ref. [52] is among the earliest experimental observation of the bond-softening effect, where broadening of photoelectron kinetic energy spectrum from H_2 in strong field as 100TW/cm^2 was attributed to the subsequent low-energy dissociation. Later studies [49, 113–115] directly observe of dissociated ionic fragments, and low-energy ionic fragments with relatively sharp angular distribution (i.e. strongly aligned in the polarization axis) is attributed to arise from the bond softening. As for the bond hardening, the experimental evidence is much more controversy; an earlier report by Zavriyev and co-workers[55] observed the ionic kinetic energy spectrum from H_2^+/D_2^+ and attributed the higher energy peak to arise from ionization from trapped state followed by Coulomb explosion. Whereas later studies by Frasinski and coworkers [113, 114] attribute lowest (near zero) energy proton fragments with a broad angular distribution to be arising from the trapped state.

In these experimental studies, key observables are the kinetic energy distribution of the ionic fragments or ionized electrons, either angle-resolved or angle-integrated. Earlier studies, for example, Ref. [113] used the time-of-flight (TOF) measurement techniques [116] to measure the kinetic energy of ionic fragments released in the direction parallel to the detector axis. They also measured energy-integrated angular distribution to supply the orientational information. In more recent studies, the velocity map imaging techniques [117] have been particularly favored, in which the velocity distribution perpendicular to the axis is projected on the detector plane.

Theory-Experiment correspondence Quantitative correspondence of theoretical calculation and experimental observation (from theoretical side) was studied in Ref. [115]. The first step to achieve this was to solve the time-dependent Schrödinger equation in three-dimensional space with molecular rotational degrees explicitly taken into account [118]. They thus obtained energy-angle-resolved probability distribution $P_{v,J,m}(\theta, k)$, where v, J and m denotes the inital state vibrational and angular quanta. Then in the second step the results are then averaged over initial state distribution (experimentally determined vibrational distribution and the Boltzmannian angular state distribution). The numerical results compared

well with the experimental ones in the finite angle ($\pi/7$ and $\pi/4$) but not in zero-angle to the laser polarization. The divergence was attributed to small-angle Coulomb explosion, that was missing in the theoretical treatment. A critical factor for such correspondence, suggested in Refs. [115, 118] is the channel-dependent energy/angular distribution of ionic fragments. Correctness of such distribution as well as branching ratio then makes a test of theoretical calculations.

Studies in the opposite direction, experimental identification of the underlying dissociation pathway has also been investigated [119]. In fact such attribution has not been established in molecules other than H_2^+.

Reaction engineering One of the most intriguing application of laser-induced dynamics is reaction engineering. Rabitz's learning algorithm [67] automatically finds out the optimal pulse shape without any need of theoretical estimate. As we have discussed in the introduction, however, the method is not complete and there are still needs for theoretical development. Some studies [122] directly calculate Rabitz's variational functional so as to numerically find out optimized pulse shape. This work does not take this approach but seek for development of fundamental theory. One of our expectations, however, is that development in the nonadiabatic Floquet analysis can be used for estimate or interpretation of optimization results to design or improve the experimental setting before actual process of optimization.

Summary Relevant indications for our study, obtained in this review subsection is summarized as follows;

1. The idea of nonadiabatic dynamics on the field-induced PES is potentially powerful with clear physical insights, but detailed verification is required for practical applications. This will be the central theme in the Part II.

2. The obtained analyses have to be applied extensively on wider variation of molecules other than H_2^+ where much less of the mechanisms have been established. In this work, an attempt in this direction will be made through the analysis of LiF, whereas much extensive study has to be performed in the future.

3. In order to further validate theory against experimental results up to quantitative level, three-dimensional calculation of kinetic energy release including its energy/angular distribution need to be clarified. This will be left as our future task.

1-3. Generalized Floquet Hamiltonian method

We have thus seen a rapid progress in the experimental researches and growing needs for advanced theoretical calculation methods. On the other hand, the applicability of exact full-quantum treatment is limited to simplest molecules [120, 121] due to the large computational cost.

We here investigate MQC approach. We have seen the possibility of interpreting the field-induced nuclear dynamics as quasiclassical dynamics on the field-induced PES. In order to ensure the accuracy, we first establish the exact theory of generalized Floquet Hamiltonian method. Combining this theory and our discussions in Part I, we derive the gradient approximation with definite application conditions. We then perform a numerically exact (equivalent to the full-quantum treatment of TDSE) calculations on model systems to establish the exactness of the theory and validity of the gradient approximations.

In order to convert the intuitive idea of field-induced PES to exact theory, there are several problems to be resolved. We first see that the notion of the field-induced PES needs concrete definition. Its mathematical basis is on the Floquet theorem [126], which, in this case, states the stationarity of the Floquet state (eigenstate of the Floquet Hamiltonian$\mathcal{H} = H - i\hbar\partial_t$) in the periodic background Field. A field-induced PES is nothing but a quasi energy (eigenvalue of Floquet Hamiltonian) as a function of nuclear coordinate. In this view, we hereafter use the term quasi energy surface (QES) in place of field-induced PES.

The validity of the intuitive analysis is hence ambiguous when the exact periodicity (of the electronic Hamiltonian) is broken due to the nonperiodicity of the laser field and/or nuclear motion. Moreover, nuclear dynamics accompany kinematically induced nonadiabatic transitions through the intrinsic derivative couplings. In order to obtain an exact result, one has to generalize the Floquet Hamiltonian method to incorporate this nonstationarity in form of generalized nonadiabatic transitions among Floquet states. In fact such generalization has first emerged in the literature by Ho and Chu's work [128].

Here we derive the generalized Floquet Hamiltonian method using the two-time formalism of Pesikin and Moiseyev [127] (or what theses authors call (t, t')-formalism). It was found that a generalization equivalent to the Ho and Chu's work can be established in more robust ground with broader applicability.

The theory thus implemented is applied to field-induced bond dynamics mainly to see how it works. We first calculate H_2^+ and its isotope D_2^+, using a modeled Hamiltonian without

nuclear derivative couplings, to verify the present formalism. We will also examine whether this approach can provide clearer insights into the underlying mechanisms such as the bond softening[51–53] and the bond hardening[54, 55]. We next treat a problem, in which the intrinsic nuclear derivative couplings are explicitly involved. We are particularly interested in such systems where the nuclear kinematic effects play an essential role in a dissociation process. Such system can be found, for example, in a typical ionic bound diatomics, such as LiF, in which the lowest ionic and covalent PESs have an avoided crossing. We calculate *ab initio* PESs and matrix elements of LiF to perform dynamical calculations with all nonadiabatic effects fully taken into account. These results all show in the end that the present theory is promising as a general method for unified treatment of field-induced and intrinsic nonadiabatic transitions.

The organization of Part II is as follows; We first formulate the theory and method in Sec. 2. Numerical calculations of H_2^+/D_2^+ and LiF are then discussed in Sec. 3 and Sec. 4, respectively. This part concludes in Sec. 5.

2. FORMULATION OF GENERALIZED FLOQUET HAMILTONIAN METHOD

In this section, we formulate a generalized Floquet Hamiltonian method that is applicable to nonperiodic dynamics. Our derivation is based on an extended formulation of time-dependent quantum dynamics that uses two time-like variables, originally developed by Peskin and Moiseyev[127] as the name of (t, t') formalism. After briefly outlining the basic formulation in Subsec. 2-1, we formulate a nonadiabatic Floquet analysis in Subsec. 2-2.

2-1. Two-time formulation of quantum dynamics

Let us begin with the time-dependent Schrödinger equation

$$i\hbar\frac{\partial}{\partial t}|\psi_t\rangle = H_t|\psi_t\rangle, \tag{2.1}$$

where $|\psi_t\rangle$ is the state vector of the system. Up to this point, no restriction is imposed on the time dependence of the Hamiltonian H_t. The state vector $|\psi_t\rangle$ is then extended to a function of two time variables $|\widetilde{\psi}_{t,s}\rangle$, which is related to the original, or the physical state, by

$$|\widetilde{\psi}_{t,s}\rangle|_{t=s} = |\psi_t\rangle. \tag{2.2}$$

The Schrödinger equation for the extended state is then given by

$$\left(i\hbar\frac{\partial}{\partial t}+i\hbar\frac{\partial}{\partial s}\right)|\widetilde{\psi}_{t,s}\rangle = H_t|\widetilde{\psi}_{t,s}\rangle \tag{2.3}$$

or, equivalently,

$$i\hbar\frac{\partial}{\partial t}|\widetilde{\psi}_{t,s}\rangle = \mathcal{H}_{t,s}|\widetilde{\psi}_{t,s}\rangle \tag{2.4}$$

with the Floquet-type operator $\mathcal{H}_{t,s} \equiv H_t - i\hbar\frac{\partial}{\partial s}$.

2-2. Formulation of quasiperiodic quantum dynamics

Now we impose quasiperiodic assumption (the terms inducing nonperiodicity will be specified below) on the Hamiltonian. In so doing, our formalism deviate from that in Ref. [127]. We first introduce an extended Hamiltonian $\widetilde{H}_{t,s}$ that is dependent on the two time variables. It has a formal periodicity in the second variable s in the sense

$$\widetilde{H}_{t,s+T} = \widetilde{H}_{t,s}, \tag{2.5}$$

where the fundamental period T is assumed to be a fixed constant[13]. The t-variable dependence of the extended Hamiltonian $\widetilde{H}_{t,s}$ is arbitrary except that it is assumed to have a timescale T_{np} (np stands for nonperiodic) much longer than T ($\frac{T}{T_{np}} \ll 1$) so that the Hamiltonian H_t is quasiperiodic in the sense $H_{t+T} = H_t + O(\frac{T}{T_{np}})$. The physical Hamiltonian is related to $\widetilde{H}_{t,s}$ by

$$H_t = \widetilde{H}_{t,s}|_{s=t}. \tag{2.6}$$

An example of quasiperiodic Hamiltonian is that of a system under a time-dependent optical field

$$H_t = H_0 - \boldsymbol{\mu}\cdot\boldsymbol{\varepsilon}E(t)\cos\omega t, \tag{2.7}$$

where H_0 is the time-independent part, $\boldsymbol{\mu}$ and $\boldsymbol{\varepsilon}$ are the dipole operator and field polarization vector, respectively. The field amplitude $E(t)$ varies slowly with the variable t over multiple optical periods. One can then construct a two-time counterpart of this Hamiltonian as

$$\widetilde{H}_{t,s} = H_0 - \boldsymbol{\mu}\cdot\boldsymbol{\varepsilon}E(t)\cos\omega s, \tag{2.8}$$

[13] This restriction can be lifted to allow time-dependence of the frequency as is shown in the Appendix. B

which has formal periodicity in the variable s for a fixed value of t, and is related to the original Hamiltonian by Eq. (2.6).

Let $\mathcal{R}_t$ collectively represent slowly-varying system-parameters. It can be readily seen that a two-time extended Hamiltonian of the form $\widetilde{H}_s(\mathcal{R}_t)$, which is periodic in the variable s and dependent on the variable t only through $\mathcal{R}_t$, has the same type of periodicity. The parameters most relevant for the later discussions are the nuclear positions, represented by a collective vector $\mathbf{R} = (\mathbf{R}^1, \mathbf{R}^2, ..., \mathbf{R}^N)^T$, with each $\mathbf{R}^I$ being the position of Ith nucleus. The other examples are laser parameters such as the field amplitude and the polarization, which are formally represented as ζ^μ (see Eq. (2.13))

In this paper, laser frequency ω is assumed to be a constant, although it can also be among time-dependent parameters as in the case of chirped pulse. Extension of our formalism to such more general case is discussed in Appendix B

Substituting the parameterized Hamiltonian $\widetilde{H}_s(\mathcal{R}_t)$ into Eq. (2.4), the Floquet-type operator becomes $\mathcal{H}_s(\mathcal{R}_t) = \widetilde{H}_s(\mathcal{R}_t) - i\hbar\frac{\partial}{\partial s}$, which is now a true Floquet operator in the sense that it has the exact periodicity in the variable s. It thus follows that the eigenstates of this Floquet operator $\mathcal{H}_s(\mathcal{R}_t)$ are also periodic in the variable s. We define parameterized Floquet states

$$\mathcal{H}_s(\mathcal{R}_t)\,|\Phi_\alpha(s);\mathcal{R}_t\rangle = \lambda_\alpha(\mathcal{R}_t)|\Phi_\alpha(s);\mathcal{R}_t\rangle, \tag{2.9}$$

where $\lambda_\alpha(\mathcal{R}_t)$ is the αth Floquet quasienergy. Restricting our attention to the discrete spectrum, we can further impose mutual orthonormality with respect to the inner product $\langle\langle\cdot\rangle\rangle$ defined as

$$\langle\langle u|v\rangle\rangle \equiv \int_0^T \frac{ds}{T}\langle u_s|v_s\rangle, \tag{2.10}$$

where T is the fundamental period as indicated in Eq. (2.5).

We now consider an electron-nucleus coupled system. We denote the two-time extension of the total state as $\widetilde{\Psi}_{t,s}$. The corresponding Schrödinger equation, in the nuclear coordinate representation, becomes

$$i\hbar(\frac{\partial}{\partial t}+\frac{\partial}{\partial s})\langle\mathbf{R}|\widetilde{\Psi}_{t,s}\rangle = \left[\sum_I \frac{1}{2M_I}\left[\frac{\hbar}{i}\frac{\partial}{\partial\mathbf{R}^I} - \frac{Q_I}{c}\mathbf{A}\right]^2 + U_{nuc}(\mathbf{R},t) + \widetilde{H}_s^{ele}(\mathcal{R}_t)\right]\langle\mathbf{R}|\widetilde{\Psi}_{t,s}\rangle, \tag{2.11}$$

where $\langle\mathbf{R}|$ is the bra vector associated with the position eigenstate of nuclei $|\mathbf{R}\rangle$, M_I and Q_I are the mass and charge of the Ith nucleus and $U_{nuc}(\mathbf{R},t)$ is the nuclear potential term.

A is the vector potential. Throughout this paper, optical fields are treated within the long wavelength approximation. $\widetilde{H}_s^{ele}(\mathcal{R}_t)$ is the electronic Hamiltonian including electron-nucleus interactions. We then define the Floquet states $\{|\Phi_\alpha(s);\mathcal{R}_t\rangle\}$ as the eigenstates of the electronic Floquet operator $\mathcal{H}^{ele} \equiv \widetilde{H}^{ele} - i\hbar\frac{\partial}{\partial s}$. The parameter set $\mathcal{R}_t$ in this problem therefore includes nuclear coordinate in addition to laser parameters. The total state $\widetilde{\Psi}_{t,s}$ is then expanded in the form

$$|\widetilde{\Psi}_{t,s}\rangle = \sum_\alpha \int d\mathbf{R}|\mathbf{R}\rangle|\Phi_\alpha(s);\mathcal{R}_t\rangle\chi_\alpha(\mathbf{R},t), \tag{2.12}$$

where $\chi_\alpha(\mathbf{R},t)$ is the nuclear wavefunction associated with the electronic state $|\Phi_\alpha(s);\mathcal{R}_t\rangle$. Then the coupled Schrödinger equations for $\chi_\alpha(\mathbf{R},t)$ become

$$\begin{aligned} i\hbar\dot{\chi}_\alpha(\mathbf{R}) = &\sum_I \frac{1}{2M_I}\sum_\beta \left(\left[\frac{\hbar}{i}\frac{\partial}{\partial\mathbf{R}^I} - \frac{Q_I}{c}\mathbf{A} - i\hbar\mathbf{X}\right]^2\right)_{\alpha\beta}\chi_\beta + U_{nuc}(\mathbf{R})\chi_\alpha + \lambda_\alpha\chi_\alpha \\ &- i\hbar\sum_\mu \dot{\zeta}^\mu \sum_\beta \mathcal{X}_{\alpha\beta}^{(\zeta^\mu)}\chi_\beta, \end{aligned} \tag{2.13}$$

where $\mathbf{X}_{\alpha\beta}^I \equiv \langle\langle\Phi_\alpha|\frac{\partial}{\partial\mathbf{R}_I}|\Phi_\beta\rangle\rangle$ is the nuclear derivative coupling term, while $\mathcal{X}_{\alpha\beta}^{(\zeta^\mu)} \equiv \langle\langle\Phi_\alpha|\frac{\partial}{\partial\zeta^\mu}|\Phi_\beta\rangle\rangle$ are nonadiabatic coupling terms that are associated with a laser parameter ζ^μ.

In this paper, the notion of (non)adiabaticity is meant to be the (non)stationarity of the Floquet states. Under the exact periodicity as well as the absence or neglect of nuclear derivative couplings, the Floquet theorem ensures the stationarity of Floquet states. Conversely, any deviation from the periodicity can cause transitions among the Floquet states, which are, in our present formalism, uniformly treated as the generalized nonadiabatic transitions (see the first and the last terms in the right hand side of the Eq. (2.13)).

Equation (2.13), which is somewhat similar to Eq. (12) in Ref. [128], brings about several key concepts in (generalized) Floquet formalism. Examples are the formal periodicity of the Floquet operator $\mathcal{H}_s(\mathcal{R}_t)$ and the formal definition of the inner product, Eq. (2.10). Both are defined under a fixed value of t, and hence are independent of the t-dependence of parameters $\mathcal{R}_t$. This formal independence ensures broader applicability of this formalism. In fact it is formally applicable even in the cases with poor periodicity, $T/T_{np} \sim 1$ [14]. In practice, however, as nonperiodicity T/T_{np} grows, nonadiabatic contributions in Eq. (2.13)

[14] This is in contrast to the derivation of Ref. [128], in which smallness of t-dependence is explicitly assumed in formulation (see derivation of Eq. (12) of Ref. [128]).

become larger, and hence the advantages of Floquet state expansion diminish. In this aspect, it should be noted that the quasiperiodicity in our formalism is not a key assumption but a requirement for an effective use of this method.

In our formalism, the Floquet-type analysis is applied to the electronic Hamiltonian H^{el}, but not to the total Hamiltonian. As a consequence, the electronic states are expanded in the (parameterized) electronic Floquet basis, which are the eigenstates of the electronic Floquet operator. It thus follows that the eigenvalues are real if possible ionization processes are ignored. If, on the other hand, we used the total Hamiltonian (including the nuclear kinetic part) in constructing the Floquet Hamiltonian, the total state would be expanded in the electron-nucleus coupled Floquet basis. The eigenvalues would be complex-valued reflecting finite dissociation rates. This latter type of treatment has been studied[54, 129, 130] to reach many important results including life-time analysis of the bond hardening[54], time-independent analysis of photodissociation[129], and discussions on the exceptional points which induce intriguing quantum dynamics[130]. Moreover, if the relevant nuclear vibration mode were comparable to optical frequency, one cannot separate the nuclear modes in the Floquet analysis but need to take the latter approach. In this research, however, we assume the nuclear vibration mode to be slower than electronic we take the former approach to formulate a direct analogue of nonadiabatic dynamics among the field-induced PESs, whose advantages are emphasized in the introduction.

2-3. Physical observables

The two-time extended state $|\widetilde{\psi}_{t,s}\rangle$ bears arbitrariness in the variable s. In the dynamical calculations, an arbitrariness exists in the s-dependence of the initial ($t = 0$) extended-state vector, $|\widetilde{\Psi}_{t=0,s}\rangle$, which can be set to any function as long as the extended-state equals the physical initial state vector $|\Psi_0\rangle$ at $s = 0$, that is, $|\widetilde{\Psi}_{t=0,0}\rangle = |\Psi_0\rangle$. For example, two extreme choices are $|\tilde{\Psi}_{0,s}\rangle = |\Psi_0\rangle\delta(s)$ and $|\tilde{\Psi}_{0,0}\rangle = |\Psi_0\rangle$ (independent of s).

The s-dependence can be fixed for the sake of convenience in actual calculations. This arbitrariness, however, should not affect the final result as far as the "physical observables" are concerned, which are quantities obtained from physical state vector $|\widetilde{\Psi}_{t,t}\rangle$. It is then clear from the above two extreme choices that the population of an individual Floquet state is not a physical observable and is indeed affected by the choice of the s-dependence of the initial state. In order to proceed, we recall that for any Floquet state $|\Phi_\alpha(s)\rangle$ with quasienergy λ_α,

scalar multiplication of $e^{-in\omega s}$ yields another Floquet state with a quasienergy $\lambda_\alpha - n\hbar\omega$, which is hereafter referred to as an "$n\omega$-shift" of the original one. We also describe any two Floquet states to be "distinct" if one of them is not a $n\omega$-shift of the other. To obtain physical observables related to the Floquet state population, we consider the following summation over $n\omega$-shifts;

$$\xi_\alpha(\mathbf{R}, t) = \sum_n e^{-in\omega t}\chi_{\alpha - n\omega}(\mathbf{R}), \tag{2.14}$$

which is the projected amplitude of physical state vector $\langle \mathbf{R}|\widetilde{\Psi}_t(s)\rangle|_{s=t}$ on the Floquet eigenstate at $s = t$; $|\Phi_\alpha(s); \mathcal{R}_t\rangle|_{s=t}$, hence is a physical observable. Taking square and neglecting the fast oscillating components, (or equivalently, taking an average over one optical cycle) we obtain

$$\rho_{[\alpha]}(\mathbf{R}, t) = \sum_n |\chi_{\alpha - n\omega}(\mathbf{R})|^2, \tag{2.15}$$

where the subscript $[\alpha]$ indicates that the state α and its all $n\omega$-shifts are not mutually distinguished.

2-4. On the validity of quasiclassical approximation

Having formulated a generalized Floquet Hamiltonian method, we examine the validity of the gradient approximation on quasienergy surface(QES); an approximation for the nuclear dynamics by classical dynamics of a point-like particle driven by the minus of the gradient of a single QES.

Using a formal theory of mixed quantum classical representation of nonadiabatic dynamics [89] developed in Part I (also see Appendix C), the effective force acting on nuclei is given as,

$$\boldsymbol{\mathcal{F}} \approx \langle \Phi_\alpha(t); \mathcal{R}_t| - \frac{\partial H^{el}}{\partial \mathbf{R}}|\Phi_\alpha(t); \mathcal{R}_t\rangle. \tag{2.16}$$

provided that the effects of nonadiabatic transitions are negligible. Further assuming that the timescale of nuclear dynamics is large compared to the fundamental period T, we can take cycle average of Eq. (2.16) to obtain

$$\boldsymbol{\mathcal{F}} \approx \langle\langle \Phi_\alpha(t); \mathcal{R}_t| - \frac{\partial H^{el}}{\partial \mathbf{R}}|\Phi_\alpha(t); \mathcal{R}_t\rangle\rangle = -\frac{\partial \lambda_\alpha(\mathcal{R}_t)}{\partial \mathbf{R}}, \tag{2.17}$$

which is the gradient of QES.

From this derivation, we obtain three validity conditions for the gradient approximation; (a) smallness of nonadiabaticity(see Appendix C for details), (b) longer timescale of nuclear dynamics, and (c) absence of purely quantum mechanical effects, such as tunneling, where the last one being the assumption in the discussions in Part I.

Conversely, the gradient approximation breaks down around the avoided-crossings on QESs, where strength of the nonadiabatic coupling becomes large compared to the difference of adjacent quasi energies. Avoided-crossings of QESs in the weak field limit typically occur around resonant points, where the energy difference of two dipole-coupled adiabatic states equals to $n\hbar\omega$ with n being an integer (referred to as $n\omega$ resonances). Resonant points, along with intrinsic avoided crossings on the original field-free PESs are to be treated with special care in the following analysis.

Here the advantage of using Floquet state representation, rather than other choices of basis, for example, time-dependent adiabatic state is stationarity of the Floquet state; formally exact expression of the Force form, Eq. (2.24) is best-approximated by equal-time expectation value of a quasistational state. Conversely, it means, there would be little reason to use Floquet basis if the approximate stationarity of the Floquet states is severely broken or the cycle average is not appropriate.

3. APPLICATIONS TO THE FIELD-INDUCED BOND DEFORMATION OF H_2^+ AND D_2^+

To verify the theory presented above, we implement Eq. (2.13) in a computational scheme to actually obtain the extended wavefunction $\widetilde{\Psi}_{t,s}$. Each $\chi_\alpha(\mathbf{R})$ in Eq. (2.13) is represented on a spatial grid and propagated using the split-operator technique. Although this implementation scarifies applicability to larger systems, we can expect the most accurate results that are directly comparable to those obtained by a standard full quantum calculations. We first examine the method with the field-induced dynamics of H_2^+ and D_2^+, in which no nuclear derivative coupling is involved, and then in the next section we present a unified treatment of field-induced nonadiabatic dynamics and intrinsic one due to the nuclear kinetic couplings in LiF molecule.

The field-induced dynamics of H_2^+ and D_2^+ has been intensively studied in literature and hence the properties are well-known to serve as reference data. For the simplest assessment of the method, we use the two-state model proposed in Ref. [131]. The two-state models are

known to sufficiently reproduce the essential effects in the field-induced bond dynamics; the bond softening and the bond hardening. We can therefore check if these two fundamental effects are correctly treated in the present method.

3-1. Systems and computational methods

We use the two-state model potential proposed in Ref. [131], whose R-dependent electronic states are denoted as $|j;R\rangle$, with either $j = g$ or $j = u$ corresponding to the gerade and ungerade states, respectively. The derivative couplings between these states $\langle j';R|\frac{\partial}{\partial R}|j;R\rangle$ are neglected, and hence they are treated as the diabatic states in the simulation, although they are more like the adiabatic states in the context of field-free quantum chemistry. The molecular orientation is fixed so as the molecular axis to be parallel to the polarization vector of the applied laser in, say, x axis, and we concentrate only on the one-dimensional vibrational motion. The Schrödinger equation is

$$i\hbar\frac{\partial}{\partial t}\Psi_\alpha(R) = \sum_\beta \left[-\frac{\hbar^2}{2M}\frac{\partial^2}{\partial R^2}\delta_{\alpha\beta} + H^{ele}_{\alpha\beta}(R,t)\right]\Psi_\beta(R), \tag{3.1}$$

where M is the reduced mass of the nuclear relative motion and H^{ele} is the electronic Hamiltonian given as

$$H^{ele}(R,t) = \begin{pmatrix} U_g(R) & -\mu(R)E(t)\cos(\omega t) \\ -\mu(R)E(t)\cos(\omega t) & U_u(R) \end{pmatrix} \tag{3.2}$$

with $E(t)\cos(\omega t)$ being the electric field, and $\mu(R)$ is the dipole matrix element between the g and u state. Here the electric field amplitude $E(t)$ is chosen to be of a single Gaussian form with the full width half maximum (FWHM) being 150 fs; $E(t) = E_0 \exp\left(-\left(\frac{t-t_c}{t_w}\right)^2\right)$ with $t_c = 162.15$ fs, $t_w = 90.08$ fs. The effective potential and the dipole matrix element are, following Ref. [131], given as

$$U_g(R) = K\left(\exp(-2D(R-R_0)) - 2\exp(-D(R-R_0))\right) \tag{3.3}$$

$$U_u(R) = K\left(\exp(-2D(R-R_0)) - 2a\exp(-D(R-R_0))\right) \tag{3.4}$$

$$\mu(R) = \mu_0 + \frac{\mu_0'}{Dy}\left(1 - \exp(-Dy(R-R_0))\right). \tag{3.5}$$

Here the parameters are set, following Ref. [131], $D = 0.72$, $K = 0.10262$, $R_0 = 2.0$, $\mu_0 = 1.07$, $\mu_0' = 0.396$, $y = -0.055$ and $a = -1.11$, respectively. We use the atomic units throughout, except for time.

The Schrödinger equation (3.1) was numerically solved using a standard grid-based split operator method[132]. Here the one-dimensional space is limited to the range $[0, R_{max}]$ and divided into N_S equal-spaced lattice, whose lattice points are given as $R_k = k\frac{R_{max}}{N_S}$, $k = 0, ..., N_S - 1$. The actual parameters used are $N_S = 4096$ and $R_{max} = 20$. The results were confirmed to be qualitatively independent of the system size by comparison with those of the smaller size simulation $N_S = 2048$ and $R_{max} = 16$. An imaginary potential term V_I is applied near the boundary in order to eliminate unphysical reflections by absorption;

$$V_I = \begin{cases} -iA_0 \left(\frac{R-R_b}{R_w}\right)^2 & R_a \le R \le R_b \\ 0 & \text{otherwise,} \end{cases} \tag{3.6}$$

where we chose $A_0 = 2.4K$ (this K is the parameter introduced in Eq. (3.3) and below), $R_w = 3.6$, $R_a = 14.0$ and $R_b = 18.0$.

The extended state $|\widetilde{\Psi}_{t,s}\rangle$, is propagated using the Trotter formula (see Eq. (3.7) below). We use the Fourier series expansion to represent the s-dependence of the extended state as $|\widetilde{\Psi}_{t,s}\rangle = \sum_n e^{-in\omega s}|\widetilde{\Psi}^F_t[n]\rangle$, where $|\widetilde{\Psi}^F_t[n]\rangle$ represents the nth Fourier component of the extended state vector, and n runs through $-N_w$ to N_w with a fixed large number N_w for cutoff (actually set to 50). The Fourier series is then represented in the column vector as $|\widetilde{\Psi}^F_t\rangle = \left(|\widetilde{\Psi}^F_t[-N_w]\rangle, |\widetilde{\Psi}^F_t[-N_w+1]\rangle, ..., |\widetilde{\Psi}^F_t[N_w]\rangle\right)^{\mathrm{T}}$, where the superscript T indicates the vector transposition. We then have

$$|\widetilde{\Psi}^F_t\rangle = \prod_{j=0}^{P-1} \left\{ e^{-\frac{i}{\hbar}\frac{\epsilon}{2}\mathbf{T}^{nuc}} e^{-\frac{i}{\hbar}\epsilon\mathbf{H}^{eff}(t_j)} e^{-\frac{i}{\hbar}\frac{\epsilon}{2}\mathbf{T}^{nuc}} \right\} |\widetilde{\Psi}^F_0\rangle, \tag{3.7}$$

where P is the number of the time steps in the Trotter decomposition, $\epsilon \equiv \frac{t}{P}$ is the infinitesimal time step, $t_j \equiv j\epsilon$ is the jth time point, $\mathbf{T}^{nuc}$ and $\mathbf{H}^{eff}(t_j)$ are the Fourier series representation of the nuclear kinetic term T^{nuc} and the effective electronic Hamiltonian $H^{eff} \equiv \mathcal{H}^{ele} + \mathbf{V}_I$ in a matrix form, respectively. In the actual computation, the nuclear kinetic term was calculated using the fast Fourier transformation (FFT) technique[132]. The electronic state was expanded with the Fourier-transformed diabatic basis; $e^{-in\omega s}|j; \mathbf{R}\rangle$. The total state in this representation has the form $|\widetilde{\Psi}\rangle = \sum_j \sum_k \sum_{n=-N_w}^{N_w} e^{-in\omega s}|\mathbf{R}_k\rangle|j; \mathbf{R}_k\rangle\chi_{j,k}[n]$ where $\chi_{j,k}[n]$ is the nth Fourier series component of the discretized nuclear wavefunction $\chi_{j,k} \equiv \chi_j(R_k)$.

The initial conditions of the present dynamical simulation are chosen such that the electronic state is in the ground (gerade) state and the nuclear state is at one of the vibrational eigenstates (quantum number v) of the gerade electronic state. The corresponding extended-state vector at $t = 0$ is then fixed as $\chi_{j,k}[n] = \delta_{j,g}\delta_{n,0}\phi_v(R_k)$, with the vth vibrational

eigenstate wavefunction $\phi_v(R)$. As stated above, the initial choice of the extended state at $t = 0$ has arbitrariness with respect to the dependence on the variable s. The choice here corresponds to $|\widetilde{\Psi}_{t=0,s}\rangle = |\Psi_0\rangle$ (independent of s) and is found to be favorable for the present numerical implementation since, by this choice (together with the only weakly nonperiodic nature of the problem), only a small number of n is populated during the whole simulation. The simulation starts at $t = 0$ fs and end at $t \gtrapprox 400$ fs. The duration of simulation time is taken long enough. (We recall that the pulse is Gaussian of FWHM= 150 fs centered at $t_c = 162.15$ fs.)

The Floquet state population at an arbitrary time point is obtained by projecting the extended state vector on the Floquet eigenstate vector, which is obtained by diagonalization of the Floquet operator $\mathcal{H}^{ele}$. Formally, the physically meaningful quantity should be given as in Eq. (2.14). However, within the parameter choice in our practice, the Floquet states of the higher order are scarcely populated, and therefore the summation in Eq. (2.14) was replaced with a single term.

3-2. Typical QES and positions of $n\omega$ resonances

Some of the relevant QESs in the zero field limit are plotted in Fig. 1. Also plotted are squared amplitudes of the initial wavefunctions to show their spatial distributions. In Fig. 1, one can see two resonances; a 3ω resonance at around $R \approx 3$ and an 1ω resonance at $R \approx 5$. The corresponding QESs under finite field intensity are shown in Fig. 2, where, and throughout this paper, the temporal and the pulse-peak field intensity are indicated by I_t and I, respectively, in units of TW/cm^2. Since QESs are dependent on the temporal field amplitude E_t, the different lines of Fig. 2 can also be understood as snapshots of time-dependent QESs as they evolve according to the time-dependent pulsed laser field. From Figs. 1 and 2, one can see that the gap already exists at lower intensity as $I_t = 10$TW/cm^2 around the 1ω resonant point, while that around 3ω resonant point opens around $I_t = 50$TW/cm^2, reflecting the difference in the strength of dipole coupling around the each resonant point.

Smooth QESs are obtained by smoothly connecting a set of local data (the Floquet states and the corresponding quasienergies) at each grid-point. The connection process starts from the innermost grid-point, where the dipolar coupling is negligibly small relative to the field-independent terms in the Hamiltonian. The Floquet states at this point is almost identical to either gerade(g) or ungerade(u) state, or their n-shifts, hence they are labeled accordingly.

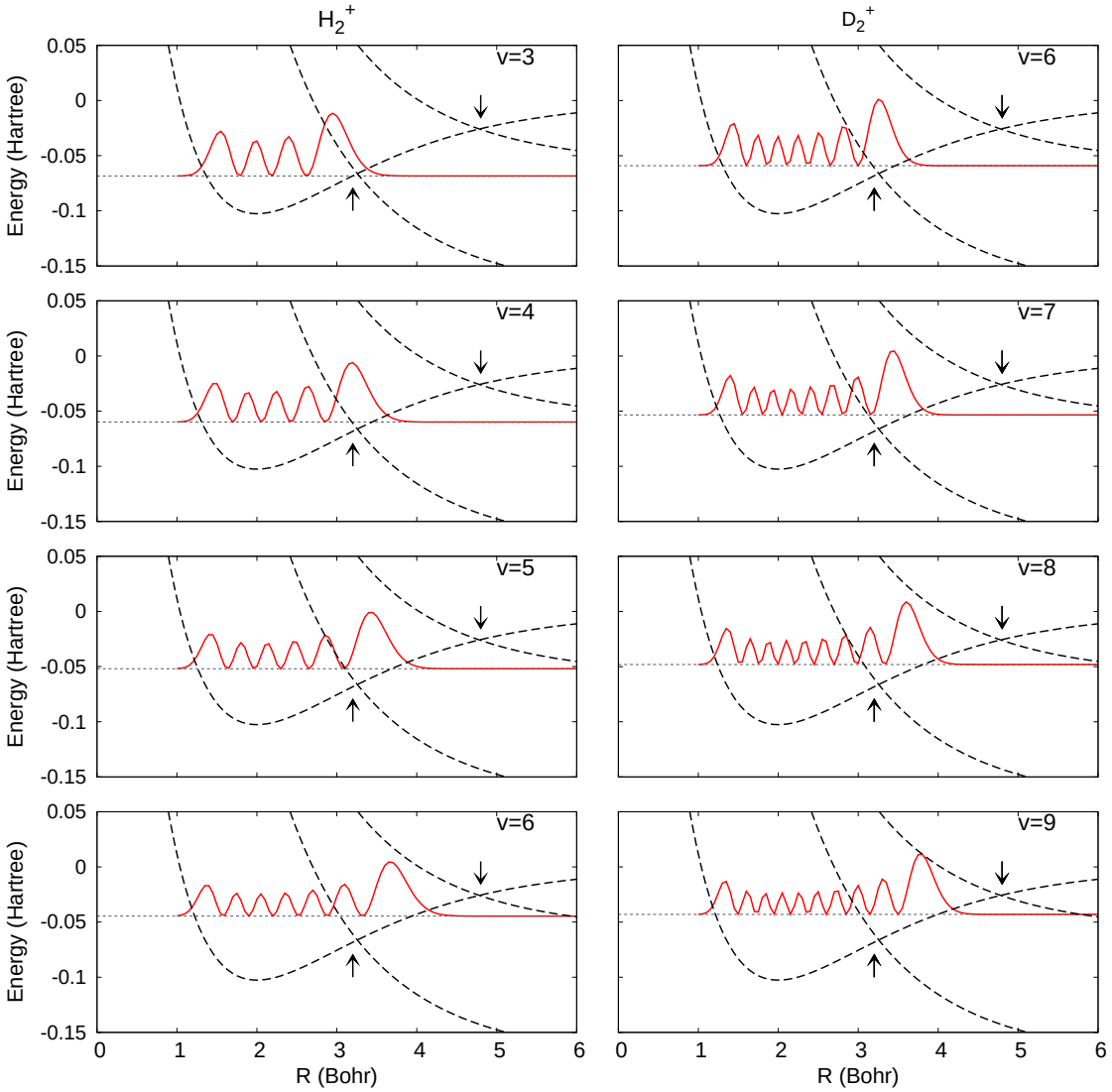

FIG. 1: The spatial distribution of the initial wavefunctions for several vibration quantum numbers. Panels in the left vertical row show the results for H_2^+, from the top to bottom, $v = 3, 4, 5, 6$. Panels in the right vertical row show that for D_2^+, from the top to bottom, $v = 6, 7, 8, 9$. The red solid lines indicate the squared amplitude of the wavefunction, whereas the black dashed lines indicate QESs corresponding to the gerade, 1ω shift of the ungerade and 3ω shift of the ungerade states in the zero field limit, indicating the location of the 1ω resonance (at $R \approx 5$) and the 3ω resonance (at $R \approx 3$) as the crossing points.

Then in the following steps, each local Floquet state at a grid-point R_{k+1} is given one of these labels generated at the preceding point R_k in such a way that the largest overlap $|\langle\langle \Phi_\alpha; R_k | \Phi_\alpha; R_{k+1} \rangle\rangle|^2 \approx 1$ is ensured. Those grid-local Floquet states are thus connected in a stepwise manner to form a global state. At resonant points, where two QESs come close to each other, there are two possibilities. A straight-forward application of the above procedure almost always connects the lower energy state on the left (smaller in R coordinate) of the

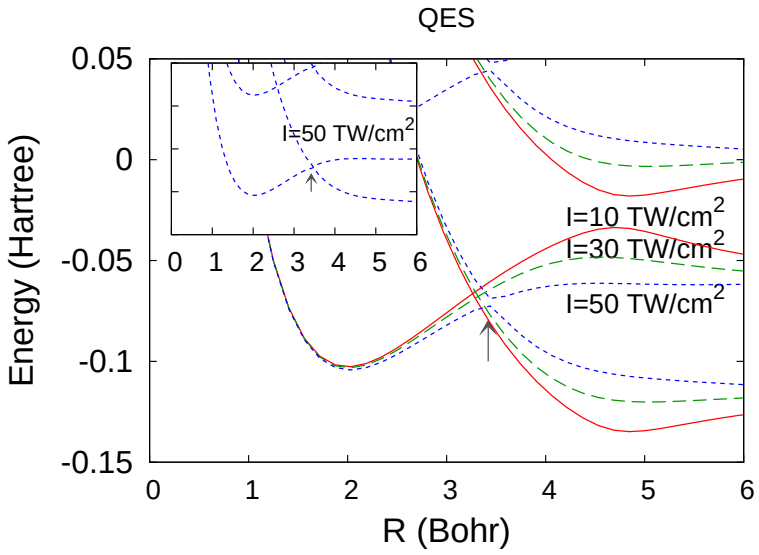

FIG. 2: Typical QESs relevant to the dissociation dynamics. Red solid, green dashed and blue dotted lines indicate the QES for (instantaneous) field intensity 10, 30 and 50TW/cm^2, respectively. The QES given by 50TW/cm^2 in the main panel shows the adiabatic connection at the 3ω resonant point, whereas the inset shows the diabatic connection (see the text). The small arrows show the point where the difference of the connection occurs.

resonant point with the lower energy one on the right (larger in R coordinate) and vice-versa ("adiabatic connection"). Yet there is another way of connection, "diabatic connection", in which the lower energy state on the left is connected with the higher energy state on the right. In some of the situations we will see below, the diabatic connection is favorable for description of the spatial distribution of the wavepackets. In Fig. 2, the main panel exhibits the adiabatic connection applied on the 3ω resonant point, while the inset shows the QES at temporal field intensity $I_t = 50$ TW/cm^2 with the diabatic connection applied at the 3ω resonant point.

3-3. Dissociation probability and underlying wavepacket dynamics

We next show the calculated dissociation probability in Fig. 3. The results for H_2^+ are in good agreement with Fig. 18 of Ref. [47], in which no further analysis has been reported. As we notice in Fig. 3, the dissociation probability versus the field intensity are classified into three overall patterns.

Pattern 1. Near-zero probability at low field followed by rapid monotonic increase at higher

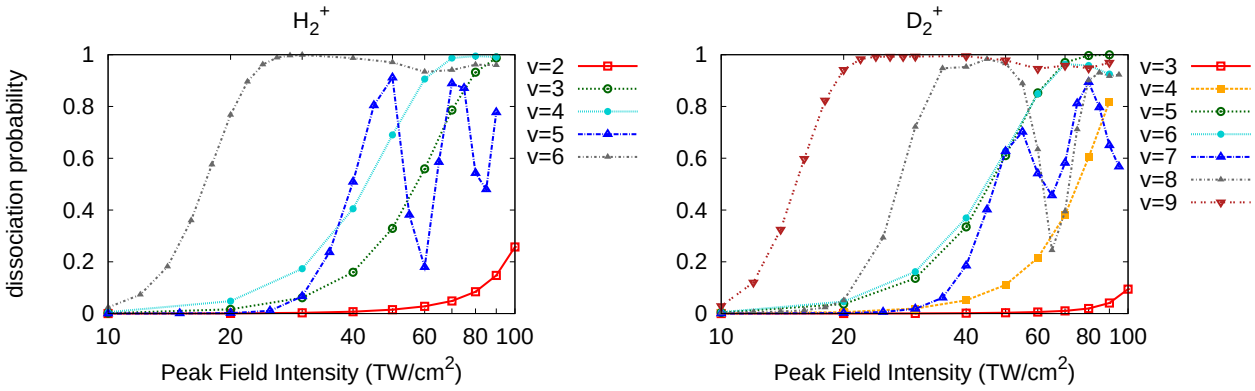

FIG. 3: The dissociation probability calculated from the total population lost from the simulation space $0 \leq R \leq R_{max}$ during the laser radiation. Left and right panel shows the results for H_2^+ and D_2^+, respectively. Each line shows the result obtained from the initial vibration state indicated on the right of each panel. The horizontal axis is plotted in log scale.

intensity: $v = 2, 3, 4$ in H_2^+ and $v = 3, 4, 5, 6$ in D_2^+.

Pattern 2. Non-monotonic oscillatory behavior; $v = 5$ in H_2^+ and $v = 7, 8$ in D_2^+.

Pattern 3. Similar to the pattern 1, but the increase occurs at much lower field; $v = 6$ in H_2^+ and $v = 9$ in D_2^+.

In order to analyze the dynamics behind each pattern, we show in Fig. 4 selected snapshots of wavepackets represented by the squared amplitude of the dominant Floquet state. The time-dependent behavior of the related QESs are also superimposed in the figure. One can observe that the wavepacket motion is in accordance with the QES gradient, thereby qualitatively verifying the quasiclassical interpretation. Throughout the present simulation, the population of the $n\omega$-shifts of the dominant Floquet state was negligibly small in the entire parameter range. The population of the second-dominant Floquet state, which is distinct from the dominant, is also negligible in the parameter region in Fig. 4. The second-dominant state population, however, may grow to a finite value in other parameter region (not plotted) especially around the resonant points. Discussions below are based on the dominant state behavior, which nevertheless characterizes the overall behavior.

3-4. Mechanisms of the individual patterns

Pattern 1: Bond softening

The snapshots of the dynamics of initial state $v = 3$ and the peak field intensity $I = 80$ TW/cm^2 are shown in the three panels, (a-1) to (a-3) in Fig. 4, where one can see that the

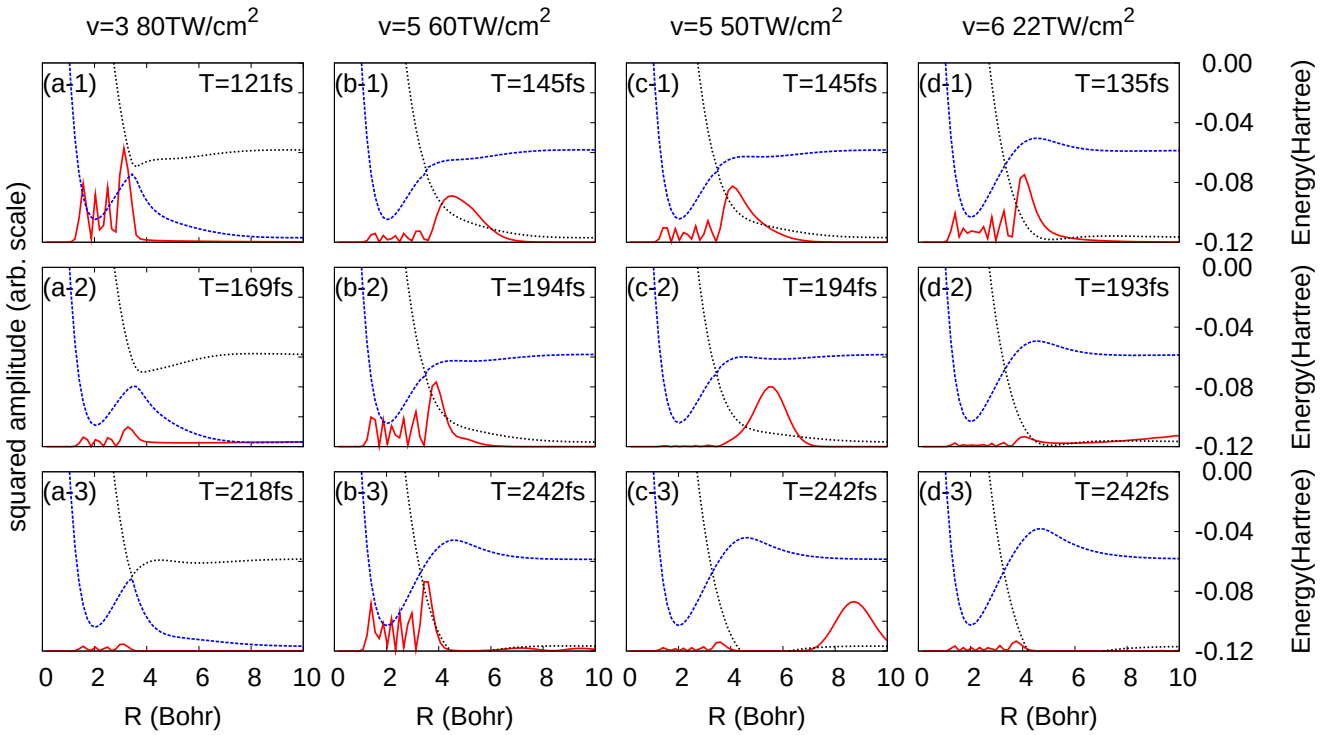

FIG. 4: Snapshots of the squared wavepacket amplitude and Floquet quasienergy surface. Each panel shows the snapshot at the time point which is indicated at the right top. For each panel, the red solid line represent the squared amplitude of the dominant Floquet state, and the blue dashed curve does the corresponding quasienergy surface. Another closely related QES is also plotted with black dotted line for reference. Three panels in each vertical row show snapshots of the dynamics starting from the initial vibrational state and the peak field intensity indicated at the top.

wavepacket moves out through deformed QES after the opening of the gap at the 3ω resonant point, which is a typical behavior in the bond softening [47]. Dynamics in other parameters categorized in this pattern also shows a similar behavior at intensities higher than an onset intensity, where a sharp increase of dissociation probability (see Fig. 3) occurs. We thus identify the present pattern as bond softening.

It is expected that the onset intensity is closely related to the suppression of the peak, or the local maximum, of QES, which seems to act like a barrier near the 3ω resonant point. To verify this assertion, we show the value of the QES peak in Fig. 5. One can see that the onset intensity approximately correspond to the value at which the QES peak becomes smaller than the original vibrational energy. Since the energy does not have to be conserved in this short-term dynamics under external field, the correspondence found above is rather unexpected. From the viewpoint of the quasiclassical dynamics, however, QES peak position

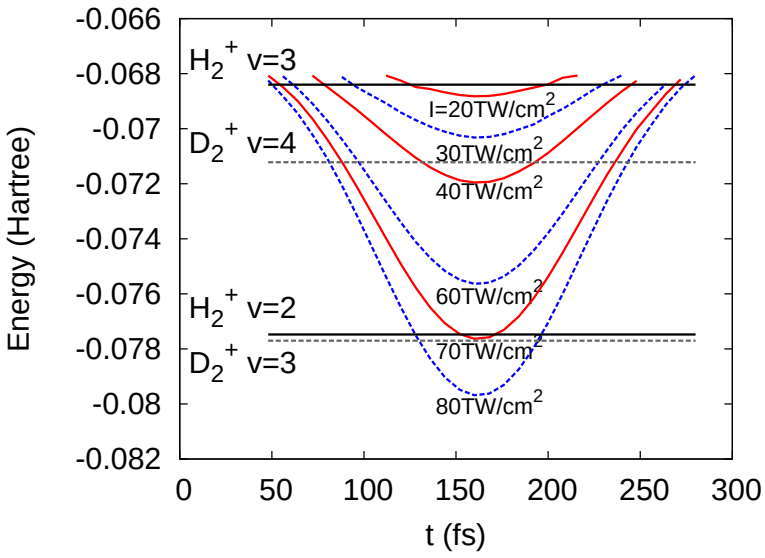

FIG. 5: Time evolution of the peak energy of the QES for different laser peak intensities. Each curve is assigned to the individual laser peak as indicated in the figure. Horizontal solid lines and dashed lines are the field-free vibrational energy levels of H_2^+ and D_2^+, respectively.

is the point where the gradient force changes its sign, whereas the point where the original vibrational energy crosses the QES (in the field free limit) roughly corresponds to the range of the distribution of the wavefunction. Transfer of large population therefore should start when these two points come close to each other.

Pattern 2: Bond hardening and inverse bond hardening

The snapshots of the wavepacket dynamics of $v = 5$ at the peak field intensity $I = 60$ TW/cm^2, which is at the bottom of the dissociation probability oscillation (see Fig. 3), are shown in the panels (b-1) to (b-3) of Fig. 4. One can see that the increase of the QES local maximum near the 1ω resonant point prevents the wavepacket from dissociation, which is a typical behavior in the bond hardening[47, 54, 55, 133].

We also show, in the panels (c-1) to (c-3) in Fig. 4, the snapshots of the dynamics of $v = 5$ with the peak field intensity $I = 50$ TW/cm^2, which is at the peak of the dissociation probability oscillation. Here the development of a local maximum in QES near the 1ω resonant point seems to push out a portion of the wavepacket. Hence the underlying mechanism is the same as the normal bond hardening seen in the dynamics at the peak field intensity $I = 60$TW/cm^2, although the outcome is opposite. We thus term it "inverse bond hardening".

Pattern 3: Bond softening (at 1ω resonant point)

The snapshots of the dynamics of $v = 6$ at the peak field intensity $I = 22$ TW/cm^2 are shown in the panels (d-1) to (d-3) in Fig. 4. Here we can see the wavepacket move out through the gap formed by the 1ω resonance. The onset occurs at much lower intensity due to the stronger dipole coupling at the 1ω resonant point than that at the 3ω resonant point. Nevertheless, the essential mechanism is the bond softening, the same as the Pattern 1.

3-5. Topography of QES and the spatial distribution of nuclear wavefunctions

Let us discuss the physical origin that consistently explains the different behaviors of three patterns. We first note that the convention of the state connection in Fig. 4 are different among the first vertical row ($v = 3$) and the rest ($v = 5, 6$); that of the former being adiabatic while that of the latter is diabatic. The state connection scheme is chosen so that the spatially integrated Floquet populations do not have discontinuity in the timeline as the 3ω gap increases. The traveling part of the wavepacket is therefore on the lower QES in case of $v = 3$ and on the upper QES for $v = 5, 6$. The quasiclassical analysis has been found to be consistent with this attribution.

The above difference is more easily understood by comparing the spatial distributions of the initial wavefunctions of $v = 3$ and $v = 5$, which are shown in Fig. 1. In the panels in the left row in Fig. 1, one can see the entire wavefunction of $v = 3$ lying left (smaller in R coordinate) of the 3ω resonant point, while the rightmost (largest in R coordinate) peak of the wavefunction of $v = 5$ stays to the right of the resonant point. Thus the outermost part of the $v = 5$ wavefunction propagates into the upper QES. The $v = 3$ wavefunction, on the other hand, does not have an amplitude right to the 3ω resonant point at $t = 0$ and it moves out adiabatically on the lower QES after the $n = 3$ gap has developed, and hence the whole motion remains on the lower QES. Thus the appropriate state connection and the origins of pattern 1 and 2 are explained in terms of the spatial distribution of the initial wavefunctions relative to the singular points on QES.

The same analysis applies to the case of $v = 6$ where the wavefunction distributes close to the 1ω resonant point although all the peaks are inside the resonant point. Thus the situation in the state of $v = 6$ at the peak laser intensity around $I = 10$TW/cm^2 is analogous to that of $v = 3$ in higher laser intensity, and therefore bond softening through the 1ω resonance is expected.

We also apply the same analysis to D_2^+ to explain the similarity of behavior as H_2^+. Since the larger mass of D_2^+ makes the spatial distribution of vibrational state narrower than that of H_2^+ with the *same* vibrational quantum numbers, the similar spatial distribution occurs at larger vibrational quanta than that of H_2^+. The right side of Fig.1 shows $v = 6, 7, 8, 9$ of D_2^+, whose distribution relative to the resonant point show approximate correspondence to $v = 3, 4, 5, 6$ of H_2^+.

3-6. Summary

We have thus verified the present formalism by successfully reproducing the dissociation probabilities of H_2^+ reported in Ref. [47], including the oscillatory feature. We also show that an interplay of bond softening and bond hardening can be clearly seen in the snapshots of time-dependent QESs and wavepacket dynamics on them, which is clearly understood in terms of quasiclassical approximation. In fact our simulation serves as a direct real-time demonstration of possibly competing bond softening and bond hardening mechanisms. It lead to detailed understanding of the interplay of the two mechanisms, including theoretical possibility of inverse bond hardening[15]. The additional calculations for D_2^+ dissociation have been found to be consistent with these interpretations. Thus the present theory and its numerical realization have been shown to work well for this prototype field-induced dynamics.

4. APPLICATION TO THE CURVE-CROSSING DISSOCIATION DYNAMICS OF LIF

We next proceed to a system in which the intrinsic nuclear derivative couplings directly affect the dissociation process in laser fields. We take LiF as a case study, which is among the simplest molecules having an avoided crossing of ionic and covalent PESs (see Fig. 6 (a)). In such a system, the nuclear derivative interaction around the avoided-crossing should affect the dissociation process by inducing transition between the dissociative (covalent) state and non-dissociative (ionic) state. In the presence of strong laser field, these ionic and covalent PESs are expected to be largely deformed, since these two and other possible excited states are dipole-coupled. Thus a qualitative description of the field-induced dissociation dynamics should require full consideration of nuclear kinematic effects as well as dynamical deformation

[15] We note that the experimental observability of inverse bond hardening requires further discussions.

of QES.

4-1. Systems and computational details

Theoretical studies on LiF in recent years include static *ab initio* calculation of PESs[134, 135], and calculations of field-induced dynamics[123, 136]. To the best of our knowledge, no experimental study on its field-induced dynamics has ever been reported, but it still serves as a prototype for studying an interplay of field-induced and intrinsic nonadiabatic transitions.

The full quantum-mechanical calculations in Ref. [136] suggests onset of dissociation under strong infrared ($\lambda = 9.4$ μm) laser field of order 10^0 to 10^1 TW/cm^2. Mixed quantum classical calculations in Ref. [123], on the other hand, reports dissociation under higher field intensities around 10^2 to 10^3 TW/cm^2 although the laser wavelengths are different from Ref. [136]. Here we consider the laser field of wavelength $\lambda = 227$ nm.

***ab initio* calculation of electronic matrix elements**

We first calculate PESs and relevant matrix elements of LiF by *ab initio* calculations. We use the program package GAMESS[137] to perform configuration interaction calculations limited to single and double excitation(CISD) using the graphical unitary group approach (GUGA)[138] and obtain PESs as well as the relevant matrix elements including electronic dipole and derivative couplings. Our choice of basis set is Dunning's second order augmented correlation-consistent basis set (aug-cc-pCVDZ)[139], which generates the total of 48 atomic orbitals. In the CISD calculations, 2 core-like and 27 higher-lying orbitals out of 48 molecular orbitals are frozen. The number of symmetry-adapted configuration state functions (CSFs) was 870.

The adiabatic PESs are shown in Fig. 6. Although the calculation level is rather lower than the previous works on the same molecule[135], it is however sufficient to qualitatively reproduce the features obtained from more accurate calculations[135]. The position of the avoided crossing of the lowest two PESs is obtained at around internuclear distance $R_c = 11.85$. (Ref. [135] reports $12 \leq R_c \leq 13$ with larger size calculations.) Since the value of R_c is sensitive to the level and size of calculations, the present R_c seems to be within a tolerable range. The necessary matrix elements in the adiabatic representation are first calculated using the $N_{tot} = 870$ CSFs as described above. Dimension of the basis set is then reduced by restricting to the lowest $N_b = 8$ adiabatic states.

The obtained $N_b \times N_b$ matrices are further transformed to an approximately diabatic

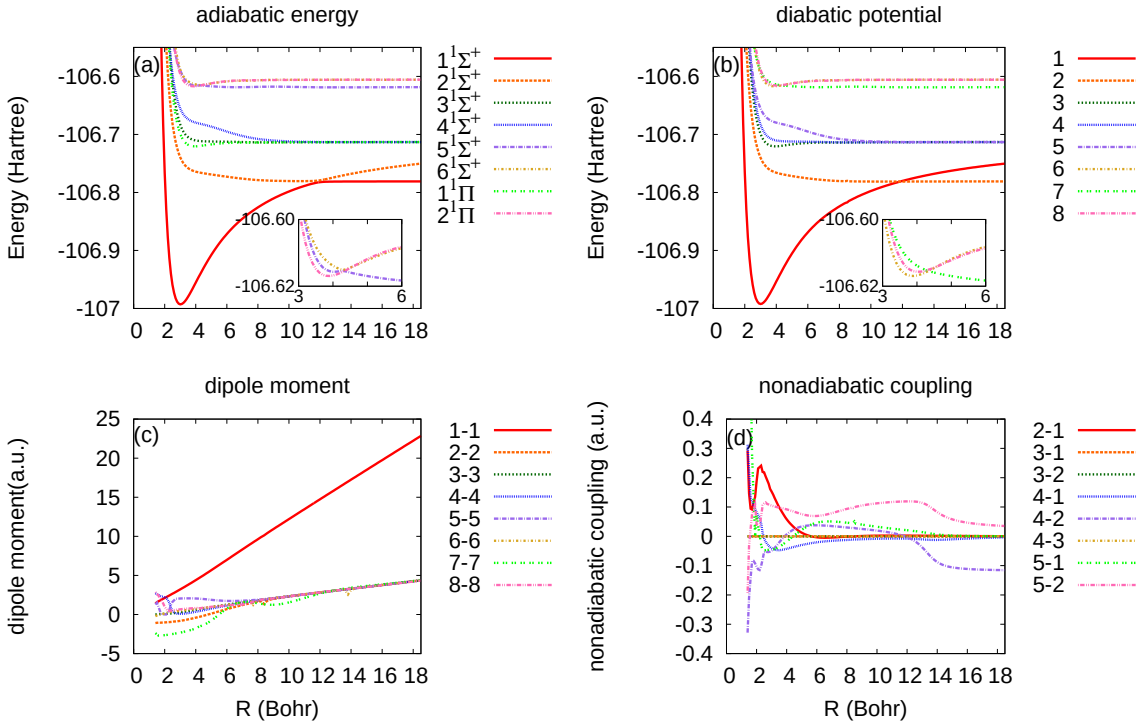

FIG. 6: The adiabatic PESs (panel (a)) and the relevant elements (panels (b) to (d)) of matrices obtained by *ab initio* calculations. Matrices in (b) to (d) are in the approximate diabatic representation as describerd in the text. (a) Adiabatic energies of the lowest 8 adiabatic states. (b) Diagonal elements of the Hamiltonian matrix. (c) Diagonal elements of the electric dipole matrix. (d) Off-diagonal elements of the nuclear nonadiabatic coupling matrix. The adiabatic states are labeled as $1^1\Sigma^+$ to $6^1\Sigma^+$, $1^1\Pi$, $2^1\Pi$, where numbers are given in an increasing order in the adiabatic energies.

basis to avoid the derivative couplings. Here an approximate diabatization is applied to the lowest two adiabatic states, whereas the rest $N_b - 2$ basis states are kept as adiabatic states. We diagonalize the lowest 2×2 block of the dipole matrix to obtain new states with either 'ionic' or 'covalent' character. Thus the nonadiabatic coupling between these states has been significantly reduced around the avoided crossing, although being finite. The residual derivative couplings are evaluated as is separately described in Appendix D.

The relevant elements of thus obtained matrices are shown in Fig. 6. All the matrices are calculated at 171 grid-points with the internuclear distance $R^{(p)} = 1.4 + 0.1p$ ($p = 0, 1, 2, ..., 170$).

Quantum wavepacket calculations

Here again we assume one-dimensional nuclear motion along the molecular axis, which is fixed parallel to the field polarization. The quantum wavepacket calculations are then

performed using Eq. (3.7) in a similar manner as was described in the preceding section but with several modifications. The nuclear degrees of freedom is represented by internuclear distance R, whose corresponding reduced mass is $M_{eff} = \frac{M_{Li}M_F}{M_{Li}+M_F}$ and the effective charge $Q_{eff} = \frac{M_F Q_{Li} - M_{Li}Q_F}{M_{Li}+M_F}$, which are, in the atomic unit, 9265.97 and -0.591950, respectively.

The grid points are chosen as $R = R_{min} + k\frac{R_{max}-R_{min}}{N_S}$ with $k = 0, 1, ..., N_S - 1$, $R_{min} = 1.4$ and $R_{max} = 18.312$. Number of grid points, N_S is set to 2048. An imaginary potential term of the form Eq. (3.6) is applied with modified parameters; $A_0 = 0.5084$, $R_a = 16.312$, $R_b = 18.312$ and $R_w = 2.0$. Matrices at each grid point R_k are obtained by a linear interpolation technique using the nearest two data points ($R^{(p)}$ and $R^{(p+1)}$ which satisfies $R^{(p)} \leq R_k < R^{(p+1)}$). The cut-off of the Fourier series N_w is set to 30, which is confirmed to be sufficiently large by comparing the results with those of $N_w = 45$.

Due to the existence of finite diagonal components in the dipole matrix, better convergence is expected by using the velocity gauge rather than the length gauge. We calculate the electronic dipole velocity momenta in the adiabatic representation using the formula $\frac{q_e}{m_e c}(\mathbf{p})_{\alpha\beta} = \frac{i}{\hbar}(\mathcal{E}_\alpha - \mathcal{E}_\beta)(\boldsymbol{\mu})_{\alpha\beta}$, where $\mathbf{p}$ and $\boldsymbol{\mu}$ are the electronic momentum and the dipole matrices, $\mathcal{E}_\alpha$ is the αth adiabatic energy, respectively. We also redefine the field in terms of the vector potential as $A(t)\cos(\omega t)$ with a Gaussian pulse envelope $A(t) = A_0 \exp\left(-\left(\frac{t-t_c}{t_w}\right)^2\right)$. In this paper, pulse width is set 300 fs (FWHM) and t_c and t_w are chosen to be 324.3 fs and 180.2 fs, respectively. The width is set longer than that used in H_2^+/D_2^+ to take account of the heavier reduced nuclear mass.

To obtain the initial vibrational states, we fit the first diagonal element of the Hamiltonian matrix (this is almost equal to the ground adiabatic surface in the range of R in which the vibrational states of our interest lie) to a Morse potential and derived the vibrational eigenstates.

4-2. Dissociation dynamics

The graph of the dissociation probability against the laser intensity under a pulse of FWHM 300fs is depicted in Fig. 7. It shows globally monotonic increase of the dissociation probability with pulse peak intensity, but with a slight oscillatory behavior, which implies existence of a trapping mechanism. However, this effect is less clear than in the case of H_2^+ and D_2^+.

A typical dissociation process is shown in Fig. 8, which shows the behavior of the Floquet

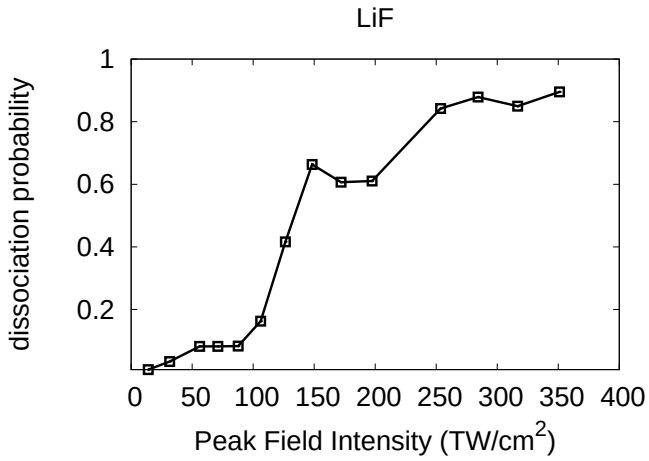

FIG. 7: Dissociation probability calculated from the total population lost from the simulation space $R_{min} \leq R \leq R_{max}$ during the simulation time. Pulse FWHM was set 300 fs and the initial vibration state was set to $v = 3$.

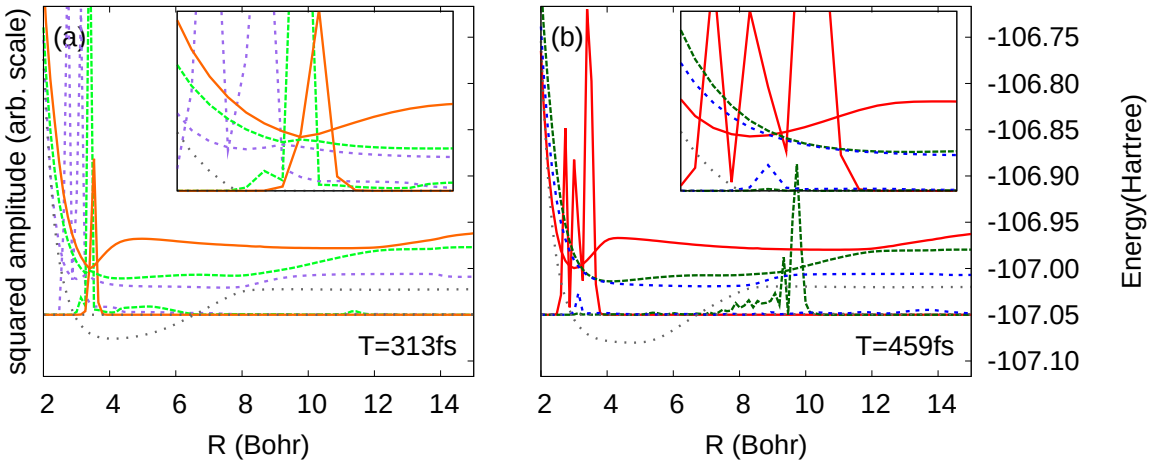

FIG. 8: The squared Floquet state amplitudes and QESs in the dissociation dynamics of LiF under a laser pulse of width 300fs (FWHM) and the peak intensity $I = 126.36$ TW/cm^2 ($A_{max}/c = 0.30$). Each panel shows the snapshot at the time indicated on the panel; (a) $t = 313$ fs and (b) $t = 459$ fs from the pulse onset. The scale for the QES plot is indicated on the right of each panel, while that for the amplitude plot is arbitrary. Each Floquet state population and the corresponding QES is plotted with the same color and the same line style. 1'. Orange solid, 2'. light green dashed and 3'. purple dotted lines in panel (a) are related to 1. red-solid (S1), 2. dark green dashed (S2) and 3. blue dotted (S3) lines in panel (b) (see also text). The gray thin dotted curve in each panel, which shows the QES of the fourth dominant Floquet state (S4), is plotted to help understanding although the corresponding state population is almost negligible.

populations and corresponding QESs obtained in the simulation under a laser pulse of width 300 fs (FWHM) and the peak intensity $I = 126.36$ TW/cm^2 ($A_0/c = 0.30$). Here again the population of higher order Floquet states are small, and therefore we can use the single Floquet state populations to represent the actual dynamics. Note the difference of the topology of QESs between the two panels; the three QESs in panel (a), plotted with orange solid, purple dotted and light green dashed lines correspond to those in panel (b), plotted with red solid, blue dotted, and dark green dashed lines. The correspondence is one-to-one in the asymptotic region, but not in the region with small R. For the sake of convenience of later discussion, we label each Floquet state accordingly; those plotted with (1) red solid, (2) dark green dashed and (3) blue dotted lines will be referred to as the Floquet state S1, S2 and S3, respectively. The wavepacket begins to flow out of the initial bound potential ($R \lesssim 4$) around the time when the laser pulse intensity reaches the peak. An example is seen in panel (a) of Fig. 8, in which the field is strong enough to induce significant deformation of QES at even around the equilibrium bond length ($R \approx 3.0$). In panel (a) three QESs avoid-cross around $R \approx 3$ and part of the initially bound vibration state population goes out along the QES plotted by the light green dashed line (see also the inset for details). The dynamics in this region is therefore similar to that in the bond-softening pattern of H_2^+/D_2^+.

In contrast to what we saw in H_2^+/D_2^+, the outgoing wavepacket in this system further undergoes trapping at a "later stage", or at a larger value of R. As is shown in panel (b) of Fig. 8, the outgoing wavepacket is trapped by the upward slope of the corresponding QES around $8 \lesssim R \lesssim 12$, which essentially comes from the character of the ionic PES. Some proportion on it, on the other hand, undergoes nonadiabatic transition through the avoided crossing at $R \approx 9$ to another Floquet state (a blue dotted curve) of the covalent type and leading to dissociation. We note however that in this simulation, this later-stage trapping at the intermediate region $8 \lesssim R \lesssim 12$ is led to dissociation as the field diminishes.

4-3. Characterization of QESs

To facilitate understanding of the above dynamics, we correlate the field induced QESs in Fig. 8 to those in the zero-field limit (ZF-QESs), which are field-free PESs and their $n\omega$-shifts (see Fig. 6 (a)). Such an approximate assignment would allow an intuitive characterization of the finite field QESs. Figure 9 presents the QESs of Fig. 8 and related ZF-QESs. We first study the global features; the upward slope of QES seen in the region $8 \lesssim R \lesssim 12$ reflects

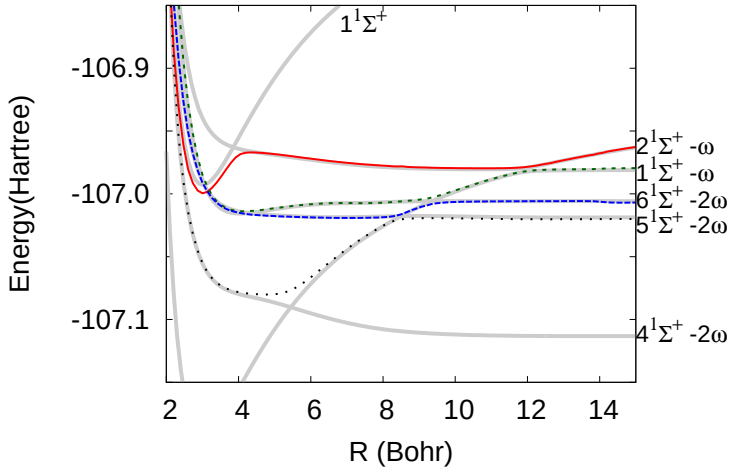

FIG. 9: The same QESs as Fig. 8 (b), with the zero-field limit QESs (ZF-QESs) being added in gray lines (refer to Fig. 6). The characters of ZF-QESs are indicated in right hand side of the figure. The red solid, blue dotted and dark green dashed lines, on the other hand, show QESs identical to Fig. 8(b).

$-\omega$-shifted $1^1\Sigma^+$, whereas the blue dotted QES, the asymptote to -2ω-shifted $6^1\Sigma^+$, leads to dissociation. We can also see that the QES forming the initial bound state ($1^1\Sigma^+$ or its finite-field correspondence) and those leading to dissociation (-2ω shifted $5^1\Sigma^+$, $6^1\Sigma^+$ or their finite-field correspondence) are indirectly coupled with -2ω shifts. This type of coupling would be zero in the two-state model of H_2^+/D_2^+, but is finite here due to the existence of more than two dipole-coupled states.

4-4. Role of the nuclear derivative couplings

We finally discuss the role of the nuclear derivative couplings. It is expected that the "later stage trapping" observed above should be affected by the kinematically induced nonadiabatic transitions at around the avoided crossing of QESs. In order to confirm this, we perform additional calculations in which the nuclear derivative coupling terms (in Eq. (2.13)) are intentionally ignored (zero nuclear derivative coupling limit denoted as Z-scheme). We note that the nuclear derivative couplings here is partly reduced from those in the adiabatic representation because of partial diabatic transformation. Nevertheless, the differences of

the two schemes represent kinematic effects [16]. The resultant nuclear wavepacket behavior is shown in Fig. 10, contrasted to that of the full standard calculations of nuclear derivative couplings (N-scheme)). Figure 10 shows the snapshots of the squared amplitudes and QESs of the relevant Floquet states at each parameter shown in the figure. In particular, the panel (b) shows the results obtained at the same parameters as those in Fig. 8 (b). The results of N-scheme calculation is plotted in the same manner as that of Fig. 8 (b), whereas the results of Z-scheme calculations are added using orange dash-dotted, light green dot-dot-dashed and purple dot-dot-dot-dashed lines for the Floquet state S1, S2 and S3, respectively. We first see Fig. 10 panel (b) where the differences of the two schemes are most pronounced. It shows larger population of state S2 around $R \approx 10$ in the N-scheme result whereas larger population have leaked off to dissociate through the state S3 in the Z-scheme result (compare the purple dot-dot-dot-dashed lines against the blue-dotted ones), indicating enhanced trapping due to the derivative coupling term. The result does not match naive perturbative expectation; if one assumes the nonadiabatic term as small perturbation term added on the local Floquet Hamiltonian, any addition of "small" off-diagonal term would induce transitions among the Floquet states. Such simple guess, however, does not apply here because the nonadiabatic term is not necessarily a small perturbation at the avoided crossing of Floquet states.

We further compare the result with those obtained in different values of laser parameters. In the weakest peak field amplitude, $I = 56.16\mathrm{TW/cm^2}$ ($A_{max}/c = 0.2$) the effect of derivative coupling is negligible because the population passes through the avoided crossings is small. In stronger peak field amplitudes, $I = 224.64\mathrm{TW/cm^2}$ ($A_{max}/c = 0.4$) and $I = 351.0\mathrm{TW/cm^2}$ ($A_{max}/c = 0.5$), the differences are small. The difference appear to decrease with the peak intensity. This is partly accounted for as the suppression of nonadiabatic transitions by larger gap among Floquet states.

In principle, the effect of nonadiabatic terms should be small when the (temporal) laser intensity is large and gaps among the Floquet states are large, but it may become relevant otherwise. It is also affected by the 'velocity' of the wave packet in the form $i\hbar\mathbf{v}\cdot\mathbf{X}$, where $\mathbf{v}$ is the wavepacket velocity (more precise description will be given in the appendix E). In dynamics under a pulsed laser field, one can then expect nonnegligible effect if an accelerated wavepacket passes through the avoided crossing on the falling edge of the pulse. The reality

[16] The dynamics in the adiabatic limit is independent of basis set. Any deviation from this, either through diabatic coupling or derivative coupling arises from kinematic effects.

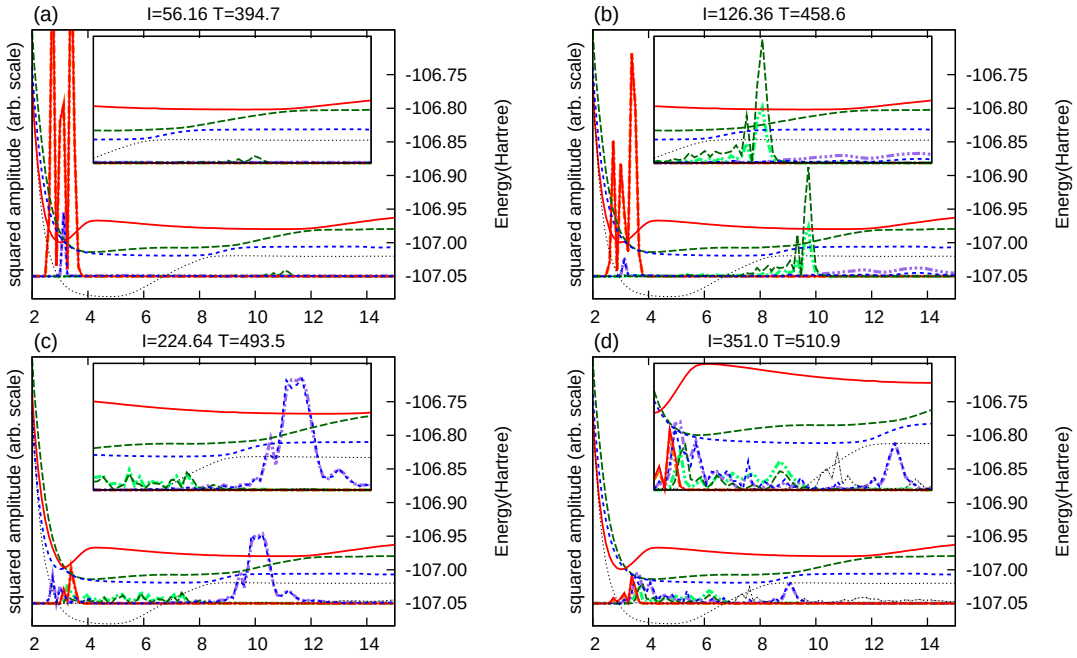

FIG. 10: Comparison of the squared wavepacket amplitudes between the results obtained by the two calculation schemes (see text). In each calculation, the laser pulse FWHM is fixed at 300 fs and the peak intensity is set (a) $I = 51.16\text{TW/cm}^2$ ($A_{max}/c = 0.20$), (b)$I = 126.36\text{TW/cm}^2$ ($A_{max}/c = 0.30$), (c)$I = 224.64\text{TW/cm}^2$ ($A_{max}/c = 0.40$) and (d)$I = 351.0$ TW/cm^2 ($A_{max}/c = 0.50$), respectively. The snapshot at fixed time $T = 459$ fs from the pulse onset is taken for comparison. The external conditions for the panel (b) is hence identical to that of Fig. 8 (b). The Floquet state populations and their corresponding QESs obtained by the N-scheme calculations are plotted with the same line styles as Fig. 8 (b) ; S1: red full, S2: green dashed, S3: blue dotted, and S4: black thin dotted, respectively, whereas the Floquet state populations in the Z-scheme are plotted with S1': orange dash-dotted, S2': light-green dash-dot-dotted, S3': purple dash-dot-dot-dotted and S4'. gray thin dotted lines, respectively.

is, however, that much is dependent on the details of dynamics.

We must also note that the effects are transient and the total dissociation probability (evaluated at large t from the onset, where laser pulse diminishes) is almost identical between the two schemes. However, the result may differ if there are multiple dissociation channels and one distinguishes between them[71].

We have thus applied our generalized Floquet method on the field-induced dissociation of ionic bound LiF using *ab initio* PESs and matrix elements, and observed that, even in the presence of nuclear derivative couplings, wavepacket dynamics can be qualitatively understood in terms of quasiclassical dynamics on QESs. We have also explicitly shown

nontrivial effects of kinematically induced transitions on the wavepacket amplitudes.

5. CONCLUDING REMARKS

We have formulated a generalized Floquet Hamiltonian method that is applicable to dynamics including nonperiodicity arising from time-dependence of laser parameters and/or the nuclear kinematic effects. Use of the two-time formalism led to a clear method that is formally independent on the details of the time-dependent parameters. In this method, effects from these two types of nonperiodicity are treated in a unified manner under the notion of generalized nonadiabatic transitions. This unified treatment naturally allows for quasi-classical analysis in the (field-free) nonadiabatic dynamics with use of the gradients of QESs, to which we have given analytic and numerical verification. A numerical implementation of this method has been applied firstly to the field-induced dynamics of H_2^+/D_2^+ within the two-state model with no derivative coupling. The dissociation probabilities obtained for them have been in good agreement with previously reported results. Analysis of time-dependent QESs and wavepacket dynamics has exposed some more details about the bond softening, bond hardening, and inverse bond hardening. In the second application to the curve-crossing dynamics of LiF, we have performed calculations of the generalized Floquet-based method in the level of *ab initio* electronic states, including the nuclear dervative coupling elements among them. In fact we have shown a nontrivial effect of the intrinsic (kinematic) nonadiabatic interaction in the system of field-induced nonadiabatic dynamics. The present method, giving simple and clear view of field-induced and intrinsic nonadiabatic transitions will contribute to the study of laser control of chemical reactions and therefore deserves further study.

APPENDIX A: GAUGE CHOICE

In principle one can choose arbitrary gauge in calculation and the resultant physical quantities are independent of gauge choice. In practical calculation, which is inevitably an approximation, however, the result does depend on the gauge choice.

In non-relativistic quantum mechanics using Coulomb gauge, the Schrödinger electron

interacting with transversal (external) vector field $\mathbf{A}^{tr}$, which satisfies $\nabla \cdot \mathbf{A}^{tr} = 0$ is given as

$$i\hbar\partial_t \Psi = \left(\frac{1}{2m} \left[\frac{\hbar}{i}\nabla - \frac{q_e}{c}\mathbf{A}^{tr}\phi \right]^2 + V \right) \Psi, \tag{A.1}$$

where V includes Coulombic interaction among materials. Here the scalar field as well as the longitudinal vector field is absent but there is instantaneous Coulomb interactions. Noting the original form in mind, we can dare rewrite Eq. (A.1) as follows;

$$\left[i\hbar\partial_t - q_e\phi \right] \Psi = \left(\frac{1}{2m} \left[\frac{\hbar}{i}\nabla - \frac{q_e}{c}\mathbf{A}\phi \right]^2 + V \right) \Psi, \tag{A.2}$$

where we have introduced 'scalar field' ϕ, whose role should be limited to a transformation of the external field $\mathbf{A}^{tr}$ given in Eq. (A.1) so that it does not contradict to the Coulombic description of interactions in V. A general gauge transformation in this case can be given as $\Psi = \hat{\mathcal{R}}\widetilde{\Psi}$, and associated transformation of the Schrödinger equation

$$\begin{aligned} &\left(i\hbar\partial_t - q_e\phi\right)\widetilde{\Psi} + \hat{\mathcal{R}}^{-1}\left[\left(i\hbar\partial_t - q_e\phi\right), \hat{\mathcal{R}}\right]\widetilde{\Psi} \\ &= \left(\frac{1}{2m}\hat{\mathcal{R}}^{-1}\left[\left(\frac{\hbar}{i}\nabla - \frac{q_e}{c}\mathbf{A} \right)^2, \hat{\mathcal{R}} \right] + \left(\frac{\hbar}{i}\nabla - \frac{q_e}{c}\mathbf{A} \right)^2 + \hat{\mathcal{R}}^{-1}V\hat{\mathcal{R}} \right) \Psi, \end{aligned} \tag{A.3}$$

In the simplest case, $\hat{\mathcal{R}} = \exp(\frac{i}{c\hbar}q_e\chi)$ so that only the potentials changes as $\tilde{\phi} = \phi + \dot{\chi}/c$ and $\tilde{\mathbf{A}} = \mathbf{A} - \nabla\chi$.

Important gauge choices in atomic problem is Dipole gauge: $\hat{\mathcal{R}} = \exp\left[\frac{i}{c\hbar}q_e\int^{\mathbf{r}}\mathbf{A}_t \cdot d\mathbf{r}'\right]$
Velocity gauge: $\hat{\mathcal{R}} = \exp\left[-\frac{i}{\hbar}\int^t dt' \frac{1}{2m}\left(\mathbf{p} - \frac{q_e}{c}\mathbf{A}_{t'}\right)^2\right]$
Acceleration gauge: $\hat{\mathcal{R}} = \exp\left[\frac{i}{\hbar}s_t\boldsymbol{\epsilon}\cdot\hat{\mathbf{p}} - \frac{i}{\hbar}\int dt' \frac{1}{2m}\left(\frac{q_e}{c}\mathbf{A}_{t'}\right)^2\right]$ where $\mathbf{s}_t \equiv \int^t dt' \frac{q_e}{mc}\mathbf{A}_{t'}$ assuming linear polarization
Here the second one merely cancels the phase arising from the quiver energy.

In practical calculation using ab-initio quantum chemical calculation techniques, exponential transformations like $e^{\frac{i}{\hbar}\mathbf{A}\cdot\mathbf{r}}$ usually cannot be exactly expanded in a finite number of basis set. It follows that if, within some small number of basis set, one can describe the true wave function in good approximation, the same basis set would give poor approximation of the equivalent wave function in another gauge choice.

We can further see that, in analytic approaches, the appropriateness of favored assumption that the initial bound state is well approximated by the field-free ground state $\Psi(0) \approx \phi_g$, depends on the gauge choice; if it is good in the dipole gauge, the equivalent description in the radiation gauge should be obtained using $\Psi(0) \approx \exp\left[\frac{i}{c\hbar}q_e\int^{\mathbf{r}}\mathbf{A}_t \cdot d\mathbf{r}'\right]\phi_g$.

Since existing calculation packages work best for field-free low energy states, a practical choices in molecular problem should then be judged by smallness of difference from the field-free wavefunctions. The field interaction terms in each gauge choices are $V^{rad} = -\frac{q}{mc}\mathbf{A}\cdot\mathbf{p} + \frac{1}{2m}\left(\frac{q}{c}\mathbf{A}\right)^2$, $V^{vel} = -\frac{q}{mc}\mathbf{A}\cdot\mathbf{p}$, $V^{dip} = -q\mathbf{r}\cdot\mathbf{E}$ and $V^{acc} = U_{en}(\mathbf{r}-\mathbf{s}_t) - U_{en}(\mathbf{r})$, where U_{en} is the electron-nucleus interaction, respectively.

In adiabatic basis, $\frac{1}{m}(\mathbf{p})_{\alpha\beta} = \frac{i}{\hbar}(E_\alpha - E_\beta)\mathbf{r}_{\alpha\beta}$, hence the velocity/radiation gauge interaction tends to be larger [smaller] than the dipole gauge interaction in core [outer] region. On the other hand, the interaction term in the acceleration gauge tends to be large and impractical in core-to-valence region but in the asymptotic region, far from the atomic core, V_F^{acc} diminishes as s_t/r^2.

It then follows that, comparing the dipole gauge and velocity/radiation gauge;

1. bound state wavefunction, in particular, whose behavior near atomic core, should be best described by the dipole gauge.

2. unbound state or high Rydberg state wavefunction in particular, whose behavior far from atomic core, should be better described by the velocity or radiation gauge. The asymptotic region would be best described by the acceleration gauge.

APPENDIX B: EXTENSION TO TIME-DEPENDENT FREQUENCY

In the (generalized) Floquet formalism, time dependent variation of the optical frequency requires special care since it alters the fundamental period T. Nevertheless laser frequency is undoubtedly an important control parameter in experiments. Pulse chirping, for example, is considered to be a powerful tool for molecular dissociation control and/or quantum population control[140, 141]. The apparent difficulty in its Floquet based formulation, however, was shown[142] to be circumvented by using the phase variable θ instead of periodic time variable s[142]. Here we apply this idea to derive the nonadiabatic time evolution equation including frequency variation in terms of two-time formalism. We use the phase variable θ instead of short time variable s to define the extended Hamiltonian $\widetilde{H}_{t,\theta}$, which is periodic in θ in the sense $\widetilde{H}_{t,\theta} = \widetilde{H}_{t,\theta+2\pi}$. It reduces to the physical Hamiltonian at $\theta = \Theta(t)$, where $\Theta(t)$ is the physical phase as a function of t. The physical phase may be set as $\Theta(t) = \omega(t)t + \text{const.}$, as Guerin assumed, but it may take other forms. We here introduce the instant (differential) frequency Ω_t to define $\Theta(t) = \int^t d\tau\Omega_\tau$. The Schrödinger equation for the extended state

becomes

$$i\hbar\partial_t\widetilde{\Psi}_{t,\theta} = \mathcal{H}_{t,\theta}\widetilde{\Psi}_{t,\theta} \tag{B.1}$$

where $\mathcal{H}_{t,\theta} = H_{t,\theta} - i\hbar\Omega_t\partial_\theta$ is the Floquet Hamiltonian, which is formally periodic in θ. As we did in the main text, we assume the t dependence can be absorbed in the parameter and rewrite the Floquet Hamiltonian as $\mathcal{H}_\theta(\mathcal{R}_t)$. The nonadiabatic time evolution equation reads

$$\begin{aligned} i\hbar\dot{\chi}_\alpha(\mathbf{R}) = &\sum_I \frac{1}{2M_I}\sum_\beta \left(\left[\frac{\hbar}{i}\frac{\partial}{\partial\mathbf{R}^I} - \frac{Q_I}{c}\mathbf{A} - i\hbar\mathbf{X}\right]^2\right)_{\alpha\beta}\chi_\beta + U_{nuc}(\mathbf{R})\chi_\alpha + \lambda_\alpha\chi_\alpha \\ &- i\hbar\sum_\mu \dot{\zeta}^\mu \sum_\beta \mathcal{X}^{(\zeta^\mu)}_{\alpha\beta}\chi_\beta, \end{aligned} \tag{B.2}$$

The formal appearance of Eq. (B.2) is equivalent to that of Eq. (2.13), although the inner product is now defined as

$$\langle\langle\alpha|\beta\rangle\rangle \equiv \int \frac{d\theta}{2\pi}\langle\alpha(\theta)|\beta(\theta)\rangle, \tag{B.3}$$

and the adiabatic parameter set $\{\zeta^\mu_t\}$ includes Ω_t, which accompanies corresponding nonadiabatic coupling $\mathcal{X}^{(\Omega)}_{\alpha\beta}$ given as

$$\mathcal{X}^{(\Omega)}_{\alpha\beta} = \langle\langle\Phi_\alpha;\mathcal{R}_t|\frac{\partial}{\partial\Omega}|\Phi_\beta;\mathcal{R}_t\rangle\rangle = \frac{\langle\langle\Phi_\alpha;\mathcal{R}_t|i\hbar\partial_\theta|\Phi_\beta;\mathcal{R}_t\rangle\rangle}{\lambda_\alpha - \lambda_\beta} \tag{B.4}$$

If the physical phase is given by $\Theta_t = \omega(t)t + \phi$ (ϕ is time-independent phase) after Refs. [140–142], we have $\Omega_t = \dot{\omega}(t)t + \omega(t)$ and the resultant time-evolution of the physical wavefunction $\widetilde{\Psi}_{t,\theta}|_{\theta=\Theta_t}$ is equivalent to Ref. [142].

APPENDIX C: DETAILS OF QUASICLASSICAL APPROXIMATION

Here we discuss the details of the quasiclassical approximation. We first discuss Eq. (2.16). In Part I, it was shown that the best classical representation (within the stationary phase approximation) of nuclear dynamics is Newtonian dynamics with force form given as Eq. (2.24). Calculation of the force form requires the knowledge of the time-evolution of the electronic degrees of freedom, which, in general case, lead to a difficult self-consistency problem. In the region with negligible nonadiabatic transitions, however, the adiabatic state $|\Phi_\alpha(t);\mathcal{R}_t\rangle$, after a sufficiently short time, obviously evolves into the corresponding state on the nearby nuclear position. The effective force is hence given by the adiabatic state average. The argument here obviously extends to generalized nonadiabaticity, since it is the Floquet

state which is (quasi)stationary under the laser field. The effective force is hence given by Eq. (2.16) in the main text.

We next derive an explicit estimate of small nonadiabaticity. Using a non-dimensional estimate of nuclear derivative contribution, smallness of nonadiabaticity between two Floquet states $|\Phi_\alpha;\mathcal{R}_t\rangle$ and $|\Phi_\beta;\mathcal{R}_t\rangle$ with quasienergy λ_α and λ_β is given as

$$\frac{|i\hbar\mathbf{v}\cdot\mathbf{X}_{\alpha\beta}|}{|\lambda_\alpha-\lambda_\beta|}\ll 1 \tag{C.1}$$

where $\mathbf{v}=\dot{\mathbf{R}}$ is the velocity of the nuclei in the sense of classical representation. Using the fact $\langle\langle\Phi_\alpha|\frac{\partial}{\partial\zeta}|\Phi_\beta\rangle\rangle=\langle\langle\Phi_\alpha|-\frac{\partial\mathcal{H}^{ele}}{\partial\zeta}|\Phi_\beta\rangle\rangle/\left(\lambda_\alpha-\lambda_\beta\right)$, Eq. (C.1) is rewritten as

$$\frac{\left|i\hbar\mathbf{v}\cdot\langle\langle\Phi_\alpha;\mathcal{R}_t|\left(-\frac{\partial\mathcal{H}^{ele}}{\partial\mathbf{R}}\right)|\Phi_\beta;\mathcal{R}_t\rangle\rangle\right|}{\left(\lambda_\alpha-\lambda_\beta\right)^2}\ll 1, \tag{C.2}$$

A similar estimate for the smallness of field-induced nonadiabaticity is given as, in the dipole gauge,

$$\frac{\left|i\hbar\dot{E}\boldsymbol{\varepsilon}\cdot\langle\langle\Phi_\alpha;\mathcal{R}_t|\boldsymbol{\mu}|\Phi_\beta;\mathcal{R}_t\rangle\rangle\right|}{\left(\lambda_\alpha-\lambda_\beta\right)^2}\ll 1, \tag{C.3}$$

where $\boldsymbol{\varepsilon}$ is the field polarization vector, E and $\dot{E}$ are the electric field amplitude and its time derivative (such as pulse envelope and its time derivative), and $\boldsymbol{\mu}$ is the dipole operator. The corresponding expression for the velocity gauge can also be obtained in an obvious manner.

It obviously follows that near avoided-corssing points, adiabaticity is broken for the range where the difference of two adjacent quasienergies is smaller than the energy scale given by the square root of the numerator appearing in the left hand side of Eq. (C.2) or (C.3).

APPENDIX D: APPROXIMATE DIABATIZATION

We show some details of the approximate diabatization scheme. We start from an N_{tot} dimensional adiabatic basis set and corresponding matrices. We first select subset of adiabatic vectors $\{|F_a;\mathbf{R}\rangle\}_{a\in\Lambda}$ where Λ is a fixed subset of the adiabatic vector index set $\Lambda_0=[1,N_{tot}]$. We first diagonalize the submatrix of the dipole matrix (parallel to the molecular axis) $D^{\parallel}_{ab}|_{a,b\in\Lambda}$ as

$$\sum_{b\in\Lambda}{}' D^{\parallel}_{ab}U^b_p=\mu_p U^a_p, \tag{D.1}$$

where U^a_p denotes the ath component of pth eigenvector of the dipole submatrix and μ_p is the corresponding eigenvalue. The corresponding state is defined as $|U_p;\mathbf{R}\rangle\equiv\sum_a{}'|F_a;\mathbf{R}\rangle U^a_p$.

The derivative couplings of these state vectors are evaluated as (the derivation will be given later)

$$\langle U_p;\mathbf{R}|\frac{\partial}{\partial\mathbf{R}}|U_q;\mathbf{R}\rangle = -\frac{\sum'_{b,a\in\Lambda} U_p^{b*}\sum_{r\notin\Lambda}\left(D^{\parallel}_{br}\mathbf{X}_{r,a}-\mathbf{X}_{b,r}D^{\parallel}_{ra}\right)U_q^a}{\mu_p-\mu_q}, \tag{D.2}$$

where $\sum'_{b,a\in\Lambda}$ indicates the summation over subset Λ, while $\sum_{r\notin\Lambda}$ indicates the summation over the residual set $\Lambda_0\setminus\Lambda$. For the actual calculation of LiF in the main text, the lowest two adiabatic states are thus transformed (i.e. $\Lambda=\{0,1\}$), to $|U_I;\mathbf{R}\rangle$ and $|U_C;\mathbf{R}\rangle$, which are essentially ionic and covalent, respectively. These two transformed state vectors as well as the lowest N_b-2 of remaining adiabatic vectors, $\{|U_I\rangle,|U_C\rangle,|F_3\rangle,...,|F_{N_b}\rangle\}$ are used in the calculation of dynamics. The derivative coupling obtained in this transformation is shown in the panel (d) of Fig. 6.

We now evaluate the nuclear coordinate derivatives of state vector $|U_p;\mathbf{R}\rangle$ defined as $\sum'_a|F_a\rangle U_p^a$ where the summation with prime ($\sum'$) is used to emphasize that the summation of indices runs over the restricted set Λ. The derivative couplings among state vectors $|U_p;\mathbf{R}\rangle$ are expanded as

$$\begin{aligned}\langle U_p;\mathbf{R}|\frac{\partial}{\partial\mathbf{R}}|U_q;\mathbf{R}\rangle &= \sum_a{}'\langle U_p;\mathbf{R}|F_a;\mathbf{R}\rangle\frac{\partial}{\partial\mathbf{R}}U_q^a+\sum_a{}'\langle U_p;\mathbf{R}|\frac{\partial}{\partial\mathbf{R}}|F_a;\mathbf{R}\rangle U_q^a\\ &= \sum_a{}'U_p^{a*}\frac{\partial}{\partial\mathbf{R}}U_q^a+\sum_{b,a}{}'U_p^{b*}\mathbf{X}_{ba}U_q^a\end{aligned} \tag{D.3}$$

It follows from the fact that the coefficient vector U_q^a is the eigenvector of the matrix $D^{\parallel}_{ab}$ that

$$\sum_a{}'U_p^{a*}\frac{\partial}{\partial\mathbf{R}}U_q^a = -\frac{\sum_a{}'U_p^{a*}\frac{\partial}{\partial\mathbf{R}}\left(D^{\parallel}_{ab}\right)U_q^b}{\mu_p-\mu_q}. \tag{D.4}$$

Introducing the basis vector independent operator form of the dipole, $\hat{D}^{\parallel}$, the derivative of matrix element is evaluated as (using index i to emphasize unrestricted summation)

$$\frac{\partial}{\partial\mathbf{R}}\left(D^{\parallel}_{ab}\right)=\frac{\partial}{\partial\mathbf{R}}\langle F_a|\hat{D}^{\parallel}|F_b\rangle=\sum_i\left(D^{\parallel}_{ai}\mathbf{X}_{i,b}-\mathbf{X}_{a,i}D^{\parallel}_{i,b}\right), \tag{D.5}$$

where the dipole operator itself, being a purely electronic operator, is assumed to be independent of nuclear coordinates; $\frac{\partial}{\partial\mathbf{R}}\hat{D}^{\parallel}=0$. We hence have

$$\begin{aligned}\langle U_p;\mathbf{R}|\frac{\partial}{\partial\mathbf{R}}|U_q;\mathbf{R}\rangle &= -\frac{\sum'_{b,a}U_p^{b*}\sum_i\left(D^{\parallel}_{bi}\mathbf{X}_{ia}-\mathbf{X}_{bi}D^{\parallel}_{ia}\right)U_q^a}{\mu_p-\mu_q}+\sum_{b,a}{}'U_p^{b*}\mathbf{X}_{ba}U_q^a\\ &= -\frac{\sum'_{b,a}U_p^{b*}\sum_{r\notin\Lambda}\left(D^{\parallel}_{br}\mathbf{X}_{r,a}-\mathbf{X}_{b,r}D^{\parallel}_{ra}\right)U_q^a}{\mu_p-\mu_q},\end{aligned} \tag{D.6}$$

which proves Eq. (D.2).

APPENDIX E: EXACT DESCRIPTION OF NONADIABATIC TRANSITIONS

We show an exact expression of nonadiabatic transition moment taking into account of the extended nature of the nuclear wavefunction. We use Eq. (2.13) to derive the time derivative of the local Floquet state population $\rho_\alpha(\mathbf{R},t) \equiv |\chi_\alpha(\mathbf{R},t)|^2$. A straightforward calculation gives

$$\dot{\rho}_\alpha(\mathbf{R},t) = -\sum_I \nabla_I \cdot \mathbf{J}^I_{\alpha\alpha} - \sum_{I,\beta} \frac{1}{2}\left[\mathbf{X}^I_{\alpha\beta}\cdot\boldsymbol{\mathcal{J}}^I_{\alpha\beta} + c.c.\right] + \sum_{I,\beta}\frac{1}{2}\left[\mathbf{X}^I_{\beta\alpha}\cdot\boldsymbol{\mathcal{J}}^I_{\beta\alpha} + c.c.\right] - 2\sum_\mu \dot{\zeta}^\mu Re\left(\chi^*_\alpha(\mathbf{R},t)\chi_\beta(\mathbf{R},t)\boldsymbol{\mathcal{X}}^{\zeta^\mu}_{\alpha\beta}\right), \tag{E.1}$$

where $\boldsymbol{\mathcal{J}}^I_{\alpha\beta}$ denotes the 'covariant' current-like quantity related to the Ith nuclear coordinate defined as

$$\boldsymbol{\mathcal{J}}^I_{\alpha\beta} \equiv \frac{1}{M_I}\sum_\gamma \chi^*_\alpha(\mathbf{R},t)\left[\left(\frac{\hbar}{i}\nabla - \frac{q}{c}\mathbf{A}\right)\delta_{\beta\gamma} - i\hbar\mathbf{X}^I_{\beta\gamma}\right]\chi_\gamma(\mathbf{R},t) \tag{E.2}$$

and $\mathbf{J}^I_\alpha$ is the projected current

$$\mathbf{J}^I_\alpha \equiv \frac{1}{2}\left(\boldsymbol{\mathcal{J}}^I_{\alpha\alpha} + c.c.\right). \tag{E.3}$$

The meaning of Eq. (E.1) is now clear; the first term describes the drift contribution while the second and the third terms (each including $c.c.$) describe the transition induced by nuclear motion through the derivative coupling. The fourth term is the contribution from the time-dependent change of the laser parameters. Mixed quantum classical description, or the narrow wavepacket limit would give,

$$\frac{d}{dt}|C_\alpha|^2 = -\sum_I \mathbf{v}^I \cdot \left(C^*_\alpha \mathbf{X}^I_{\alpha\beta} C_\beta + c.c.\right) - 2\sum_\mu \dot{\zeta} Re\left(C^*_\alpha X^{\zeta^\mu}_{\alpha\beta} C_\beta\right), \tag{E.4}$$

where C_α denotes the coefficient of Floquet state α, $\mathbf{v}^I$ is the Ith nuclear velocity (in the sense of mixed quantum classical representation). The first term in Eq. (E.4) corresponds to the second and third terms in Eq. (E.1), while the second term in Eq. (E.4) corresponds to the fourth term.

APPENDIX F: INVERSE ITERATION METHOD TO DERIVE EIGENVALUES FROM LARGE SCALE FLOQUET HAMILTONIAN

The inverse iteration algorithm for Floquet eigenvalue problem

We consider the Floquet state in $\mathcal{N}_{\mathcal{H}}$ dimensional Hilbert space with the Fourier series (photon number) cutoff set as $N_p^{\pm}$, which is to say that Fourier order n runs through $-N_p^- \leq n \leq N_p^+$. The Floquet Hamiltonian has formal linear dimension $(N_p^+ + 1 + N_p^-) \times \mathcal{N}_{\mathcal{H}}$, which can be prohibitively large to perform with standard matrix diagonalization algorithm such as Householder method [143]. Moreover, in practical calculations, we want Floquet states for a few hundreds of spatial grid points and/or every time slices along the time-evolution. There clearly need some better algorithms.

In order to discuss further, we introduce supermatrix notation where each block has linear dimension $\mathcal{N}_{\mathcal{H}}$. The (n,m)-th block of the Floquet Hamiltonian is denoted as $\mathcal{H}_{n,m}$ where n and m runs from $-N_p^-$ to N_p^+. The Floquet Hamiltonian for monochromatic field has blockwise-tridiagonal structure ($\mathcal{H}_{n,n} = H^{el} - n\hbar\omega$, $\mathcal{H}_{n\pm1,n} = V_F^{\pm}$ and zero otherwise), which is to be exploited for reducing computational cost.

We consider the inverse iteration method with LU algorithm [143]. The inverse iteration method is an iterative method to solve eigenvalue problem.

Inverse iteration method

Purpose:	Iterative derivation of Kth eigenvalue λ_K and eigenvector $\mathbf{u}_K$ of a given Hermitian matrix $\mathcal{A}$
Starting Conditions:	Initial guess of eigenvalue $\widetilde{\lambda}_K^{(0)}$, which is closest to λ_K ($\lvert\lambda_K - \widetilde{\lambda}_K^{(0)}\rvert < \lvert\lambda_{K'} - \widetilde{\lambda}_K^{(0)}\rvert$ for any $K' \neq K$), and trial eigenvector $\widetilde{\mathbf{u}}_K^{(0)}$, which is not orthogonal to the true eigenvector $\mathbf{u}_K$
Procedure:	(Iterate over the following steps until convergence.)
1. **(Vector update)**	$\mathbf{w}_n^{(i+1)} = \left(A - \widetilde{\lambda}_K^{(i)}\right)^{-1} \widetilde{\mathbf{u}}_K^{(i)}$ and renormalize the result; $\mathbf{u}_n^{(i+1)} = \mathbf{w}_n^{(i+1)} / \left\lvert\mathbf{w}_n^{(i+1)}\right\rvert$
2. **(Eigenvalue update)**	$\widetilde{\lambda}_K^{(i+1)} = \widetilde{\lambda}_K^{(i)} + 1/\mathbf{w}_n^{(i+1)} \cdot \mathbf{u}_n^{(i)}$.

The matrix inversion, required for the inverse iteration, is efficiently obtained using LU algorithm [143], exploiting the tridiagonal structure. We first review the LU algorithm to calculate matrix inversion.

For our purpose, we can use the idea of step 1, the LU decomposition, in a block-wise

LU algorithm for matrix inversion

Purpose	Derivation of the inverse matrix of $\mathcal{A}$, which is assumed to be inversible through LU-decomposition $\mathcal{A} = LU$, or more explicitly, $\mathcal{A}_{ij} = \sum_{k \leq \min(i,j)} L_{ik} U_{kj}$ (†) where L and U are lower- and upper-triangle matrices, respectively. without loss of generality, L_{ii} can be set unity.
Procedure	
1. (LU decomposition)	Eq. (†) is solved for $j = 1, 2, ..., N$: in the jth step, one first solves for U_{ij} for $i = 1, 2, ..., J$ in this order and then solves for L_{ij} for $i = j+1, ..., N$.
2. (Back-substitution)	Matrix equation $LUX = 1$ is solved column by column as $LU\mathbf{x}_j = \mathbf{e}_j$ with $\mathbf{e}_j$ being the jth unit vector. Coupled equations $L\mathbf{y} = \mathbf{e}_j$, $U\mathbf{x}_j = \mathbf{y}$ are readily solved [143] using the triangular property of L and U.

manner. To be explicit, block-tridiagonal matrix $\mathcal{H}$

$$\mathcal{H} = \begin{pmatrix} \ddots & & & & \\ & H^{el} - (n-1)\hbar\omega & V_F^- & 0 & \\ & V_F^+ & H^{el} - n\hbar\omega & V_F^- & \\ & 0 & V_F^+ & H^{el} - (n+1)\hbar\omega & \\ & & & & \ddots \end{pmatrix} \tag{F.1}$$

is decomposed into blockwise LU matrix

$$\mathcal{L} = \begin{pmatrix} \ddots & & & \\ & 1_{N_\mathcal{H}} & 0 & 0 \\ & V_F^+ U_{n-1}^{-1} & 1_{N_\mathcal{H}} & 0 \\ & 0 & V_F^+ U_n^{-1} & 1_{N_\mathcal{H}} \\ & & & \ddots \end{pmatrix} \tag{F.2}$$

$$\mathcal{U} = \begin{pmatrix} \ddots & & & \\ & T_{n-1} & V_F^- & 0 \\ & 0 & T_n & V_F^- \\ & 0 & 0 & T_{n+1} \\ & & & \ddots \end{pmatrix} \tag{F.3}$$

where T_n are $N_{\mathcal{H}} \times N_{\mathcal{H}}$ dimensional submatrices subject to the equation

$$T_n = \left(H^{el} - n\hbar\omega\right) - V_F^+ T_{n-1}^{-1} V_F, \tag{F.4}$$

which is to be solved starting from $T_{-N_p^-} = H^{el} + N_p^- \hbar\omega$

Here we note the mechanism of the inverse iteration. We formally expand the ith step guess vector by the true eigenvectors as $\widetilde{\mathbf{u}}_K^{(i)} = \sum_L \mathbf{u}_K C_{LK}^{(i)}$. Application of $\left(\mathcal{A} - \tilde{\lambda}_K^{(i)}\right)^{-1}$ scales each component as $C_{LK}^{(i)} \to C_{LK}^{(i)}/(\lambda_L - \tilde{\lambda}_K^{(i)})$, hence through each step the component with eigenvalue closest to $\tilde{\lambda}_K^{(i)}$ magnifies the best.

In practical implementation, the initial guess at the onset of laser pulse can be set eigenvalues and eigenvectors of the field-free Hamiltonian.

Practical implementation

In the Floquet eigenvalue problem (in the limit $N_p^{\pm} \to \infty$), for any Floquet eigenvector $\mathbf{u}_K$ with eigenvalue λ_K, its "$m\omega$-shift", defined as $\mathbf{v}[n] = \mathbf{u}[n+m]$, is also a Floquet operator with eigenvalue $\lambda_K + m\hbar\omega$. In the practical calculation with finite cut offs $N_p^{\pm}$, the exact relation is lost but the approximate relation holds if the derived vector is well-described within the truncated Fourier series expansion. We therefore have to calculate only $N_{\mathcal{H}}$ "distinct" vectors.

The initial guess can be obtained from the eigenvalue E_K and eigenvector $\mathbf{c}_K$ of the field-free Hamiltonian as $\widetilde{\mathbf{u}}_K^0 = (\mathbf{0}, ..., \mathbf{0}, \mathbf{c_K}, \mathbf{0}, ..., \mathbf{0})^T$, $\widetilde{\lambda}_K = E_K$, which is truly the Floquet eigenvector in the zero-field limit. Once the Floquet vector for certain nuclear position and time $(\mathbf{R}, t = 0)$ is obtained, subsequent calculations can use the previous results as starting guess.

The algorithm is applied successfully to large scale problems with, for example, $N_{\mathcal{H}} = 50$, $N_p = 41$. However, there have also been found a number of problems to be overcome.

1. Convergence to unwanted vector; Some iterations do not converge to "new" one, which is distinct to already derived ones, but converge to one of the already derived vectors or their $n\omega$shifts.

2. Sometimes iterations do not converge or converge to a superposition of eigenvectors. This typically occurs on the (avoided) crossing points on the QESs, where eigenvalues come close to each other.

These problems arise from the nature of the inverse iteration algorithm, which "filters" the

trial vector only through the eigenvalues. A possible cure to avoid the former problem, convergence to undesired vector, is to project out these undesired ones (including their $m\omega$ shifts) in each iteration step $\tilde{\mathbf{u}}_K^{(i)} \to \left[1 - \sum_m \sum_j^{K-1} \mathbf{u}_{K-m\omega}\mathbf{u}_{K-m\omega}^T\right] \tilde{\mathbf{u}}_K^{(i)}$.
As for the latter problem, application of other algorithm such as Lanczos algorithm [144] was found effective in some cases.

Thus the inverse iteration algorithm tend to get more complex than initial expectation. As a practical prescription, Floquet eigenvalue problem for small ($N_{\mathcal{H}} = 8$, $N_p = 61$, for example) size system is much easier solved by standard full-size matrix diagonalization procedures. The numerical results in the main text was obtained by the latter method, not by the inverse iteration. For larger size problem, however, inverse iteration should work better both in terms of memory efficiency and time efficiency.

General Conclusion and Perspectives

As we have already given summary of each part separately, here we put emphasis on relations among sections and future perspectives.

We have first reviewed current trend in the study of nonadiabatic dynamics, with much emphasis on the field-induced dynamics to derive requirements for a new theoretical approach; (i) accurate reproduction of electronic dynamics, (ii) appropriate description of nuclear dynamics that couples to the electronic dynamics (iii) applicability to a certain variety of molecules (iv) clear description of the underlying physics.

In Part I, we have discussed MQC representation of electron-nucleus coupled nonadiabatic dynamics. We have found that one of the most rigorous description, free from empirical approximations, is the Pechukas theory, with several modifications. Although being unsuited for direct numerical implementation, it serves as a guide for theoretical discussions. We did use the formal expression of force form for derivation of QES gradient approximation in Part II Subsec. 2-4.

On the other hand, there is also a need for practical algorithms (even if we have to allow some additional assumptions). We hence have examined existing algorithms, SET and PSANB, along this framework, to clarify their properties and underlying assumptions. In seek for further improvements of these algorithms, we have proposed central requirements for branching algorithms (Sec. 4) and examined possible approaches. These discussions are to be further developed with numerical tests to construct a practical algorithms.

The general theory of MQC dynamics thus obtained covers the requirements (i) (iii) and (iv) on formal theory whereas we need further sophistication to satisfy the requirement (ii) since there have been found no practical way to reproduce the "conservation laws in the asymptotic region".

In Sec. 6, we have discussed higher order expansion of the nuclear path integrals. Existence and roles of the force-force correlation term has been found to be related to possible electron-nucleus mode couplings and is another manifest of nonadiabaticity. However, apart from several toy-model examples we discussed in this work, its effects in more realistic molecular models remains to be examined. In future work, we should also examine field effects on such nuclear-electron couplings. In fact the effects of field-nuclear or electron-field-nuclear dynamical couplings are mostly omitted (as we have assumed laser frequency to be off-resonant with respect to the nuclear vibration modes) in the discussions in Part II, but there are some

intriguing findings in the literature [130].

In Part II, we have sought for a practical theory for electron-nucleus coupled nonadiabatic dynamics in intense laser fields. We are hinted by intuitive observations on the validity of the idea of field-induced PES. In order to construct physically clear as well as rigorous approach, we formulated a generalized nonadiabatic Floquet Hamiltonian method based on the two-time formalism of quantum mechanics. We thus have formulated a unified treatment of field-induced as well as kinematically-induced nonadiabatic transitions among Floquet states. This allows analogy from conventional theory of chemical reaction dynamics. Another important outcome here was concrete formulation of the QES gradient approximation with explicit validity conditions. Exactness of the theory and validity of the QES gradient approximation have also numerically examined.

Here we note that the advantage of using the Floquet representation in evaluation of the effective force is the sationarity of the Floquet state. It is interesting to examine the validity of the QES gradient force against other derivations of effective force based on different representations including the adiabatic basis and so-called time-dependent adiabatic basis [145].

Having constructed theoretical foundations, we have achieved (i) to (iv) in the formal theoretical level let alone inclusion of higher energy processes such as field-ionizations. On the other hand, in practical level, much is left for future work including (iii). Our next goal is to construct a practical calculation method of Floquet-based field-induced dynamics in MQC representation. In such implementation, accuracy of the asymptotic nuclear velocity in each dissociation channel is crucial for reproducing the experimental observables. In order to achieve this, we have to carefully formulate branching algorithms based on the discussions on Part I. Study in this course is now going on.

Acknowledgments

The author would like to express depth of his gratitude for his supervisor, Professor Kazuo Takatsuka for many insightful conversations and encouragements throughout his course. The author is greatly indebted to Professor Takatsuka for generously accepting him as a student regardless of the author's age, and providing guidance and supports for his academic as well as his private life.

The author also greatly appreciate Dr. Satoshi Takahashi for having supported both his

academic as well as private life throughout his course with much patience. Dr. Takahashi is also among the first ones who introduced the author to this wonderful academic life.

He is greatly indebted to Dr. Yasuki Arasaki and Dr. Takehiro Yonehara for many important advices as well as stimulating discussions. They have been so generous to tell the author many of their advanced computational techniques. He also appreciates Mrs. Yukiko Kousaka for her hearty supports throughout his course. She has been a great help in the author's applying for the JSPS Fellowship. Many discussions and critical comments from (former and present) members of Takatsuka Lab., Dr. Kengo Nagashima, Mr. Shin-ichi Koda, Mr. Kentaro Yamamoto, Mr. Masaya Konishi, Mr. Kentaro Matsumoto, and Mr. Yuta Mizuno are also greatly acknowledged. Their critical comments have often been great hints for improving this research.

The author is deeply honored of having been able to share time with Professor Kozo Kuchitsu. Professor Kuchitsu has kindly told us many of his experiences in his distinguished academic career, which have been invaluable hints and stimuli for the author as well as members of Takatsuka Lab.

He also appreciates Professor Katsuyuki Nobusada for enlightening discussions, which are reflected in several topics in Part I of this research. The author has been supported by Grant-in-Aid for JSPS Fellows (DC1). Part of this work has also been supported by Grant-in-Aid for Scientific Research from Japan Society for the Promotion of Science (Grant No. $23 \cdot 9633$).

---

[1] M. Head-Gordon, J. Chem. Phys. **100**, 13213 (1996); R. A. Friesner Proc. Natl. Acad. Sci **102**, 6648 (2005).

[2] M. Born and J. R. Oppenheimer, Ann. Phys. **84**, 457(1927).

[3] A. H. Zewail, Angrew. Chem. Int. Ed. **39**, 2586 (2000).

[4] J. Burnett, V. C. Reed and P. L. Knight, J. Phys. B **26** 561 (1993).

[5] J. H. Posthumus, Rep. Prog. Phys. **67** 623 (2004).

[6] M. F. Kling and M. J. Vrakking, Ann. Rev. Chem. Phys. **59**, 463 (2008).

[7] F. Krausz and M. Y. Ivanov, Rev. Mod. Phys. **81**, 163 (2009).

[8] W. Demtröder *Laser Spectroscopy fourth Ed.* (Springer, Berlin 2008).

[9] L. D. Landau, Phys. Zts. Sov. **2**, 46 (1932).

[10] C. Zener, Proc. R. Soc. London **137**, 696 (1932).

[11] E. C. G. Stueckelberg, Helv. Phys. Acta. **5**,369 (1932).

[12] C. Zhu and H. Nakamura, N. Re and V. Aquilanti, J. Chem. Phys. **97**, 1892 (1992); C. Zhu and H. Nakamura, *ibid.* **97**, 8497.(1992); C. Zhu and H. Nakamura, *ibid.* **98**, 6208 (1993); C. Zhu and H. Nakamura, *ibid.* **101**, 4855 (1994);

[13] J. C. Tully and R. Preston, J. Chem. Phys. **55**, 5621 (1971).

[14] H. D. Meyer and W. H. Miller, J. Chem. Phys. **70**, 3214 (1979).

[15] J. B. Delos, W. R. Thorson and S. K. Knudson, Phys. Rev. A **6** 709 (1972).

[16] D. A. Micha, J. Chem. Phys. **78**, 7138 (1983).

[17] R. Kendall, T. Dunning and R. Harrison, J. Chem. Phys. **96** 6796 (1992), T. Dunning, J. Chem. Phys. **90** 1007, (1989).

[18] M. W. Schmidt and M. S. Gordon, Annu. Rev. Phys. Chem. **49**, 233 (1998).

[19] K. B. Lipkowitz, D. B. Boyd, R. J. Bartlett and J. F. Stanton, Rev. Comput. Chem. **5**, 64 (2007).

[20] N. C. Handy and H. F. Schaefer, J. Chem. Phys. **81**, 5031 (1984).

[21] J. C. Tully, J. Chem. Phys. **93**, 1061 (1990).

[22] M. Amano and K. Takatsuka, J. Chem. Phys. **122**, 084113 (2005).

[23] C. Zhu, A. W. Jasper and D. G. Truhlar, J. Chem. Phys. **120**, 5543 (2004).

[24] M. Ben-Nun and T. J. Martnez, J. Chem. Phys. **108**, 7244 (1998).

[25] T. Yonehara and K. Takatsuka, J. Chem. Phys. **129**, 134109 (2008).

[26] J. C. Tully, J. Chem. Phys. **137**, 22A301 (2012).

[27] A. M. Wodtke, J. C. Tully, and D. J. Auerbach, Int. Rev. Phys. Chem. **23**, 513 (2004).

[28] R. Valero and D. G. Truhlar, J. Chem. Phys. **137**, 22A539 (2012).

[29] S. Hammes-Schiffer and A. V. Soudackov, J. Phys. Chem. B **112**, 14108 (2008).

[30] J. Lambe and R. C. Jaklevic, Phys. Rev. **165**, 821 (1968).

[31] J. Nelson, J. Kirkpatrick and P. Ravirajan, Phys. Rev. B **69**, 035337 (2004).

[32] C. V. Shank and E. P. Ippen, App. Phys. Lett. 24, 373 (1974).

[33] T. S. Rose, M. J. Rosker and A. H. Zewail, J. Chem. Phys. **91**, 7415 (1989).

[34] P. M. Felker and A. H. Zewail, J. Chem. Phys. **82**, 2961 (1985); *ibid.* **82**, 2975 (1985).

[35] V. Engel and H. Metiu, J. Chem. Phys. **90**, 6116 (1989).

[36] Y. Arasaki, K. Takatsuka, K. Wang and V. McKoy, Phys. Rev. Lett. **90**, 248303 (2003); J. Chem. Phys. **119**, 7913 (2003);

[37] P. Agostini, F. Fabre, G. Mainfray, G. Petite and N. K. Rahman, Phys. Rev. Lett. **42**, 1127 (1979).

[38] B. W. Shore and P. L. Knight, J. Phys. B **20**, 413 (1987).

[39] J. L. Krause, K. J. Schafer and K. C. Kulander, Phys. Rev. Lett. **68**, 3535 (1992).

[40] L. V. Keldysh, J. Exp. Theor. Phys. **47**, 1945 (1964) [Sov. Phys. JETP. **20**, 1307 (1965).]

[41] A. M. Perelomov, V. S. Popov and M. V. Terent'ev, J. Exp. Theor. Phys. **50**, 1393 (1966) [Sov. Phys. JETP. **23**, 924 (1966).]

[42] M. V. Ammosov, N. B. Delone and V. P. Krainov, Zh. Eksp. Teor. Fiz. **91**, 2008 (1986) [Sov. Phys. JETP **64** 1191 (1986).]

[43] F. H. M. F.aisal, J. Phys. B **6**, L89 (1973).

[44] H. R. Reiss, Phys. Rev. A **22**, 1786 (1980).

[45] G. Gibson, R. Freeman and T. McIlrath, Phys. Rev. Lett. **67**, 1230 (1991).

[46] C. Lynga, A. L'Huillier and C. G. Wahlstrom, J. Phys. B **29**, 3293 (1996).

[47] A. Giusti-Suzor, F. H. Mies, L. F. DiMauro, E. Charron and B. Yang, J. Phys. B **28**, 309 (1995).

[48] T. Zuo and A. D. Bandrauk, Phys. Rev. A **52** R2511 (1995).

[49] D. Pavicic, A. Kiess, T. Hansch and H. Figger, Phys. Rev. Lett. **94**, 163002 (2005).

[50] T. Kanai, S. Minemoto and H. Sakai, Nature (London) **435**, 470 (2005).

[51] Giusti-Suzor, X. He, O. Atabek, and F. Mies, Phys. Rev. Lett. **64**, 515 (1990).

[52] P. Bucksbaum, A. Zavriyev, M. Muller and D. Schumacher, Phys. Rev. A. **42**, 5500, (1990).

[53] Shih-I Chu, J. Chem. Phys. **94**, 7901 (1991).

[54] G. Yao, Shih-I Chu, Chem. Phys. Lett. **197**, 413, (1992).

[55] A. Zavriyev, P. Bucksbaum, J. Squier and F. Saline, Phys. Rev. Lett. **70**, 1077, (1993).

[56] K. Codling and L. J. Frasinski, J. Phys. B **26**, 783 (1993).

[57] S. Chelkowski, T. Zuo, O. Atabek, and A. D. Bandrauk, Phys. Rev. A **52** 2977 (1995).

[58] T. Okino, Y. Furukawa, P. Liu, T. Ichikawa, R. Itakura, K. Hoshina, K. Yamanouchi and H. Nakano, Chem. Phys. Lett. **419**, 223 (2006).

[59] P. B. Corkum, Phys. Rev. Lett. **71**, 1994 (1993).

[60] M. Lewenstein, Ph. Balcou, M. Y. Ivanov, A. L'Huillier and P.B. Corkum, Phys. Rev. A **49** 2117 (1994).

[61] F. Ferrari, F. Calegari, M. Lucchini, C. Vozzi, S. Stagira, G. Sansone and M. Nisoli, Nature Photonics **4**, 875 (2010).

[62] O. Smirnova, Y. Mairesse, S. Patchkovskii, N. Dudovich, D. Villeneuve, P. Corkum and M. Y. Ivanov, Nature (London) **460**, 972 (2009).

[63] H. J. Wörner, J. B. Bertrand, D. V. Kartashov, P. B. Corkum and D. M. Villeneuve, Nature (London) **466**, 604 (2010).

[64] D. J. Tannor and S. A. Rice J. Chem. Phys. **83**, 5013 (1985).

[65] P. Brumer and M. SHAPIRO Chem. Phys. Lett. **126**, 541 (1986).

[66] S. Shi and H. Rabitz, J. Chem. Phys. **92**, 364 (1990).

[67] R. Judson and H. Rabitz, Phys. Rev. Lett. **68**, 1500 (1992).

[68] A. Assion, T. Baumert, M. Bergt, T. Brixner, B. Kiefer, V. Seyfried, M. Strehle, G. Gerber Science **282**, 919 (1998).

[69] R. Levis, G. Menkir and H. Rabitz, Science **292**, 709 (2001).

[70] C. Daniel, J. Full, L. Gonzalez, C. Lupulescu, J. Manz, A. Merli, S. Vajda and L. Woste, Science

299, 536 (2003).

[71] B. J. Sussman, D. Townsend, M. Yu. Ivanov and A. Stolow, Science **314**, 278(2006)

[72] X. Xie *et. al.*, Phys. Rev. Lett, **109**, 243001 (2012).

[73] M. D. Hack and D. G. Truhlar, J. Chem. Phys. **114**, 9305 (2001).

[74] C. Zhu, S. Nangia, Ahren W. Jasper, and D. G. Truhlar, **121**, 7658 (2004).

[75] P. Pechukas, Phys. Rev. **181**, 166 (1969); *ibid.* **181**, 174 (1969).

[76] R. J. Glauber, Phys. Rev. **131**, 2766 (1963).

[77] J. P. Blaizot and H. Orland, Phys. Rev. C 24, 1740 (1981).

[78] J. W. Neegle and H. Orland, *Quantum Many-particle Systems* (Perseus Books, 1988).

[79] L. S. Schulman, *Techniques and Applications of Path Integration* (Dover, New York, 2005).

[80] K. Nagashima and K. Takatsuka, J. Phys. Chem. A **113**, 15240 (2009); M. Okuyama and K. Takatsuka, Bull. Chem. Soc. Jpn. **85**, 217 (2012).

[81] P. Pechukas and J. P. Davis, J. Chem. Phys. **56**, 4970 (1972).

[82] K. Takatsuka, J. Phys. Chem. A **111**, 10196 (2007).

[83] D. W. Schwenke, J. Phys. Chem. A **105**, 2352 (2001).

[84] G. Stock and M. Thoss, Phys. Rev. Lett. **78**, 578 (1996).

[85] T. Yonehara and K. Takatsuka, J. Chem. Phys. **132**, 244102 (2010).

[86] T. Yonehara and K. Takatsuka, J. Chem. Phys. **137**, 22A520 (2012).

[87] A. Alnaser, B. Ulrich, X. Tong, I. Litvinyuk, C. Maharjan, P. Ranitovic, T. Osipov, R. Ali, S.Ghimire, Z. Chang, C. Lin and C. Cocke, *Phys. Rev. A.* **2005** *72*, 30702.

[88] K. Hanasaki and K. Takatsuka, Phys. Rev. A **81**, 052514 (2010).

[89] T. Yonehara, K. Hanasaki and K. Takatsuka, Chem. Rev. **112**, 499 (2012).

[90] W. H. Miller and T. F. George, J. Chem. Phys. **56**, 5637 (1972).

[91] U. Müller and G. Stock, J. Chem. Phys. **107**, 6230 (1997).

[92] B. Sutcliffe, Theor. Chem. Acc. **131**, 1215 (2012).

[93] T. Yonehara, *private communication*

[94] Y. Osamura, Y. Yamaguchi and H. F. Schaefer III, J. Chem. Phys. **77** 383 (1982).

[95] J. C. Tully, Faraday Discuss., **110**, 407 (1998).

[96] H. Kohno, Y. Sato, M. Kanno, K. Nakai, and T. Kato, Bull. Chem. Soc. Jpn. **79**, 196 (2006).

[97] L. Landau and E. M. Lifshitz, *Quantum Mechanics Non-Relativistic Theory* Butterworth-Heinemann 1981.

[98] A. Becker and F. H. M. Faisal, J. Phys. B **38**, 1 (2005).

[99] X. M. Tong and Z. X. Zhao and C. D. Lin, Phys. Rev. A **66**, 033402 (2002).

[100] D. Pavcic, K. Lee, D. Raynev, P. Corkum and D. Villeneuve, Phys. Rev. Lett. **98** 243001 (2007).

[101] I. Thomann *et. al.*, J. Phys. Chem. A **112**, 9382 (2008).

[102] S. Son and Shih-I. Chu, Phys. Rev. A **80**, 011403 (2009).

[103] P. Li and Shih-I. Chu, Phys. Rev. A **86**, 013411 (2012).

[104] S. Chelkowski, A. Conjusteau, T. Zuo, and A. D. Bandrauk, Phys. Rev. A **54**, 3235 (1996).

[105] Shih-I Chu, J. Chem. Phys. 123, 062207 (2005).

[106] M. Spanner and S. Patchkovskii, Phys. Rev. A **80** 064311 (2009).

[107] E. Runge and E. K. U. Gross, Phys. Rev. Lett. **52**, 997 (1984).

[108] A. M. Lane and D. Robson, Phys. Rev. **151**, 774 (1966).

[109] P. G. Burke, P. Francken and C. J. Joachain, J. Phys. B **24** 761 (1991).

[110] L. Torlina and O. Smirnova, Phys. Rev. A **86** 043408 (2012); L. Torlina, M. Ivanov, Z. B. Walters and O. Smirnova, *ibid.*, 043409 (2012).

[111] A. Conjusteau, A. D. Bandrauk, and P. B. Corkum, J. Chem. Phys. **106**, 9095 (1997).

[112] M. V. Korolkov and K. Weitzel, J. Chem. Phys. **123**, 163408 (2005).

[113] L. J. Frasinski, J. H. Posthumus, J. Plumridge, and K. Codling, Phys. Rev. Lett. **83**, 3625 (1999).

[114] L. J. Frasinski, J. Plumridge, J. H. Posthumus, K. Codling, P. F. Taday, E. J. Divall, and A. J. Langley, Phys. Rev. Lett. **86**, 2541 (2001).

[115] V. Serov, A. Keller and O. Atabek, Phys. Rev. A **72**, 033413 (2005).

[116] N. Mirsaleh-Kohan, W. D. Robertson and R. N. Compton, Mass Spec. Rev. **27** 237 (2008).

[117] A. T. J. B. Eppink and D. H. Parker, Rev. Sci. Instr. **68**, 3477 (1997).

[118] R. Numico, A. Keller, and O. Atabek, Phys. Rev. A **60**, 406 (1999).

[119] A. M. Sayler, P. Q. Wang, K. D. Carnes, B. D. Esry and I. Ben-Itzhak, Phys. Rev. A **75**, 063420 (2007).

[120] S. Chelkowski, A. Conjusteau, T. Zuo and A. D. Bandrauk, Phys. Rev. A. **54** 3235 (1996).

[121] C. M. Dion, A. Keller, O. Atabek, and A. D. Bandrauk, Phys. Rev. A **59**, 1382 (1999).

[122] J. Werschnik and E. K. U. Gross, J. Phys. B **40**, R175 (2007).

[123] K. Yagi and K. Takatsuka, J. Chem. Phys. **123**, 224103 (2005).

[124] K. Takatsuka and T. Yonehara, Phys. Chem. Chem. Phys. **13**, 4987 (2011).

[125] M. Richter, P. Marquetand, J. Gonzaalez-Vazquez, I. Sola, and L. Gonzalez, J. Chem. Theory Comput. **7**, 1253 (2011).

[126] (a) G. Floquet, Ann. l'Ecol. Norm. Sup. **12**,47 (1883). Application to physical problems are established in (b) S. H. Autler and C. H. Townes, Phys. Rev. **100**, 703 (1955); J. Shirley, Phys. Rev. **138**, B979 (1965). Recent review is (c) Shih-I Chu and D. A. Telnov, Phys. Rep. **390**,1 (2004).

[127] U. Peskin and N. Moiseyev, J. Chem. Phys. **99**, 4590 (1993).

[128] T. Ho and Shih-I Chu, Chem. Phys. Lett. **141**, 315 (1987) see also related discussions in Ref. [126] (c)).

[129] M. Chrysos, O. Atabek, and R. Lefebvre, Phys. Rev. A **48**, 3845 (1993).

[130] R. Lefebvre, O. Atabek, M. Šindelka and N. Moiseyev, Phys. Rev. Lett. **103**, 123003 (2009).

[131] F. Bunkin and I. Tugov , Phys. Rev. A. **8**, 601 (1973)

[132] D. Kosloff and R. Kosloff, J. Comput. Phys. **52**, 35 (1983).

[133] G. N. Gibson, M. Li, C. Guo and J. Neira, Phys. Rev. Lett. **79**, 2022, (1997).

[134] L. Kahn, P. Hay, and I. Shavitt, J. Chem. Phys. **61**, 3530 (1974).

[135] A. Varandas, J. Chem. Phys. **131**, 124128 (2009)

[136] A. Bandrauk and J. Gauthier, J. Phys. Chem. **93**, 7552 (1989).

[137] M. Schmidt, K. Baldridge, J. Boatz, S. Elbert, M. Gordon, J. Jensen, S. Koseki, N. Matsunaga, K. Nguyen, S. Su, T. Windus, M. Dupuis and J. Montgomery, J. Comput. Chem. **14**, 1347 (1993).

[138] J. Paldus, Phys. Rev. A **14**, 1620 (1976); I. Shavitt, Int. J. Quant. Chem. **12** (S11), 131 (1977).

[139] R. Kendall, T. Dunning and R. Harrison, J. Chem. Phys. **96** 6796 (1992), T. Dunning, J. Chem. Phys. **90** 1007, (1989).

[140] S. Chelkowski, A. Bandrauk and P. Corkum, Phys. Rev. Lett. **65**, 2355 (1990).

[141] S. Zhdanovich, E. Shapiro, M. Shapiro, J. Hepburn and V. Milner, Phys. Rev. Lett. **100**, 103004 (2008).

[142] S. Guerin, Phys. Rev. A. **56**,1458 (1997).

[143] W. H. Press, S. A. Teukolsky, W. T. Vetterling and B. P. Flqnnery, *Numerical Recipes in C* Cambridge University Press 1999.

[144] Reference for the Lanczos algorithm can be found in, for example, E. Dagotto, Rev. Mod. Phys. **66**, 763 (1994).

[145] Y. Sato, H. Kono, S. Koseki and Y. Fujimura, J. Am. Chem. Soc. **125**, 8019 (2003).